8-2011

Modeling And Development Of A MEMS Device For Pyroelectric Energy Scavenging

Salwa Mostafa
to.salwamostafa@gmail.com

Recommended Citation

Mostafa, Salwa, "Modeling And Development Of A MEMS Device For Pyroelectric Energy Scavenging. " PhD diss., University of Tennessee, 2011.
https://trace.tennessee.edu/utk_graddiss/1208

To the Graduate Council:

I am submitting herewith a dissertation written by Salwa Mostafa entitled "Modeling And Development Of A MEMS Device For Pyroelectric Energy Scavenging." I have examined the final electronic copy of this dissertation for form and content and recommend that it be accepted in partial fulfillment of the requirements for the degree of Doctor of Philosophy, with a major in Electrical Engineering.

Syed K. Islam, Major Professor

We have read this dissertation and recommend its acceptance:

Leon M. Tolbert, Jayne Wu, Michael J. Sepaniak

Accepted for the Council:
Dixie L. Thompson

Vice Provost and Dean of the Graduate School

(Original signatures are on file with official student records.)

Modeling and Development of a MEMS Device for Pyroelectric Energy Scavenging

A Dissertation Presented for the
Doctor of Philosophy
Degree
The University of Tennessee, Knoxville

Salwa Mostafa
December 2011

DEDICATION

My better half

Ashraf Bin Islam

My parents

Md. Golam Mostafa & Jasmin Akter

My brother

Safwat Mostafa

ACKNOWLEDGEMENTS

I would like to thank my advisor Dr. Syed K. Islam for all his support and guidance throughout my time at graduate school. Special thanks to Dr. Leon M. Tolbert, Dr. Jayne Wu, Dr. Michael Sepaniak and Dr. Scott R. Hunter for serving in my committee and critically reviewing my work. Sincere thanks to Dr. Donald Bouldin for his continuing support in progressing my career.

I am forever indebted to Dr. Scott Hunter for taking me on board to work on this novel research project that eventually became my dissertation and putting his trust on me. I am also grateful to Dr. Panos Datskos for his encouragement and advices. I am thankful to members of Micro and Nanosystems Group in Measurement Science and Systems Engineering Division of Oak Ridge National Laboratory. I have learnt a lot about conducting research by working with Drs. Nicolay Lavrik, Slobodan Rajic, Thirumalesh Bannuru and Barton Smith and I humbly acknowledge the impression they have left on my career. Special thanks to Dr. Nicolay Lavrik for fabricating the MEMS devices used in the research.

I thank and congratulate my husband, Ashraf Bin Islam, for sharing this journey through graduate school with me and for always being there. I would not have dared to walk this path had he not taken every step with me. Thanks to my mother, my life line, just for being herself. Thanks to my father for being my idol, for setting my goal to become an engineer and for supporting me along the way. Thanks to my brother for being my worst critic and my best friend.

Also thanks to my in-laws, the rest of my family and friends for their constant prayers and the confidence they instilled in me.

I would also like to thank all the past and present members of Analog VLSI and Devices Laboratory for their help and support in various aspects. I have the warmest gratitude for Ms. Dana Bryson, Mr. William Rhodes and all staff members of EECS department for their loving support with many issues.

Lastly I thank the almighty for giving me this great opportunity and for providing a chance to interact with such wonderful people.

ABSTRACT

As the world faces an energy crisis with depleting fossil fuel reserves, alternate energy sources are being researched ever more seriously. In addition to renewable energy sources, energy recycling and energy scavenging technologies are also gaining importance. Technologies are being developed to scavenge energy from ambient sources such as vibration, radio frequency and low grade waste heat, etc. Waste heat is the most common form of wasted energy and is the greatest potential source of energy scavenging.

Pyroelectricity is the property of some materials to change the surface charge distribution with the change in temperature. These materials produce current as temperature varies in them and can be utilized to convert thermal energy to electrical energy. In this work a novel approach to vary temperature in pyroelectric material to convert energy has been investigated.

Microelectromechanical Systems or MEMS is the new technology trend that takes advantage of unique physical properties at micro scale to create mechanical systems with electrical interface using available microelectronic fabrication techniques. MEMS can accomplish functionalities that are otherwise impossible or inefficient with macroscale technologies. The energy harvesting device modeled and developed for this work takes full benefit of MEMS technology to cycle temperature in an embedded pyroelectric material to convert thermal energy from low grade waste heat to electrical energy. Use of MEMS enables improved performance and efficiency and overcomes problems plaguing previous attempts at pyroelectric energy conversion. A Numerical model provides accurate prediction of MEMS performance and sets design criteria, while physics based analytical model simplifies design steps. A SPICE model of the MEMS device incorporates electrical conversion and enables electrical interfacing for current extraction and energy storage. Experimental results provide practical implementation steps towards of the modeled device. Under ideal condition the proposed device promises to generate energy density of 400 W/L.

TABLE OF CONTENTS

LIST OF FIGURES

LIST OF TABLES

LIST OF ATTACHMENTS

1. COMSOL Model (COMSOL File)…………………….......... Selfoscillation.mph
2. Analytical Model of multilayer MEMS (Matlab File)……............................... Multilayer_cantilever.m
3. Analytical Model for temporal response…………… thermomechanical_t.m
4. SPICE Circuit Model (SPICE file)………................... Electrothermal_mems.asc
5. Video of oscillating cantilever (Windows Media Audio/video file) ………....……..6-flat oscillating cantilever.wmv
6. Video of self-oscillating cantilever (Windows Media Audio/video file) ..…………. ……..7-resonating flat cantilever.wmv
7. Video of self-oscillating Si-Au cantilever(Windows Media Audio/video file) ..…………. ATM_Cooling.wmv

Chapter 1

INTRODUCTION

The objective of this chapter is to present motivation and context of the study performed. First it discusses the world energy usage trend and waste energy sources. This is followed by a discussion on common energy scavenging approaches, specifically waste heat energy harvesting based on a review of thermodynamics. Particularly pyroelectric energy conversion and recent advances in MEMS technology is highlighted to provide context to the basis of the study. The chapter concludes with research objectives identified for the scope of this study.

1.1 Motivation

With the growth of earth's population to over seven billion and the advent of technology, demand for energy is skyrocketing. Modern life takes advantage of many technologies that are dependent on supply of energy produced mostly from mineral resources found on earth. To keep pace with the growing demand the energy production has also increased twice in the last twenty-five years [1]. Figure 1.1 shows the trend for energy supply in the world between 1973 and 2008. In 1973 world's total energy production was 6115 Megatons of oil equivalent (Mtoe), which increased to 12,267 Mtoe in 2008. As the demand rises with upcoming superpowers such as China and other Asian countries, the overall energy crisis in the world is worsening leading to increase in energy price.

Although excavation and mining for mineral resources started only a couple centuries ago, the available sources are already depleted, and production is past its peak in the United States. This also contributes to rise in energy price as utilizing mineral sources becomes cumbersome and costly. To keep the economy running, energy hungry developed countries are running after resources in other countries with armed forces thus creating conflicts and unrest. This has led scientists to search for alternate and renewable sources of energy. In the last couple decades nuclear, hydroelectricity, solar and wind energy production efforts have significantly increased to complement the energy production from fossil fuels.

Another inspiration towards renewable energy research is the global warming. Production of electricity from fossil fuel involves inefficient conversion of generated

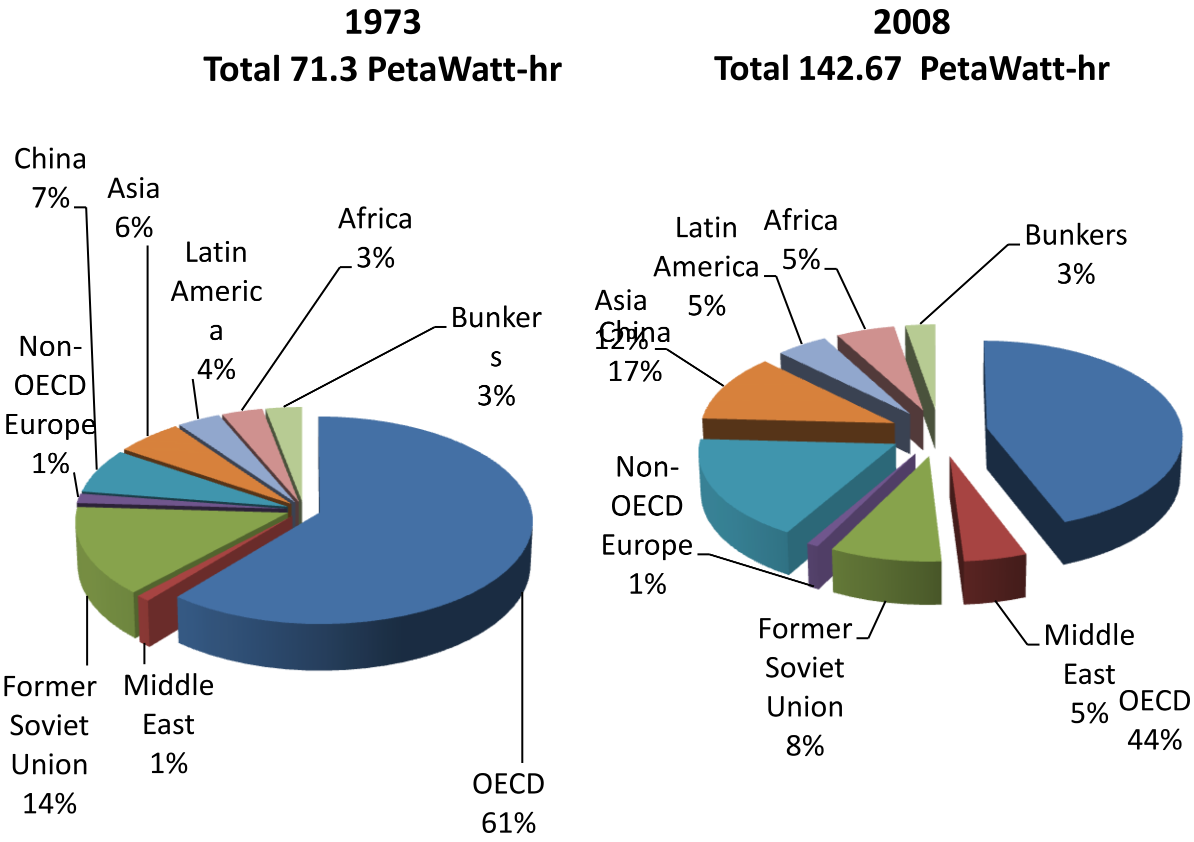

Figure 1.1: Total primary energy supply in different regions of the world in 1973 and 2008 [1].

thermal power, most of which is released to the environment as waste heat. Continuing in this path, researchers are now focusing on reusing waste forms of energy. Therefore, green, clean energy production and related research are of prime importance to sustained growth of human knowledge and technology.

1.2 Energy Flow Trend

The supply of energy to meet the demand to power cars, buildings, industries etc. comes from various sources such as fossil fuels (oil, natural gas and coal), nuclear, hydroelectric, solar, wind, geothermal as well as biofuels. In most cases the produced energy is used for its primary purpose and in the process is converted to a form of energy that is not typically reusable such as thermal or acoustic. **Error! Reference source not found.** gives an overall idea on the trend of energy flow from production to end consumption in the United States in the year 2002. The figure shows that the main source of energy comes from petroleum, coal, natural gas complemented with biomass, hydro, nuclear providing to account for the total energy supply. The main consumption sectors are transportation, industrial, residential and commercial. Majority of the petroleum goes into transportation sectors where only 5.3 quadrillion BTU (here forth termed as quads) of the 26.5 quads consumed, is converted to useful energy to drive the automobiles and the rest is wasted as heat. Electric power sector consumes 38.2 quads of energy in the form of coal, gas and nuclear but generates and distributes only 11.9 quads as electricity, the rest lost as heat in the generation process. Similarly residential and industrial sectors consume energy in different forms but usefully utilize only 29.9 quads and wastes 8.7 quads. Overall of the 97 quads of energy consumed from the primary sources, only 35.2 quads is converted useful energy and 56.2 quads is lost, primarily as waste heat.

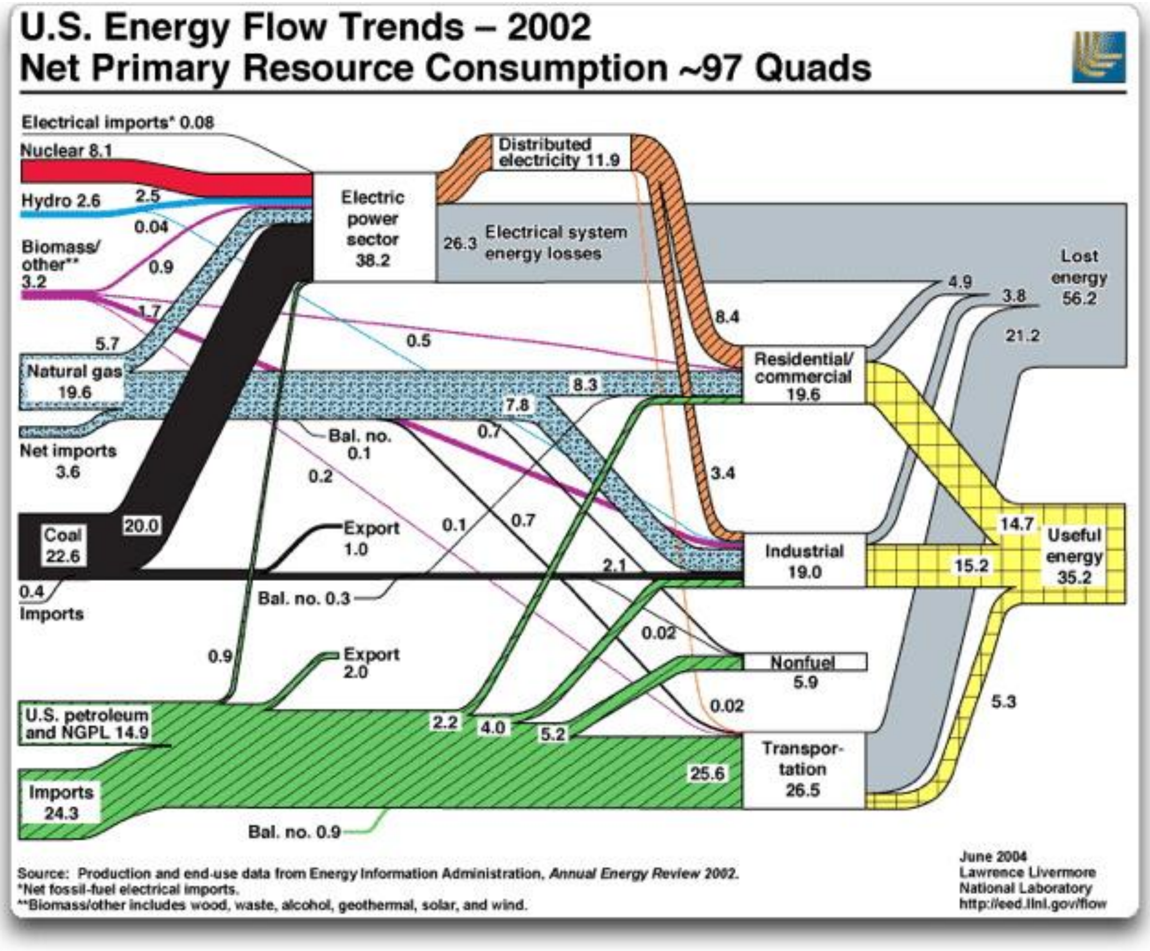

U.S. Energy Flow Trends – 2002
Net Primary Resource Consumption ~97 Quads

Source: Production and end-use data from Energy Information Administration, *Annual Energy Review 2002.*
*Net fossil-fuel electrical imports.
**Biomass/other includes wood, waste, alcohol, geothermal, solar, and wind.

June 2004
Lawrence Livermore National Laboratory
http://eed.llnl.gov/flow

Figure 1.2: Flow chart of the energy produced, used, and wasted in the United States in 2002 (unit in quadrillion BTU), [2].

1.2.1 Energy Production

Fossil fuel has been the most widely used source of energy production for many years. Fossil fuels are layers of hydrocarbons found in different forms (solid, liquid and gaseous) created by millions of years of extreme heat and pressure exposure to fossils of plants and animals. Fossil fuel resources are therefore limited in quantity and cannot be renewed within a short period in human timescale. As resources deplete at a fast rate, alternate energy sources are of prime importance that are renewable even if they are not highly efficient to produce. To complement the fossil fuel generated energy, nuclear, hydroelectric, solar and wind power started drawing attention in the late sixties and has been growing ever since.

In 2008 the world produced 142.67 Petawatt-hour (PWh) of energy compared to 71.3 PWh from 1973. Renewable energy production has grown from 1.35 PWh to 4.14 PWh although fossil fuel always remains the source for over 80% of the produced energy sources. Figure 1.3 shows energy generated in the world in 1973 and 2008 by source of energy [3].

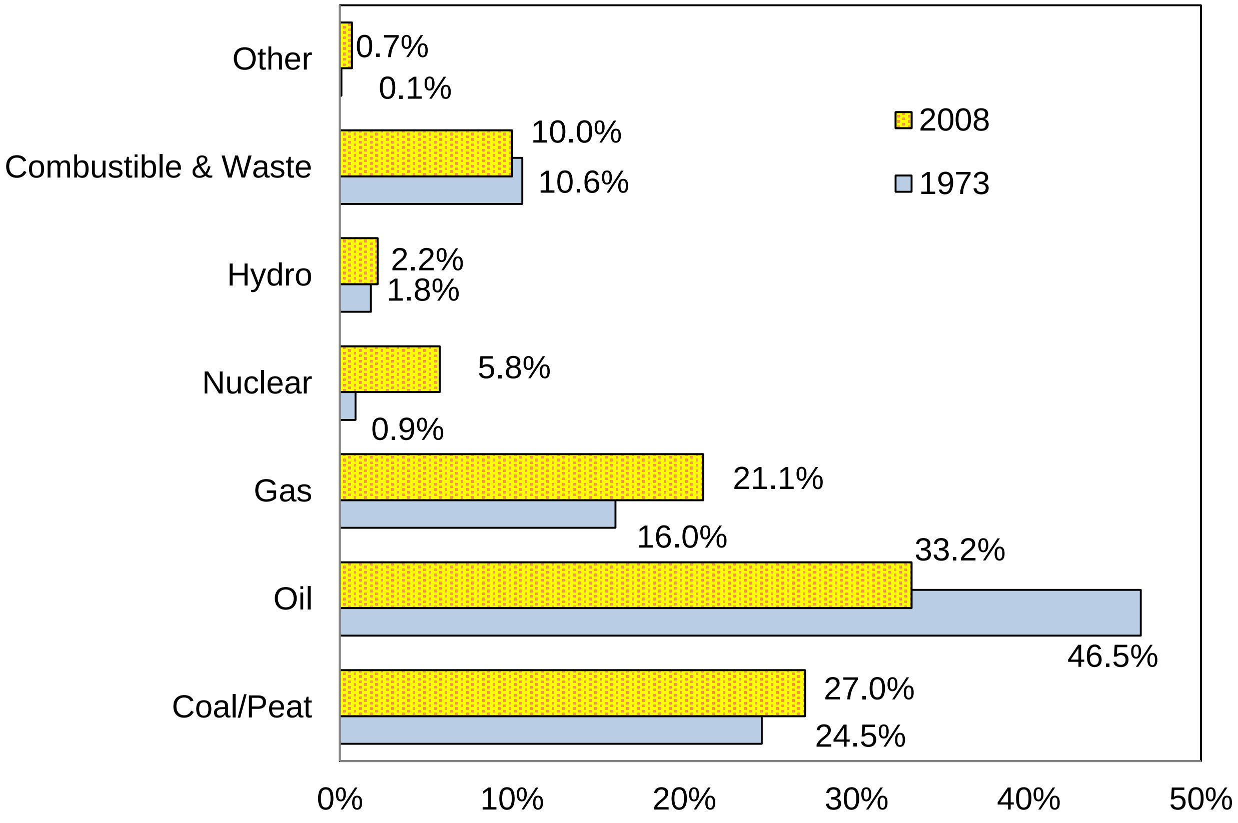

Figure 1.3: Evolution from 1971 to 2008 of world total primary energy supply. *Other includes geothermal, solar, wind, heat, etc [1]

1.2.2 Energy Consumption

In 2008, nearly half of the 142.67 PWh energy produced was consumed by the industrial sector and one-third was consumed by residential and commercial users while the rest was being used for transportation and non-energy related usage (Figure 1.5) [3]. In 2009 United States alone consumed 27.73 PWh of energy produced from different fuel sources used in different sectors. Figure 1.4 shows the energy flow trend from source to end use sectors, which clearly demonstrate a large portion of energy going to transportation and electric power sector [2].

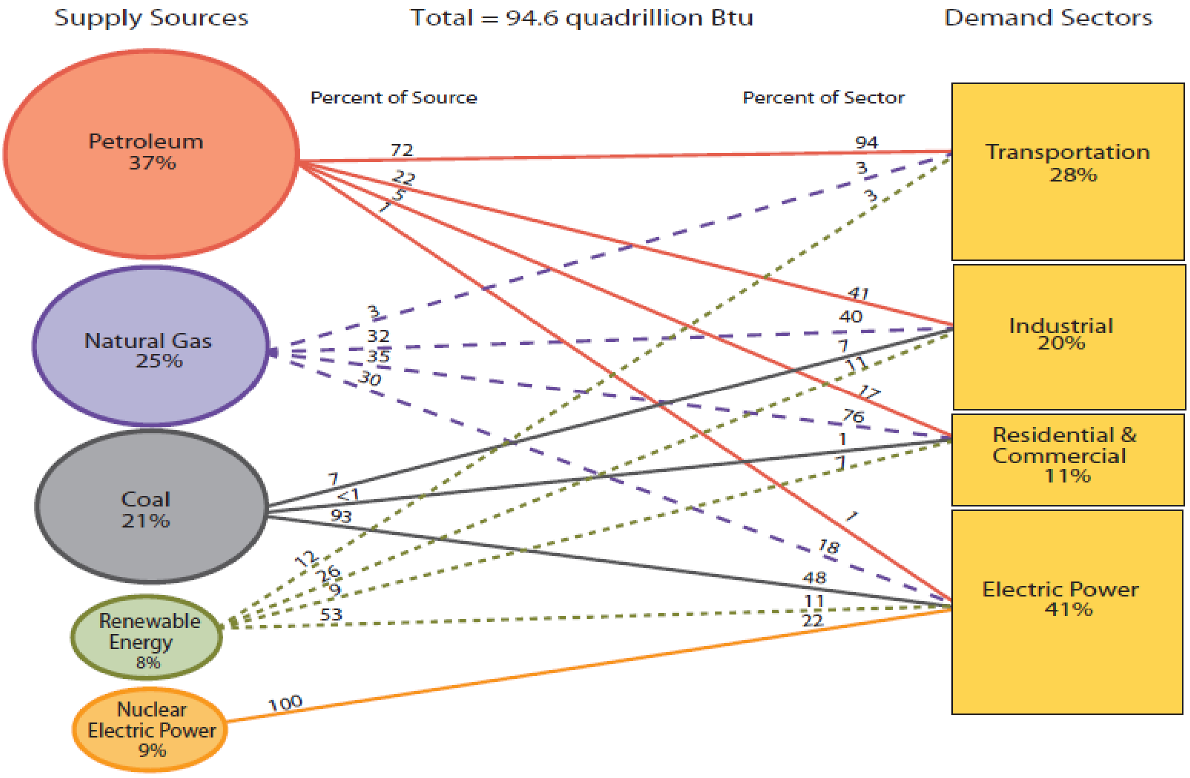

Figure 1.4: Primary Energy Flow by Source and Sector, 2009 in the United States (in Quadrillion BTU) [2].

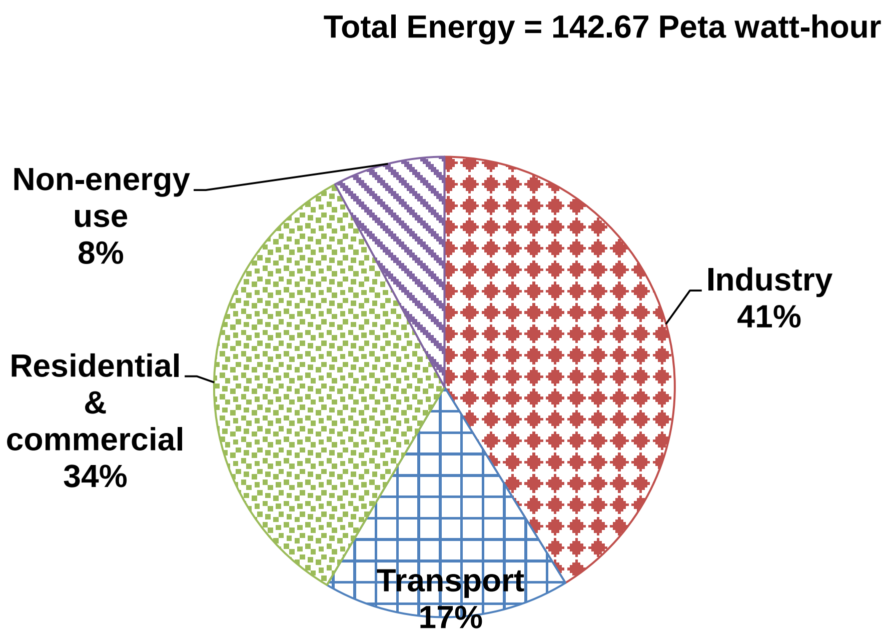

Figure 1.5: Distribution of world's total energy consumption in 2008 by end-use sectors [1].

Since electric power is the largest form of energy consumption, further breakdown of electric power consumption can provide more detailed insight into energy usage pattern. In Figure 1.6 electric power used in residential and commercial buildings is broken down into different consumption purposes [2]. The largest amount of energy consumption is for the purpose of space and water heating. A close second is powering different appliances such as television, computers, kitchen appliances, etc. Lighting for spaces also consumes considerable amount of electric power.

An in-depth analysis of the end-use of produced energy helps to determine energy pricing, as well as fossil fuel pricing. A study of the efficiency of usage also provides insight into the change needed to make the best use of the produced energy. It can also help with an overall idea where fossil fuel generated electricity can be replaced with renewable energy.

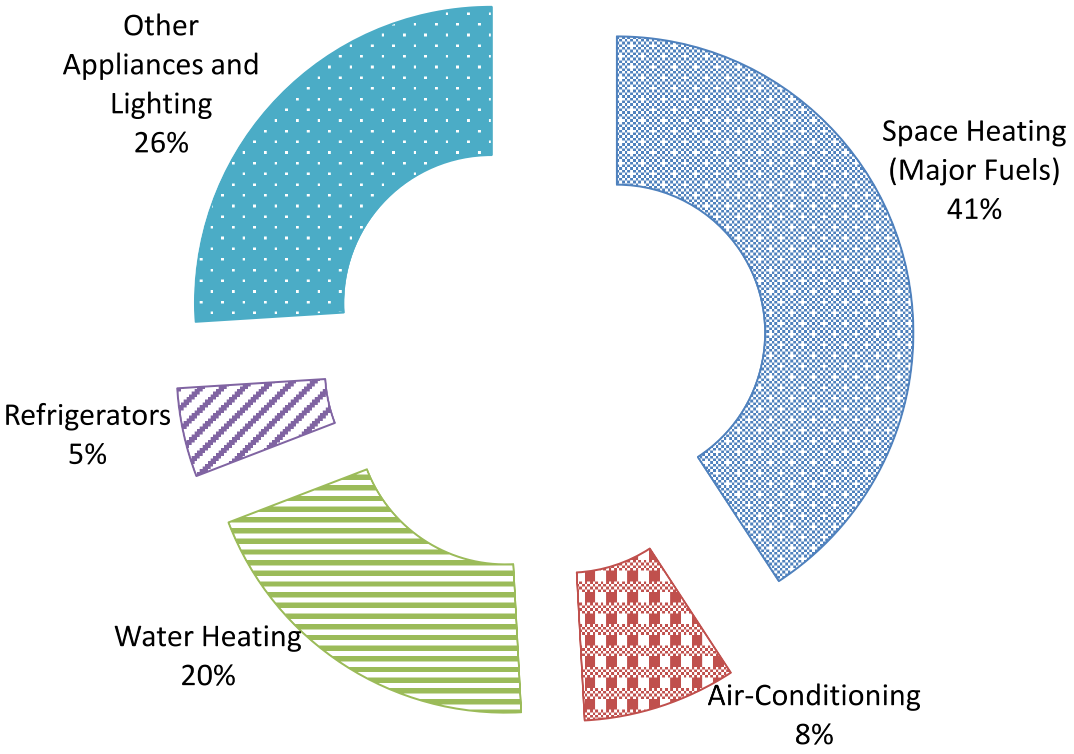

Figure 1.6: Breakdown of electrical energy consumption in residential and commercial sector in the United States, 2005 [2, 4].

1.2.3 Waste Energy

In fossil fuels the energy is contained in chemical form in the chemical bonds between atoms. When fossil fuel is burned to produce thermal energy, a portion of the energy is lost as heat. During thermal to electrical conversion a considerable amount of energy cannot be transformed due to compromised mechanical efficiency of the turbines used and other process limitations.

Other energy production technologies such as nuclear, solar, hydroelectric and wind are also inefficient processes

Table 1-1: Energy conversion process and respective efficiency [5].

Conversion process	**Energy efficiency**
Electricity generation	
Gas turbine	up to 40%
Gas and steam turbine (combined cycle)	up to 60%
Water turbine	up to 90% (practically achieved)
Wind turbine	up to 59% (theoretical limit)
Solar cell	6%-40% (technology dependent, 15% in practice, 85%-90% theoretical)
Fuel cell	up to 85%
World Electricity generation (2008)	Gross output 39%, Net output 33%.
Energy consumption	
Combustion engine	10-50%
Electric motors	30-60%
Household refrigerators	low end systems ~ 20%; high end systems ~ 40-50%
Incandescent light bulb	5-10%
Light-emitting diode	up to 35%
Fluorescent lamps	28%
Electric heaters	around 95%

solar, hydroelectric and wind are also inefficient processes

Table 1-1 lists the efficiency of different energy production processes. In [3] International Energy Agency states that gross efficiency of electricity generation is approximately 39% considering all processes combined. The rest 61% of the energy is lost as waste energy. Since 80% of the energy generation still comes from burning fossil fuels, most of the waste energy is lost as heat.

Energy consumption process is not efficient either. Nearly one third amount of energy produced from petroleum goes to run automotive transports and the automobile engine is one of the most inefficient technologies out there. In industries electrical energy is used to drive huge electric motors which have their efficiency limitations. Household heating, ventilation and air conditioning systems are also limited by thermal efficiency. Lighting fixtures are also efficiency limited depending on different technologies used. solar, hydroelectric and wind are also inefficient processes

Table 1-1 lists the efficiency of different end-use energy consumption and conversion processes. The consumed energy is often converted to thermal energy and released in air as heat after the desired work is done. If this waste heat can be recycled into useful form of energy, it can become a potential source to meet rising energy demand.

1.3 Energy Scavenging

Energy scavenging is producing energy from otherwise wasted form of energy. Often the amount is smaller than that produced by thermal generation. This source of energy generation which is not significant in quantity compared to the effort is considered energy scavenging or energy harvesting. The green energy revolution has recently made energy efficiency a hot research topic and researchers are looking for ways to produce energy using more efficient methods. One of the best ways to meet the gap between the demand and the supply of energy is to reduce energy consumption or to reuse the produced energy. In addition to reducing energy consumption, recycling the used and the wasted energy is another potential source for increasing energy efficiency. In addition to recycling waste energy scientists are also looking into scopes where the energy conversion is typically very small in amount or cumbersome to generate. All of these efforts are recognized under the terminology ‘energy scavenging’.

1.3.1 Sources

Energy is present in this universe in many different forms such as potential, kinetic, chemical, light, sound, gravitational, nuclear, electrical, magnetic, thermal, etc. For mass production chemical energy in the fuel is burned to thermal energy and is converted to mechanical energy to drive a turbine that produces electrical energy. Most common example of energy harvesting is reusing of the flue gas from gas turbines to produce steam otherwise known as combined cycle generation. The finally released flue gas still contains nearly 40% of thermal energy which can be scavenged by an alternate method such as using thermal to electric transducers. Natural vibration of machineries or human movement is another source of low magnitude mechanical energy. Ambient light is a source for scavenging energy in smaller scale compared to solar or photo cells. Radio frequency (RF) signals are abundant in todays interconnected life. RF signals present in ambience can be a potential source of electromagnetic energy. Sound in the environment or loud noise which is a by-product of many processes can also be utilized for energy scavenging. Since large portion of waste energy is in the form of heat, low grade waste heat from power generation plants, industrial facilities, and household heating-cooling units as well as from automotive exhaust can be potential sources of thermal energy. Table 1-2 presents scavenged energy from different sources by different methods.

Table 1-2: Energy scavenging sources, methods and performance [6].

Source	Method	Performance
Vibrational Microgenerators	Piezoelectricity	800 mW/cm^2
Ambient Radio Frequency	Electromagnetic	< 1 mW/cm^2
Ambient Airflow	Microturbines	1 mW/cm^2
Ambient Light	Photovoltaic	100 mW/cm^2
Low Temperature Heat	Thermoelectric	60 mW/cm^2

1.3.2 Technologies

Energy scavenging takes advantage of many physical phenomena to convert waste or miniscule amount of energy into useful quantity. In energy scavenging often different types of transducers are used for energy conversion. Different energy conversion techniques are listed below by type of energy and sources.

Common techniques of energy scavenging:

- Mechanical Energy – from sources such as vibration, mechanical stress and strain. Piezoelectric materials are used as transducers to convert kinetic energy to electrical energy.

- Thermal Energy – waste thermal energy from furnaces, heaters, auto engines, data centers and friction are converted into electrical energy taking advantage of material properties such as thermoelectricity, thermocoupling and pyroelectricity.
- Optical Energy – light captured from sunlight or ambient light indoors from incandescent or other sources are scavenged via photo sensors, photo diodes, or solar panels. Solar or photovoltaic cells are common practice for harvesting energy in large quantity from solar energy. For smaller scale energy harvesting from ambient light or in the absence of direct sun light, photo sensor or photo diodes are more efficient transducers.
- Electromagnetic Energy – from ambient radio frequency signals through inductors, coils and transformers electromagnetic energy is converted to electrical energy.
- Kinetic Energy – from the natural environment such as wind, water flow, ocean using kinetic energy is converted to electrical energy by means of microturbines.
- Human Body – a combination of mechanical and thermal energy naturally generated from bio-organisms or through actions such as walking and sitting. Piezoelectric and pyroelectric effect can be utilized to harvest energy from the prior form to electrical energy.
- Acoustic Energy- electrical signal is generated from sound in a microphone. Similar idea can be utilized to scavenge energy from loud noises or ambient sound at high intensities.

1.4 Laws of Thermodynamics and Waste Heat

Before delving into more details of scavenging waste thermal energy, a review of the two laws of thermodynamics will be useful. This section reviews the thermodynamics laws and discusses thermal and Carnot efficiency to relate probability of energy scavenging.

1.4.1 Laws of Thermodynamics

Let us consider a closed system where Q is the heat input, that takes the system from state 1 to state 2 and in the process W is the amount of work done as displayed in **Error! Reference source not found.**. The sign convention ensures that heat input and work output are both positive values for the system. The first law of thermodynamics states that energy can neither be created nor destroyed [7].That means the energy exiting the system is equal to energy entering the system and the internal change of energy. Mathematically at the output,

$$(E_2 - E_1) - Q + W = 0 \tag{1-1}$$

where, E_2-E_1 is the internal change of energy due to transition from state 1 to state 2.

In the second law of thermodynamics German scientist Rudolf Clausius states that, “No process is possible whose sole result is the transfer of heat from a body of lower temperature to a body of higher temperature.” In other words it is impossible for a thermodynamic system to convert thermal energy into positive work output if energy is received by heat transfer from a single

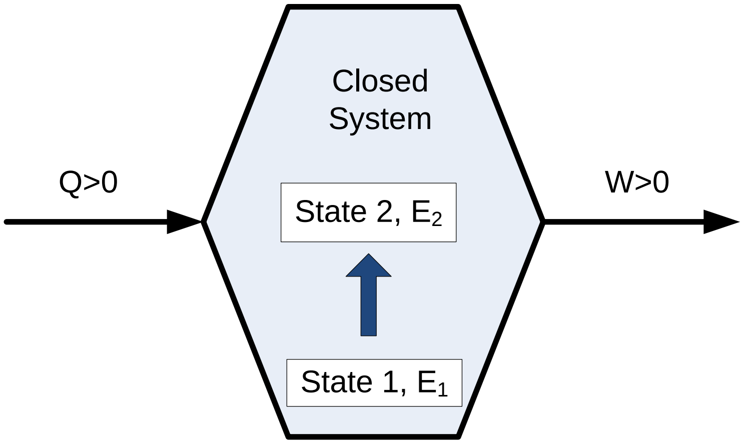

Figure 1.7: Schematic of a closed system with heat input and work output.

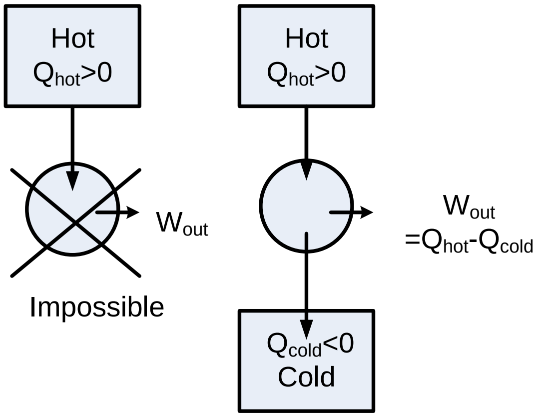

Figure 1.8: Illustration of second law of thermodynamics.

reservoir only [7]. Therefore, there are two thermal reservoirs required to produce positive work output from a system as heat flows from the higher temperature to the lower temperature reservoir. Figure 1.8 illustrates the second law of thermodynamics, where, Q_{hot} is the heat transfer supplied to system and Q_{cold} is the heat transfer absorbed from the system, and W_{out} is the work output from the close system.

Thermal efficiency: In a thermodynamic power cycle, the ratio of the net work output to the total thermal energy supplied to the cycle is termed as thermal efficiency, i.e.

$$\eta = \frac{W_{out}}{Q_{hot}} = \frac{Q_{hot} - Q_{cold}}{Q_{hot}} = 1 - \frac{Q_{cold}}{Q_{hot}} \tag{1-2}$$

Carnot Efficiency: For a reversible power cycle, $Q_{cold}/Q_{hot} = T_{cold}/T_{hot}$, where T_{cold} and T_{hot} are the temperature of the hot and cold sources, respectively in Kelvin scale. The maximum thermal efficiency that a power cycle can achieve is called the Carnot efficiency and it is defined as [7],

$$\eta_{Carnot} = 1 - \frac{T_{cold}}{T_{hot}} \quad (1\text{-}3)$$

Practically, a thermodynamically reversible heat engine is not impossible, but the maximum possible efficiency of a device can be estimated from this equation. It is to be noted that the heat transferred to the cold reservoir Q_{cold} is lost and is wasted and is the so-called waste heat.

1.4.2 Waste Heat Sources

Waste heat is the thermal energy released into the environment as a by-product of power generation, refrigeration, heat pump cycles and cooling following the second law of thermodynamics. Usually the thermal energy is released as hot gases into the atmosphere or hot water in large water resources.

From the discussion in the previous section on Carnot efficiency, it is evident that to scavenge a significant amount of energy, the heat source must maintain a large temperature difference with the heat sink. The heat source needs to be at higher temperature than the ambient if no cooling method for the sink is involved. Such high temperature heat sources can be flue gases from steam or gas turbine power plants. Industrial machineries and processes involve high temperature operation where the heat is released as by-product. Industry world-wide discharges over 100 Terajoules annually of low-grade waste heat (25°C to 250°C) from electric power stations, pulp and paper mills, steel works and petro- chemical plants[8] which represent a large source of waste heat. Household cooling units usually have an outdoor unit that releases heat from indoors to outdoors for air-conditioning. This could be a potential heat source. Car exhaust passes burnt fuel as CO_2 at very high temperature. Also automotive engines running at very high temperature need to be air/water cooled for their operation. The thermal energy lost is nearly 60% of that produced by burning the fuel which is a highly rich source of waste heat. Modern electronic equipment, especially computer's central processing units and microchips therein in particular, dissipate electricity in the form of heat. Servers and data centers are highly concentrated facilities housing computers and processing units running at full load. The total electrical energy consumed here is dissipated as heat and nearly 30% energy in a data center goes toward cooling the facility to maintain the operating temperature. This is a potential source for low grade waste heat energy scavenging. Solar panels harvest energy from sunlight at typically 15% efficiency, but the rest of the light energy is converted to heat which heats up the panels. The heated solar panel can be plausible source for harvesting low grade thermal energy [9].

1.5 Harvesting Waste Heat

A technology to recover or convert this low-grade waste heat to usable, high voltage electricity could save industrial sectors tens of millions of dollars annually, through increased process efficiencies and reduced fuel costs, while substantially reducing greenhouse gas emissions. In an attempt to scavenge energy from any possible source, many techniques have been investigated even though these technologies demonstrate very low conversion efficiency. The most common form of waste heat harvesting is using combined cycle gas and steam turbine[10]. In this process flue gas after driving primary turbine is used to heat water and produce steam which is used to turn a secondary turbine. On a smaller scale thermoelectric or pyroelectric method are used for low grade waste heat to electrical energy conversion. In thermoelectric method Seebek effect or Peltier effect are used to generate voltage. In Seebeck effect two wires of different metals joined at one end develops a potential difference at the opposite ends if there is a temperature difference between two ends of the wires. The efficiency of commercial thermoelectric generator is "typically around

5%”[11]. On the other hand pyroelectric effect takes advantage of changing temperature. Number of dipoles created by spontaneous polarization in a pyroelectric material is highly temperature dependent. As temperature changes in a pyroelectric material it creates or reduces number of dipole in it to attract opposite charge from the surroundings to its surface. When a closed circuit is formed connecting these surfaces, current flows as temperature fluctuates. Direction of current flow depends on the increase or decrease of temperature. Pyroelectric conversion is dynamic while thermoelectric conversion is more steady-state. In addition to electrical conversion, waste heat can also be converted to mechanical energy by using a Stirling engine.

1.6 Pyroelectric Effect & Converters

Pyroelectric energy converters take advantage of the pyroelectric effect to directly convert thermal energy to electrical energy [12-20]. Here time dependent temperature is transformed into alternating current. It makes use of the pyroelectric effect to create a flow of charge to and from the surface of the material through a closed circuit as a result of heating and cooling. In response to temporal changes in temperature, dipoles are created or diminished which attract positive and negative charges to the surface, establishing an electrical potential across the material. Very small change in temperature (~mK) produces considerable amount of pyroelectric current on the order of pA or nA [21]. This property has been widely used in thermal sensors successfully [22]. Prototypical pyroelectric converters have been assembled and operated in the past [13, 16, 18]. Although early research reported very low efficiencies [9, 23, 24], recent experimental studies have yielded better results.

1.7 MEMS Technology

MEMS stands for microelectromechanical systems where different physical properties of material at micro scale is utilized to electrically control the mechanical response of a microsystem and vice versa. Electro-thermal, electrostatics, piezoelectric, piezoresistivity are some of the physical phenomenon adopted by MEMS technology. They often function as transducers for conversion of energy from one form to another. For example, application of force on piezoelectric MEMS would yield electrical current signal. Conversely by applying electric field on a piezoelectric MEMS world's smallest motor has been fabricated [25]. Application of heat to a bimaterial structure can produce mechanical movement due to differential rate of thermal expansion.

Since in energy scavenging the energy harvested is very small in quantity it is quite inefficient to use regular size machines and systems for the purpose. To harvest small amount of energy, small transducers like MEMS can be more beneficial.

1.8 Research Objective and Scope of the Present Study

1.8.1 Scope of This Study

To address the demand for remote and mobile electronics devices, this research effort looks at harvesting energy from low grade waste heat source utilizing pyroelectric properties of certain materials. An efficient energy conversion scheme using MEMS technology is proposed, and by developing a finite element and an analytical model of the system, its behavior and performance is estimated for energy harvesting. The modeling is also used to find optimized design parameters for the maximum power extraction and the highest conversion efficiency. The energy generation capacity of the pyroelectric material is also studied and characterized before integrating the two components to form a thermally actuated self-governing device that harvests energy from a heat source.

The original contribution of this work towards the progress of science is to introduce a novel technique to achieve higher frequency of temperature cycling without external energy excitation. A finite element and an analytical model have been developed with identified ideal condition for a MEMS structure to thermally actuate and maintain self-oscillation. The properties and the variables involved in governing the frequency and the magnitude of oscillation and response of the MEMS structure to design parameters, thermal, mechanical condition and properties of the constituting materials are also studied.

1.8.2 Objective

To realize a microelectromechanical system with desired response, many obstacles were overcome in steps that involved studies identifying the problem at hand and researching for solutions. The challenges involved in design and development of the MEMS device are listed below chronologically as research progressed.

I. Study of the properties of materials to characterize the thermomechanical responsivity of the MEMS structure and find optimized dimension for desired range of responsivity. Develop finite element model and formulate generalized analytical model to estimate the device response under given conditions.

II. Find environmental conditions required for thermal actuation of the MEMS device and continued self-oscillation without any excitation external to the system or the source. Using finite element modeling and analytical modeling to estimate the period of oscillation of the MEMS structure and the magnitude of temperature cycling that occurs in the structure.

III. Characterize pyroelectric capacitors and their power generation capacity corresponding to temperature cycle frequency. Study thermomechanical properties of pyroelectric materials for integrating the thin-film pyroelectric capacitors with the MEMS device. Develop model to approximate the magnitude and the profile of the power generation from the combined structure.

IV. Design a low power current rectifier and energy storage circuit for storing the harvested energy from the MEMS structure for powering subsequent low power mobile or wireless electronics.

With an intention to find an innovative and more efficient way to extract pyroelectric energy a design of a self-governed temperature cycling system taking advantage of recent developments in microelectromechanical system is conceived and design properties and conditions are studied to realize a functional system with optimized performance for maximum energy conversion efficiency.

Chapter 2

CURRENT STATE OF KNOWLEDGE

In this chapter some basic physics concepts have been discussed that are utilized in this study of pyroelectric energy harvesting. First, properties of material of different crystal structures and their behavior under certain condition are focused to provide insight into the type of material used in the study. Second, a brief summary of previous attempts at assembling pyroelectric energy converters and their shortcomings are reviewed. Third, based on the shortcomings of previous efforts a MEMS approach is considered and a brief discussion on cantilever-based MEMS device and their performance is included. The chapter concludes by discussing the goals for pyroelectric energy conversion and the performance of the MEMS devices.

2.1 Material Considerations

In nature some material can be found that can produce electric charges under certain type of excitation due to their unique crystal structures. This type of material can potentially be used as transducers to convert the excitation energy into electrical energy. In this section the crystal structure of these kinds of materials and the resulting effect and dependency to excitation is discussed.

2.1.1 Material Classification

In nature, materials come in thirty-two basic lattice crystal structures. Twenty-one of all crystal structures are non-centrosymmetric and twenty of these are piezoelectric materials that demonstrate electrical polarization under external applied field. Among the twenty piezoelectric crystal structures, ten also demonstrate pyroelectric property, i.e. they have polarization that is dependent upon temperature change. These crystal structures contain a unique polar axis and possess a polarization called spontaneous polarization in the absence of an applied electric field, P_S and are called pyroelectric materials. Pyroelectric materials can be either ferroelectric or non-ferroelectric. Ferroelectric materials have two or more orientation states which can be switched from one state to another by an electric field. Ferroelectric materials show a spontaneous polarization due to non-equilibrium position of positive and negative charge centers in the non-centrosymmetric crystal structure. Ferroelectric and non-ferroelectric materials have identical crystal structures, but have opposite spontaneous polarization $+P_S$ and $-P_S$ [21]. There is also a group of dielectric materials that can be polarized by an applied electric field but have no spontaneous polarization. Such materials are called paraelectric. Under certain condition all pyroelectric material can behave like a paraelectric material. Figure 2.1 shows the breakdown of the crystal structure and associated group of materials[26].

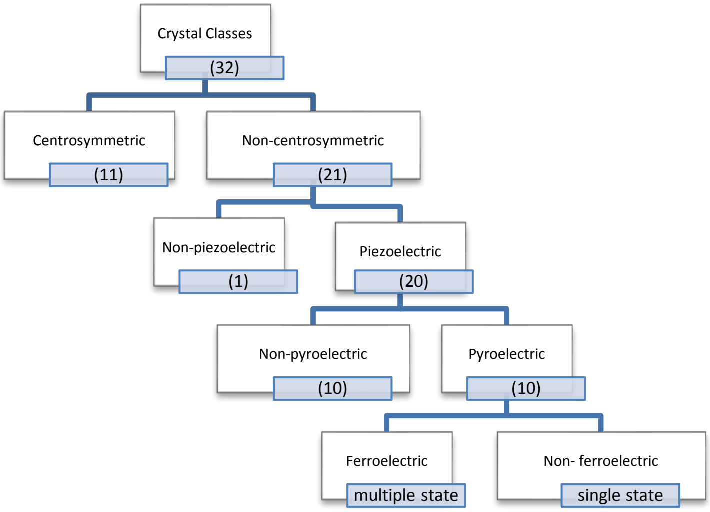

Figure 2.1: Classification of crystal symmetry relating piezoelectric, pyroelectric and ferroelectric materials.

Note that all pyroelectric materials are also piezoelectric material but not all piezoelectric materials are pyroelectric.

2.1.2 Dielectric Properties

Electrically, materials are of three types: metal, semiconductor and insulator. Insulators show strong dielectric property than the others which is critical in the energy conversion through transducer materials. Insulators or dielectric materials in general have breakdown voltages. The dielectric material sandwiched between metal electrodes forms a capacitor. Electric field, *E* is experienced by the material that creates dipole due to electrical displacement and charge is accumulated on the surface *A* across the thickness, *t* when voltage *V* is applied as shown in Figure 2.2.

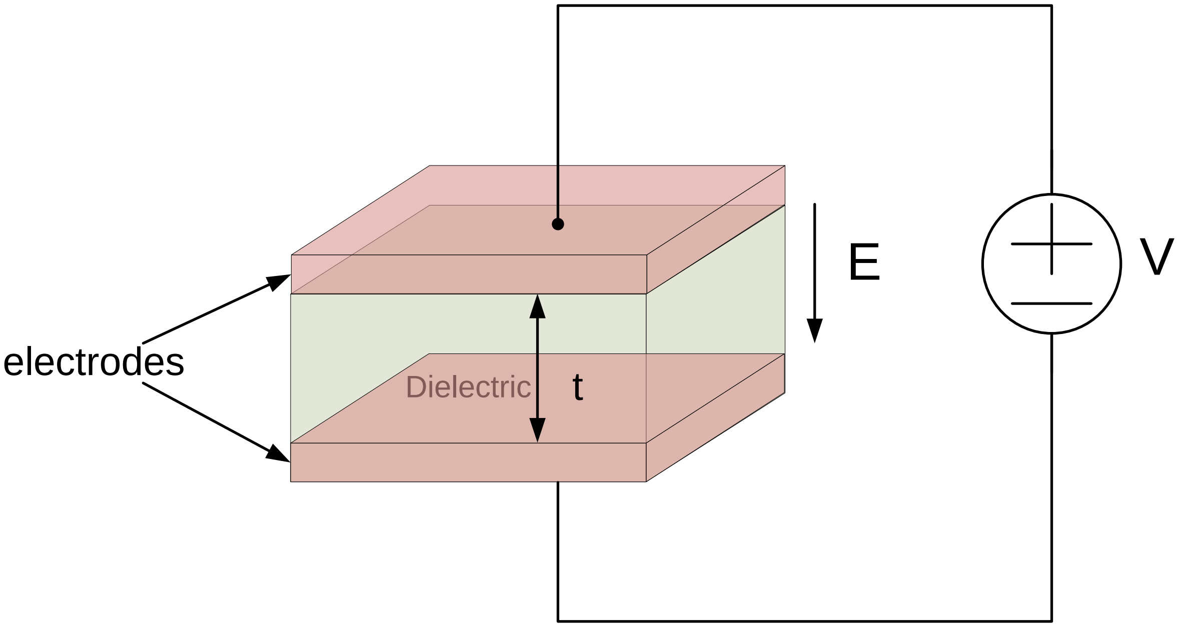

Figure 2.2: Applied voltage *V* creates electric field across capacitor thickness, *t* with surface area *A*.

The total electric displacement, D can be found by the following equation (in C/m^2),

$$D = \varepsilon_r \varepsilon_0 E + P_s \tag{2-1}$$

where, $$E = \frac{V}{t} \tag{2-2}$$

and ε_r is the dielectric constant of the material and ε_0 is the vacuum permittivity (in C/Vm) and P_S is the spontaneous polarization density of the material. Spontaneous polarization is dipoles created in materials due to external conditions other than the applied voltage. The electric displacement, electric field and polarization vectors are assumed be normal to the surface of the dielectric film. The charge is accumulated on the surface, and the dipoles internal to the material are nullified by each other except on the surface. The spontaneous polarization can thereby be expressed as,

$$P_s = \frac{M}{At} = \frac{q}{A} \tag{2-3}$$

where, M is the induced dipole moment [21].

These spontaneous dipole moments can be observed in ferroelectric materials. In addition more dipole moments can be created by piezoelectric or pyroelectric effect under pressure or heat respectively. The following sections go into more details of these effects.

2.1.3 Piezoelectric Effect

Dielectric materials that generate electric potential in response to pressure or mechanical stress and vice versa are called piezoelectric materials [27]. In the presence of pressure or stress, the positive and negative charge centers in the crystal are misaligned and lose equilibrium condition resulting in internal polarization. The dipoles internal to the bulk material are neutralized by the adjacent dipoles except on the surface. This generates an overall electric potential across the thickness of the

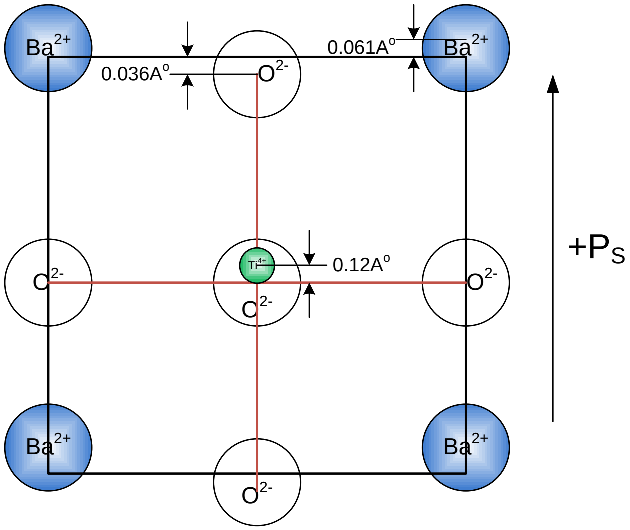

Figure 2.3: Electric polarization in piezoelectric material BaTiO3 crystal structure due to mechanical stress.

material when measured by electrodes connected to both surfaces. Conversely applying an electric field normal to the material surface displaces the charge centers along with the atoms and cause material deformation. The direction of the deformation depends on the crystal orientation and the associated electric field application. Figure 2.3 shows the crystal structure of a BaTiO3 crystal which is a piezoelectric material experiencing electric dipole moment due to deformation as the atoms are displaced from their equilibrium lattice position by application of mechanical stress.

2.1.4 Pyroelectric Effect

Pyroelectric effect is transition of energy from thermal to electrical and mechanical forms. Most pyroelectric materials experience a spontaneous polarization in the absence of an applied electric field. It is assumed that the dipoles created due to the spontaneous polarization are normal to the surface of the pyroelectric film. Within the material the dipoles cancel each other out by the adjacent dipoles of opposite polarity except on the surface where one end of the dipoles are not neutralized and attracts opposite charges from the surroundings (Figure 2.4a). The polarization is strongly temperature dependent due to pyroelectric material's crystal structure. When heated or cooled, the atoms in the lattice gain kinetic energy from the thermal energy causing displacement of equilibrium dipoles. The movement of atoms create imbalance in the previously neutralized dipoles in the bulk material and changes the number of non-neutralized dipole ends on the surface. This results in attraction or release of charges on the surface. Electric displacement is proportional to temperature change according to equation (2-4).

$$dD = \rho dT \tag{2-4}$$

where, ρ is the pyroelectric coefficient in C/m^2K defined by,

$$\rho = \left(\frac{\partial D}{\partial T}\right)_{E,\sigma} = \frac{\partial P_S}{\partial T} \tag{2-5}$$

where, σ is the elastic stress due to inherent piezoelectric properties.

When the two surfaces of a pyroelectric film are connected to form a closed circuit as in Figure 2.4 the charge on the surface flows through the circuit when the material is heated or cooled. The generated current, I_P can be calculated from equation (2-6) as[16],

$$I_P = A\rho \frac{\partial T}{\partial t} \tag{2-6}$$

The direction of the current flow depends on the slope of the temperature change, i.e. whether the material is being heated or cooled. Note that equation (2-6) is valid only for small changes in temperature, while large changes result in non-linear behavior [28].

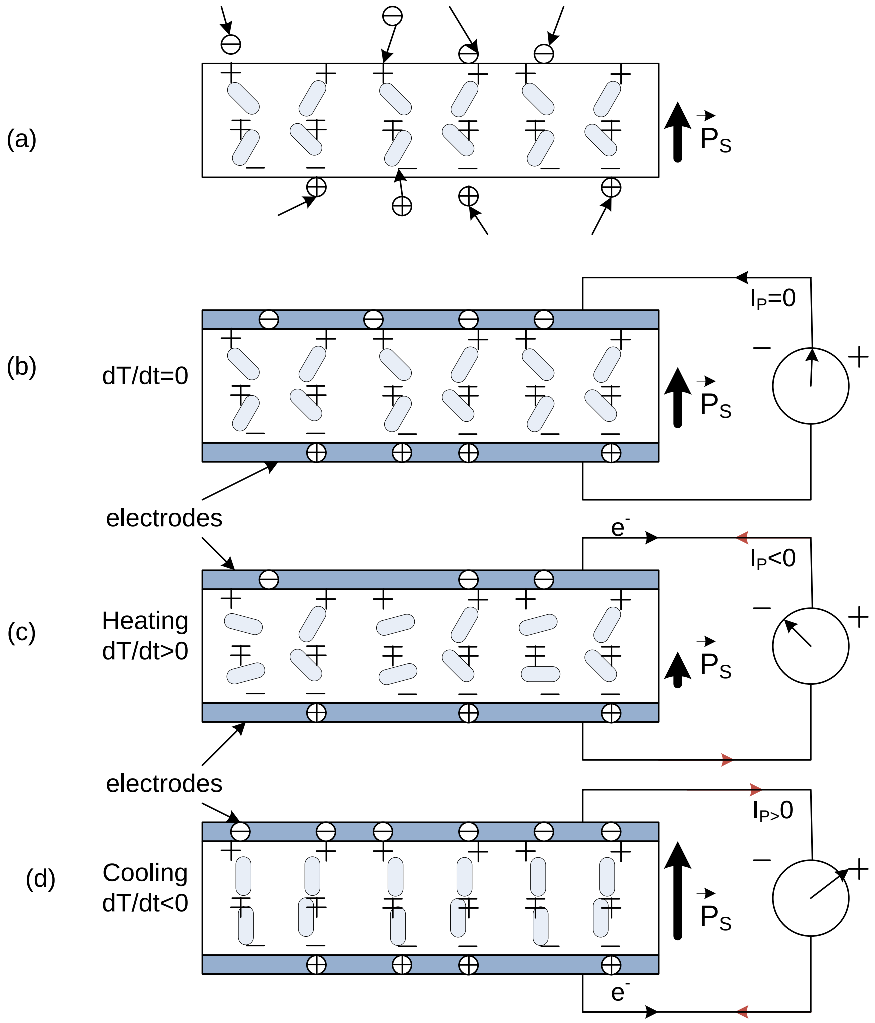

Figure 2.4: Schematic of pyroelectric film (a) Spontaneous polarization (b) at constant temperature (c) while being heated and (d) while being cooled.

Figure 2.4 illustrates different states of a pyroelectric material. Due to the spontaneous polarization of the materials, free charges accumulate on the surface. At steady-state temperature (*dT/dt=0*), the spontaneous polarization remains constant and no current flows. If a pyroelectric crystal with an intrinsic dipole moment is connected to a circuit with electrodes on each surface, an increase in temperature *T* (*dT/dt>0*) prompts the spontaneous polarization *Ps* to decrease as the dipole moments on the surface, on average diminish in magnitude as they tilt horizontally. The surface charges redistribute to cause a current flow to compensate for the change in bound charge that accumulates on the crystal edges. Alternately, when the material is cooled, the spontaneous polarization increases, and charge is supplied from one surface to the other to redistribute and neutralize the dipole moments on the surface. In this case the current flows in a direction opposite to that when material was being heated.

In addition to direct pyroelectric effect, when heated, the material experiences thermal expansion and therefore mechanical stress. Since all pyroelectric materials are subset of piezoelectric materials, piezoelectric effect induces further polarization. This is in addition to the thermally induced change in spontaneous polarization and is termed as the indirect effect. Typically the indirect effect is less than 10% of the total polarization and can be omitted.

2.1.5 Ferroelectric Effect

Ferroelectric property of a material enables it to have a spontaneous polarization, that can be reversed by applying an electric field [27]. But the relation between applied electric field and corresponding polarization or electrical displacement is not linear and displays hysteresis. Figure 2.5 provides a graph for electrical displacement versus applied electric field and shows the hysteresis behavior. It indicates that the lower half of the hysteresis loop occurs when the electric field, E in increasing and the upper half occurs when E is decreasing. The electric displacement at zero applied electric field is the spontaneous polarization, P_S. The electric field required to achieve zero polarization is called the critical field and is denoted by E_C [29].

The electrical displacement also has a saturation level, D_{Sat}, i.e. the electrical displacement value will not increase beyond this number when the electric field is increasing. The highest possible electric field that a material can withstand before breakdown is called the breakdown electric field, and is denoted by E_b. At applied E_b, material loses its insulating property and begins to conduct. When electric filed is applied to ferroelectric material and is cycled isothermally, the electrical input provided to the system is dissipated by Joule heating. The energy dissipated per unit volume, ∀ of ferroelectric material is equal to the area enclosed by the *D-E* diagram of the hysteresis loop.

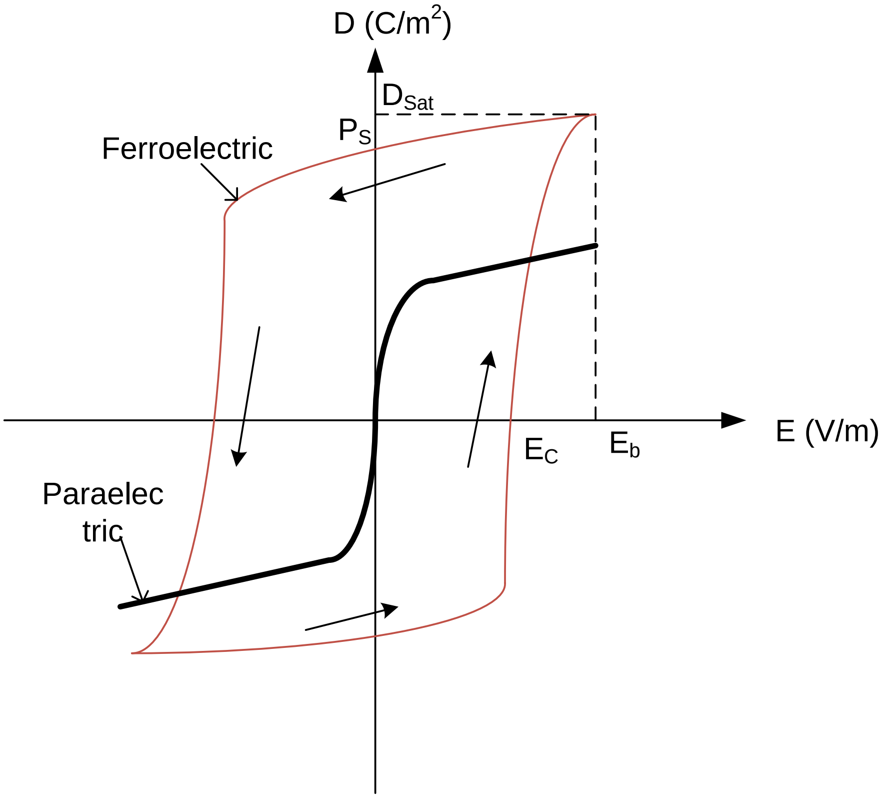

Figure 2.5: Typical electric displacement D versus applied electric field E for ferroelectric and paraelectric materials.

$$\frac{W}{\forall} = \oint dDE \tag{2-7}$$

Ferroelectric and pyroelectric materials both have spontaneous polarization. The difference between the two is that in ferroelectric material the spontaneous polarization can be reversed by an applied electric field which is not achievable in a pyroelectric material. Only temperature change above the Curie temperature can remove spontaneous polarization in a pyroelectric material [30].

2.1.6 Paraelectric Effect

Paraelectricity is the ability of materials to become polarized under applied electric field in the absence of any spontaneous polarization [31]. The paraelectric phenomenon occurs due to distortion in the individual ions due to applied electric field and polarization of the molecules. Paraelectricity is observed in materials that have dipole moments that are not aligned and can be potentially aligned by application of electric field. The domains in the material are also disordered and the internal electric field is weak and therefore no spontaneous polarization is present as evident from Figure 2.5. However an electrical displacement occurs when electric field is applied. In reality paraelectric materials have a very small spontaneous polarization and demonstrate hysteresis loop. The paraelectric *D-E* curve is non-linear as the electric permittivity ε is also dependent on E.

2.1.7 Phase Transition

Under certain condition a material can transition from ferroelectric to paraelectric. Figure 2.6 displays the *D-E* diagram of a dielectric material that transitions from ferroelectric to paraelectric as temperature increases from T_1 to T_2 to T_3. The material displays ferroelectricity at T_1 with positive and negative spontaneous polarization $+P_S$ and $-P_S$. As the material is heated to temperature $T_2>T_1$, the spontaneous polarization diminishes as the area enclosed by the *D-E* diagram also decreases indicating decrease in polarization. When the material is heated to $T_3>T_2$, the spontaneous polarization vanishes and the material behaves like a paraelectric material [27, 32]. The temperature at which the material transitions from ferroelectric to paraelectric is called the Curie temperature

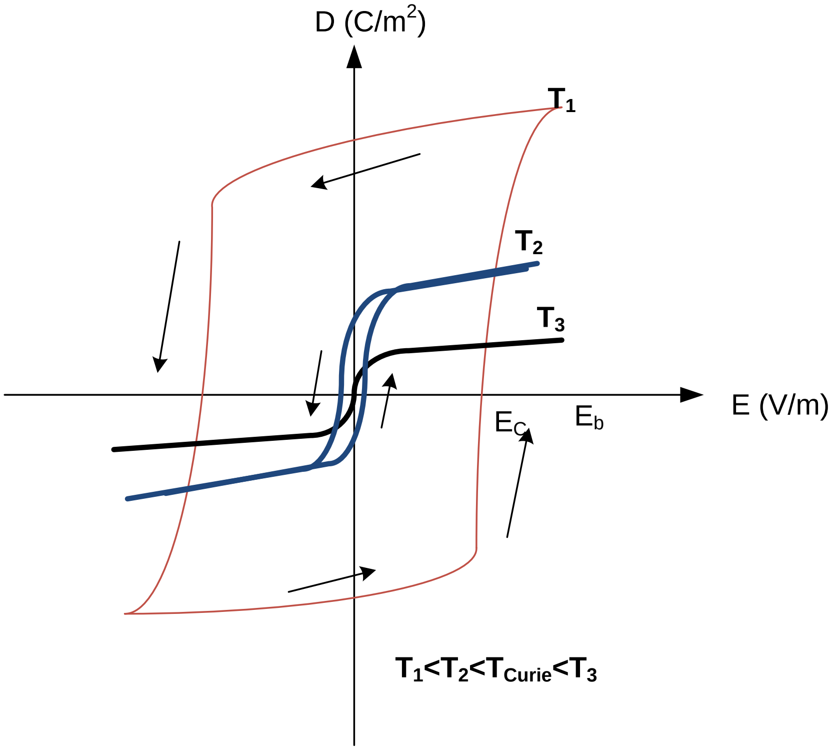

Figure 2.6: Electric displacement, *D* versus electric field, *E* for a dielectric material that transitions from ferroelectric to paraelectric at temperature above and below the Curie temperature, $T_{curie,\uparrow}$ ($T_1<T_2<T_{Curie,\uparrow}<T_3$).

and denoted by $T_{Curie,\uparrow}$ or phase transition temperature. As the material temperature rises to $T_{Curie,\uparrow}$ hysteresis becomes narrower until it turns into a line through the origin. The slope of the *D-E* curve also decreases as temperature increases.

Pyroelectric material experience another phase transition from para- to ferroelectric when the material is cooled from temperature T_3 to T_2 at a temperature different than $T_{Curie,\uparrow}$.This temperature is denoted by $T_{Curie,\downarrow}$ and can be lower than $T_{Curie,\uparrow}$ by as much as 50°C [27]. The difference between these two phase transition temperatures is called phase transition difference and is written as ΔT_{Curie}. Pyroelectric energy converters make use of these phase transitions to generate current.

2.2 Pyroelectric Materials

The existence of pyroelectricity has been known since Theophrastus wrote about the ability of a mineral called tourmaline to attract straw and such other small particles when heated[33]. In 1824 David Brewster, an optical physicist, named the effect pyroelectric. Modern interest in pyroelectricity was fueled by classified research during World War II [21]. Lately pyroelectric property is vastly studied for their use as heat sensors as well as small scale energy harvesting purposes.

2.2.1 Pyroelectric Performance

The performance of pyroelectric material depends on the application. In general the following properties are of interest when assessing performance of pyroelectric material.

1. A large pyroelectric coefficient, ρ is desired so the generated current according to equation (2-6) is higher.

2. Larger the saturation electric displacement, D_{Sat}, of a pyroelectric material, more the charges it can store on its surface. Therefore higher the current from the pyroelectric material is.

3. A large breakdown voltage, E_b is desired so that a large electric field can be applied before the material breaks down.

4. Some application such as energy converters takes advantage of the phase transition difference, ΔT_{Curie}. In such application a small ΔT_{Curie} is desired.

5. In other applications, time required to discharge the surface charges is critical and preferably short. As a result, short discharge period t_D is desirable.

6. Ideally, the dielectric material should act like an insulator and should not conduct. But in practice, the material does not possess infinite resistance but a large resistance allowing a small leakage current to conduct. For best pyroelectric performance the leakage current should be as low as possible.

2.2.2 Pyroelectric Materials in Nature

First known pyroelectric material found in nature is tourmaline. There are also many other ceramics found in nature that display pyroelectric property. For example:

1. Ceramics such as lead zirconate titanate (PZT), barium titanate (BATiO3) and lithium titanate (LITiO3). Aluminum nitride (AlN) and zinc oxide (ZnO) also demonstrate some pyroelectric behavior.

2. Some polymers such as polyvinylidene fluoride (PVDF), polyvinylidene fluoride trifluroethylene (P(VDF-TrFE)), and polyvinylidene fluoride trifluroethylene chlorofluroethylene (P(VDF-TrFE-CFE)) and
3. Biological materials such as collagen, femur bones and bovine phalanx.

Some materials have higher pyroelectric coefficient than other and are more useful for certain application. But the choice of material is often a trade-off between expense and performance. Polymer materials are cheaper and often the choice of the researchers. Research has been ongoing to improve the pyroelectric performance of polymeric materials.

2.2.3 Polymeric Pyroelectric Materials

Although ceramic pyroelectric materials demonstrate better performances, polymeric pyroelectric materials are more popular because they are inexpensive and easy to manufacture. They also have sufficient pyroelectric coefficient for most applications and a high electric breakdown voltage as well which is much desirable.

PVDF and it co-polymers and terpolymer (P(VDF_TrFE-CFE)) are the commonly used polyemeric pyroelectric materials. This is a carbon backboned polymer with the repeat unit (-CH2-CF2-). It has several different conformation or phases with varying properties. Not all of these phases are polar. The trans-gauche configuration or the α-phase has molecules stacked up so it produces a non-polar unit cell. The all-trans configuration is obtained from the α-phase by mechanical stress and or electric field application and it is a polar form. In the β-phase the PVDF polymers display pyroelectric like spontaneous polarization but it is not a stabilized form whereas the α-phase is stabilized [34].

Polyemeric pyroelectric materials' pyroelectric coefficient (27×10^{-6} C/Km^2) is not very impressive compared to PZT. But it is easier and inexpensive to manufacture. Especially, large thin films can be easily made from polymers that have better pyroelectric properties due to stretching and applied mechanical stress. This form is important, as it can generate a large charge which can be easily detected. This advantage overshadows all other shortcomings of polymeric pyroelectric.

The large area thin films are widely used for cheap infrared detection and security equipment. Especially such films are used in laboratories to measure energy of laser beams where large area needs to be covered with pyroelectric sensing materials, polymeric PVDF is a convenient and inexpensive solution.

2.3 Pyroelectric Energy Conversion

Pyroelectric materials have been widely studied and used for a variety of applications such as infrared detection, infrared and thermal imaging etc. A relatively uncharted territory is pyroelectric energy harvesting, possibly due to the poor conversion efficiency achieved from early attempts in comparison to other energy conversion methods. Initial research attempts investigated the process of energy harvesting using pyroelectric material, but not explored innovative ways to increase efficiency of energy conversion from this type of transducers [15, 35]. In recent years some researchers have struggled to improve energy conversion efficiency by improving the physical properties of the materials and/or by using more energy efficient techniques to create a temperature variation in the material whose energy conversion behavior is highly dependent on the time derivative of temperature[17, 36-42]. This section discusses some of the methods and attempts at pyroelectric energy conversion.

2.3.1 Pyroelectric Energy Conversion Based On Clingman Cycle

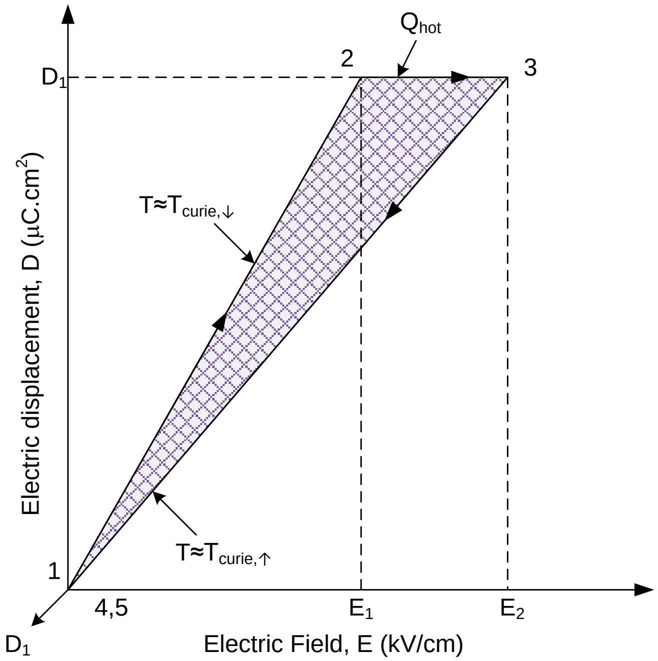

Figure 2.7: Pyroelectric energy conversion cycle used by Clingman and Moore.

In the early 60's Clingman and others attempted pyroelectric energy conversion via what is known as the Clingman cycle [9, 23, 24]. The cycle is illustrated in Figure 2.7 and is performed as follows,

1. Initially the pyroelectric sample is at a temperature $T \approx T_{Curie,\downarrow}$ and the electric displacement and applied electric field both are equal to zero at point 1.
2. Next, the applied electric field is isothermally increased from zero to E_1 and the electric displacement also increases from zero to D_1 at point 2.
3. In the next step, the pyroelectric sample is heated at constant electric displacement D_1 from $T = T_{Curie,\downarrow}$ to $T > T_{Curie,\uparrow}$ resulting in increase of electric field from E_1 to E_2 at point 3.

4. Afterwards, the sample is isothermally discharged at temperature $T = T_{Curie,\uparrow}$ until electric displacement and applied electric field both return to zero at point 4.
5. In the final step, the sample is cooled to its initial temperature $T = T_{Curie,\downarrow}$ to close the cycle at point 5.

The efficiency of this cycle was theoretically calculated to be well below 1% because the energy required to increase the temperature was much larger than the energy that can be converted to electrical energy from the cycle. The results discouraged further research efforts in pyroelectric conversion until R.B. Olsen in the early 1980's attempted to convert energy using a newly proposed electrical-thermal cycle named after him.

2.3.2 Olsen Cycle

The Olsen pyroelectric energy converter is essentially an electric form of a heat engine. In order to repeatedly extract electrical energy from the pyroelectric medium it is necessary to cycle the temperature as well as the electrical condition of the pyroelectric. Figure 2.8 displays the *D-E* diagram for PZST at temperatures above $T_{Curie,\uparrow}$, below $T_{Curie,\downarrow}$ and in between. The cycle in Figure 2.8 consists of two isotherms and two constant overlapping electric field lines. In the cycle the shaded area bounded by 1-2-3-4 is the Olsen energy conversion cycle. Energy density, N_D is represented by the shaded area of the cycle and is expressed in J/L. The total converted energy can be calculated by equation (2-8),

$$W_E = N_D \forall_{PE} = \oint E_{PE} dD_{PE} \forall_{PE} \tag{2-8}$$

where, $\forall_{PE}$ is the volume of the pyroelectric element (PE).

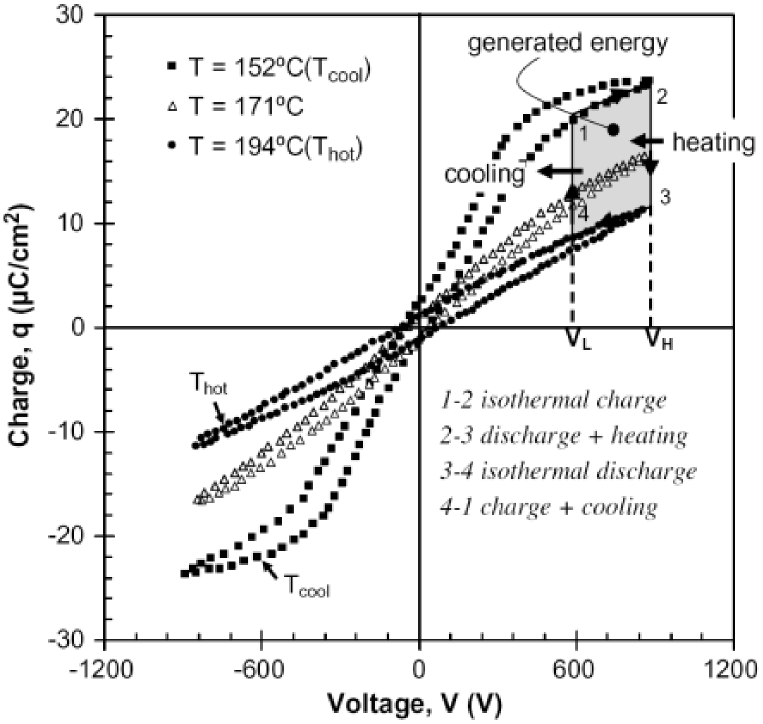

Figure 2.8: Electric Ericsson cycle superimposed on the charge-voltage hysteresis curve of a ferroelectric material showing energy harvested from employing such a cycle.

The Olsen cycle is performed as follows,

1. First the PE is charged by isothermally increasing the applied voltage from V_L to V_H at temperature T_L (process 1-2).
2. Then, the PE is discharged by increasing the temperature to T_H above $T_{Curie,\uparrow}$, at constant electric field (process 2-3).
3. Next, further discharge is achieved by decreasing the voltage isothermally from V_H to V_L (Process 3-4).

4. Finally, the PE is recharged to its spontaneous polarization at constant electric field with applied voltage V_L by cooling it below $T_{Curie,\downarrow}$ (process 4-1).

It is not required to heat and cool beyond the Curie temperatures, but doing so generates more current conversion from heat. The heat supplied to increase temperature above $T_{Curie,\uparrow}$, is entirely converted into electrical energy during the phase transition of ferro- to paraelectric at this temperature.

Efficiency of the conversion cycle is calculated by comparing the electrical energy generated to the thermal energy or heat supplied to the PE. The thermodynamic efficiency of the system is denoted by η and is calculated by equation (2-9) where, $\dot{Q_{in}}$ is the total heat transferred to the material during one cycle (in Watt) and $\dot{W}_E$ is the total electrical energy generated during that one cycle (in Watt) with time period, τ.

$$\eta = \frac{\dot{W}_E}{\dot{Q_{in}}} \tag{2-9}$$

$$\dot{W}_E = \frac{W_E}{\tau} \tag{2-10}$$

Heat losses to the surrounding and leakage current have been accounted for in measured $\dot{Q_{in}}$ and $\dot{W}_E$.

2.3.3 Pyroelectric Converter Prototypes

Since the late surge of research in the field of pyroelectricity during the Second World War, a few research groups have attempted to harvest energy from heat using the pyroelectric property of materials. Here the top three successful prototypes are discussed in the following sub-sections.

2.3.3.1 Olsen Prototype

The pioneer group in this research is Olsen et al. [12-15, 35, 43-45] Their initial attempt at harvesting energy from pyroelectric ceramic material included a heater, a cooling unit, a pump and a heat exchanging fluid to cycle the temperature in a cylinder where the pyroelectric ceramics were stacked as shown in Figure 2.9 [15]. In addition to mechanically cycling the temperature they applied a high voltage across the ceramic stack to take advantage of the Ericsson cycle. Later Navid et al adopted a similar approach for energy harvesting [17, 40-42, 46-49]. Their prototype efficiency was better due to choice of ceramic pyroelectric material with high pyroelectric coefficient and use of multi-staging and heat regeneration. Multi-staging consists of placing different pyroelectric materials with increasing Curie temperatures from cold to hot sources. Heat regeneration consists of cycling the heat required to increase the temperature of the PE back and forth between the working fluid and the PE so heat is not lost to the surroundings. Using this technique the Olsen cycle can almost reach Carnot efficiency.

To measure the pyroelectric generated power Olsen et al. used a modified Sawyer-Tower circuit as shown in Figure 2.10. Voltages V_1 and V_2 were measured across capacitor C_1 and resistor R_2 to calculate for charge and pyroelectric voltage. Resistor R_1 is used as voltage divider to comply with the data acquisition input voltage limit. The magnitude of the electric displacement is found by,

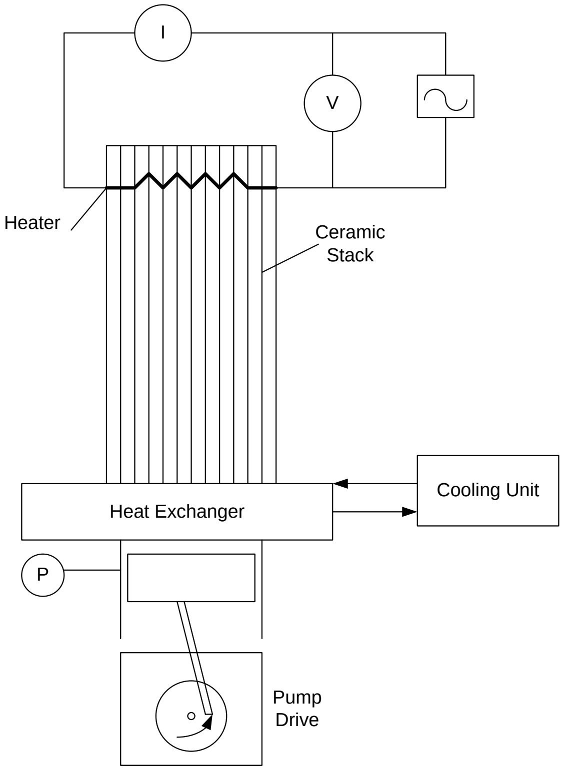

Figure 2.9: Diagram of the thermal and mechanical aspects of the pyroelectric conversion cycle experiment by Olsen et. al using heated fluid pump [13].

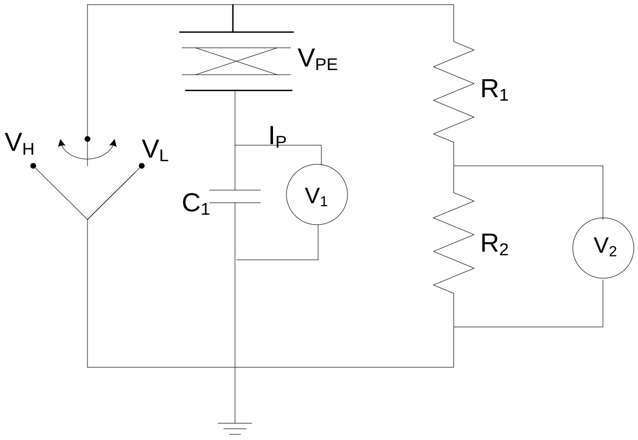

Figure 2.10: Modified Sawyer-Tower circuit used by Olsen et al. to measure the charge and voltage across a pyroelectric element.

$$D_{PE} = \frac{C_1 V_1}{A} \tag{2-11}$$

where, A is the surface area of the pyroelectric element. The magnitude of the electric field was found by Kirchhoff's voltage law

$$E_{PE} = \frac{V_{PE}}{d} = \frac{V_2\left(1 + \frac{R_1}{R_2}\right) - V_1}{d} \tag{2-12}$$

where, d is the thickness of the PE.

A *D*-*E* diagram plotted from the measurement is used to calculate for the energy density, N_D using equation (2-8). The power density P_D, defined as the power per liter of material, for one cycle is estimated as

$$P_D = \frac{N_D}{\tau} = \frac{\dot{W}_E}{\forall_{PE}} \tag{2-13}$$

where τ is the period of one cycle.

2.3.3.2 Guyomar Prototype

Guyomar et al. has also been researching methods of energy conversion using pyroelectric material, and they focused on the electrical energy extraction and polarization capability of the pyroelectric material [18-20, 36-39, 50-55]. Their experimental setup included a stack of pyroelectric films housed in a cylinder that is periodically heated using a controlled heat gun which is a simple dryer [19, 38]. Notable in this approach is the absence of applied electric field to achieve greater polarization. Figure 2.11 depicts a schematic of the experimental setup.

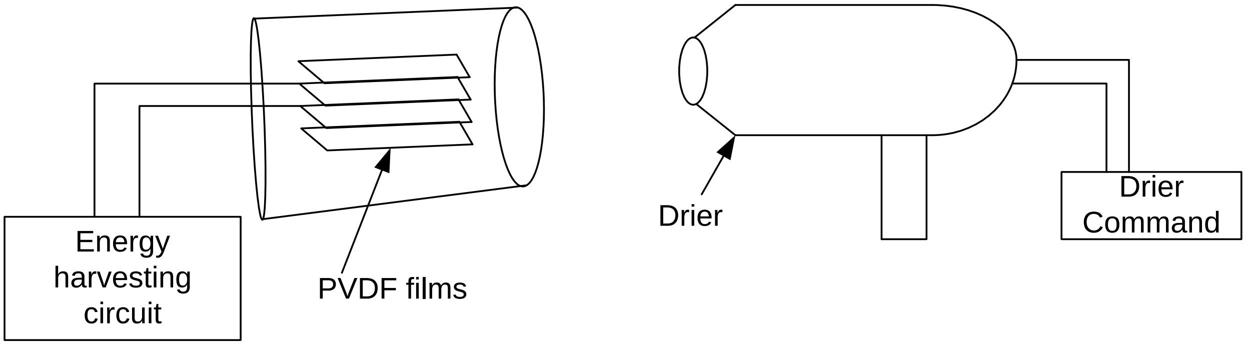

Figure 2.11: Experimental setup used by Guyomar et al., using a controlled drier to cycle temperature in the pyroelectric material [20].

Guyomar et al. also used a cantilever electromechanical structure to take advantage of the pyroelectric materials piezoelectric property for energy harvesting. To extract the electrical energy from the PE and use it as a power supply, they focused on four different harvesting techniques, which are discussed below.

Figure 2.12 shows the four techniques used by Guyomar et al. to extract the current from the pyroelectric material. The standard technique uses a diode rectifier bridge and capacitor to rectify the bidirectional current and charge the capacitor when the PE voltage V_0 rises above V_{DC}. When V_0 falls below V_{DC}, the capacitor discharged through load R. In the recent efforts they have incorporated an inductor in the circuit to maintain the direction and flow of current to charge the capacitor with more steady voltage. Note that in the SECE technique the output voltage $\pm V_{DC}$ is bidirectional, whereas in the other approaches the voltage is with reference to ground. The extraction method is an important part of useful energy harvesting and minimizes electrical losses from thermal to useful electrical energy.

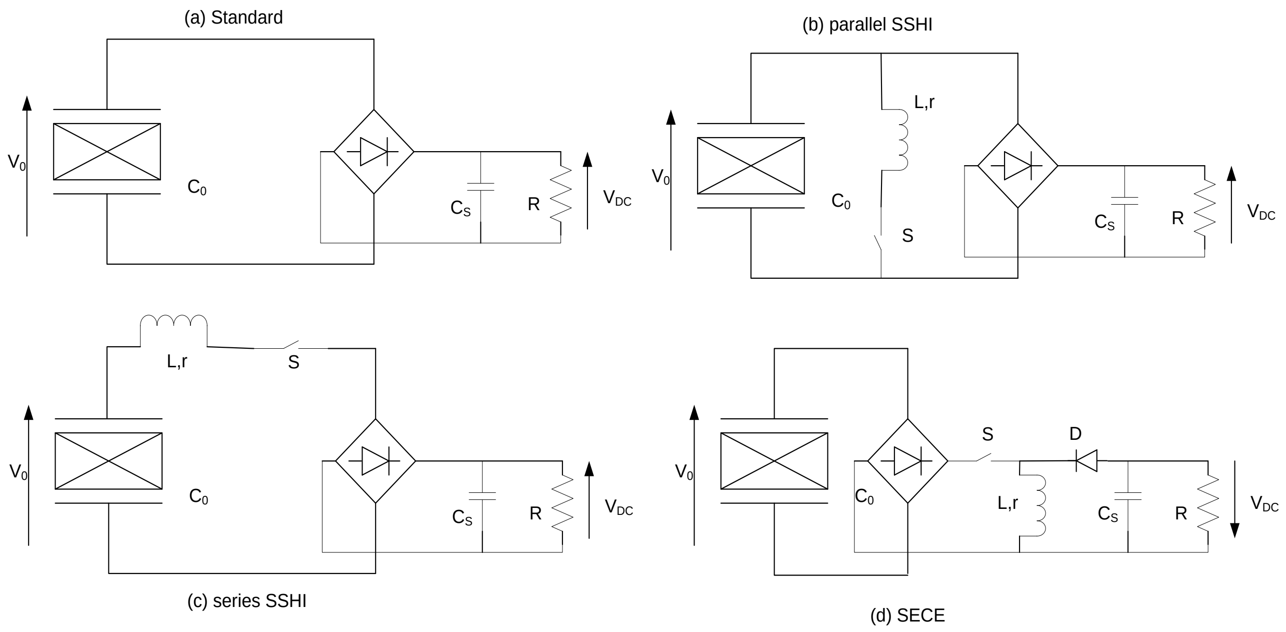

Figure 2.12: Energy harvesting technique schematics: (a) standard, (b) parallel SSHI, (c) series SSHI and (d) SECE.

2.3.3.3 Ikura Prototype

Another group recently pushing the research in low grade waste heat to electricity conversion is the Pyroelectric R&D consortium supported by CANMET Energy and is led by Ikura et al. [8, 16, 56, 57]. In their attempts to harvest energy from low grade heat sources, pellets of pyroelectric polymer were sandwiched between two metal plates that were used as electrodes to create a thin film assembly. The temperature was varied by alternately flowing hot and cold water over the film assembly and polarization was achieved by using high voltage application. The complete experimental housing is shown in Figure 2.13.

Figure 2.13: Water flow control and thin film assembly system housing for temperature cycling used by Ikura *et al* [17].

Ikura et al. followed the Olsen cycle to extract pyroelectric current, but they modified the Sawyer-Tower circuit further to measure for charge and voltage across the PE. The circuit used by this group is shown in Figure 2.14.

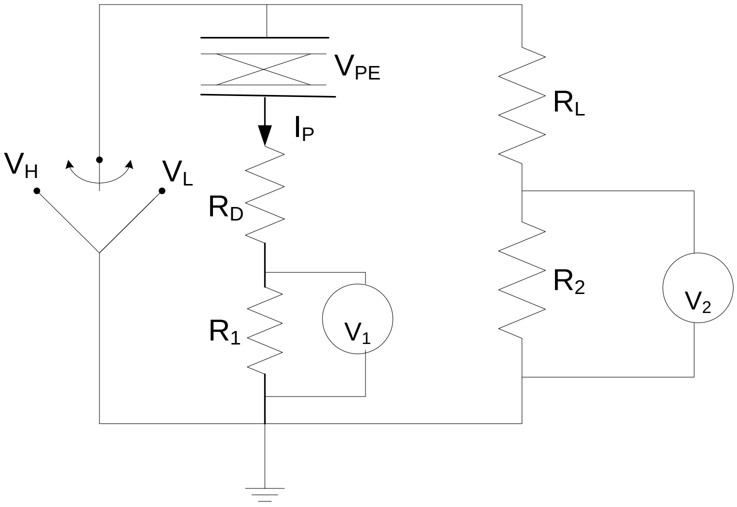

.

Figure 2.14: Energy harvesting circuit used by Ikura et al.

Instead of using a capacitor to measure the released charges, a resistor is used to measure the pyroelectric current and the instantaneous power. The instantaneous power is calculated as,

$$\dot{W}_{E,inst} = I_P V_{PE} \tag{2-14}$$

where, I_P is found by measuring the voltage, V_1 across R_1 and V_{PE} is found from Kirchhoff's and Ohm's laws as follows,

$$I_P = \frac{V_1}{R_1} \text{ and } V_{PE} = V_2\left(1 + \frac{R_L}{R_2}\right) - I_P(R_D + R_1) \tag{2-15}$$

Here, $\dot{W}_{E,inst}$ is time averaged over one cycle to obtain the generated power per cycle $\dot{W}_E$ as,

$$\dot{W}_E = \frac{1}{\tau}\int_0^\tau \dot{W}_{E,inst}\,dt \tag{2-16}$$

Where, τ is the time period of one power cycle.

All of the approaches discussed above fall short of achieving an impressive efficiency. Their performance is summarized and shortcomings are investigated in the following section.

2.3.4 Performance Summary and Shortcomings

Despite different approaches to thermally cycling temperature in the pyroelectric element and achieve greater polarization, the overall efficiency of the prototypical systems remains low. Table 2-1 summarizes the different approaches, their temperature cycling performance, harvested energy density, Carnot and overall efficiencies.

Table 2-1: Comparison between Early Attempts of Pyroelectric Energy Harvesting.

Reference	Thermal cycling method	Temperature change rate, $\frac{\partial T}{\partial t}$ (K/s)	Harvested Energy, (W/L)	Efficiency, η	Carnot efficiency, ηCarnot	Pyroelectric material
Olsen [44] - 1985	Fluid flow between heater and cooler using pump	1.764	14	1%	-	PZST
Guyomar [19] - 2008	Periodic hot air flow from drier	17.5	80	2.15%	2.15%	PZN-PT
Ikura [56] - 2008	Alternating hot/cold water flow	57	279	5.7%	37.5%	PVDF
Navid [47] - 2010	Fluid flow between heater and cooler using pump	11	38.4	5.2%	55.4%	PZST

Most of the early attempts to harvest energy using pyroelectric effect yielded unattractive numbers for efficiency. They were also very expensive in terms of the cost per KW-hr since they were mostly performed in laboratory scale. Despite adopting thin-film structures to increase the surface area these approaches suffered from very low output current because the temperature cycling method was not fast enough to provide a high value for time derivative of temperature. The rate of temperature variation is of highest importance as seen in equation (2-6), because it is directly proportional to the current produced. The reasons for low efficiency can be identified as

- Using thermal fluid, water or air as convective medium to transfer the heat energy to the pyroelectric material. The thermal mass that needs to be heated or cooled in this process is large and takes more time than it would be required to heat or cool only the pyroelectric material.
- Carnot efficiency of this heat transfer reduces the magnitude of temperature change and therefore the temperature range that changes over a cycle is reduced.

- Convective heating compared to conductive heating is slower and therefore reduces the temperature change rate and corresponding current magnitude.
- To produce more energy, large mass of pyroelectric polymer is used. But large volume of material also has larger thermal time constant and therefore slower temperature change. Thus increasing the size of material reduces the peak magnitude of the pyroelectric current.
- There is external power consumption required in the fluid pumps, drier, heater, cooler etc. used to harvest the pyroelectric energy. This reduces the overall efficiency of the energy harvesting system.
- Requires external voltage supply for creating dipole when using the Olsen thermoelectric cycle, which requires additional energy consumption reducing the efficiency somewhat.
- All of them need some method of control circuitry to control the temperature cycling by controlling the hot or cold fluid flow etc.

2.4 MEMS Devices

MEMS stands for microelectromechanical systems. It is an emerging technology using the microfabrication tools and techniques of integrated circuit manufacturing industry to fabricate micron scale machines driven by electrical energy. Typically MEMS technology consists of devices or structures that may or may not have a moving part but utilizes some mechanical properties and are electronically controlled. Functional elements of MEMS devices are miniaturized structures that are used as sensors and actuators. Notable application of MEMS devices are sensors, micromirrors, microactuators, micropumps, accelerometers, gyroscope, radio frequency resonators etc.[58-64].

In functional MEMS devices few basic structures are used to control the mechanical movement or electrical performances. In microscale the regular macroscale physics such as gravity, inertia becomes obsolete and other properties such as stress, thermal capacity or ferroelectricity become more important. In sensors these properties are utilized to sense pressure, presence of particular gas, light etc. and to produce electrical signals that are further conditioned by associated microelectronics to produce useful information. In MEMS actuator similar properties are utilized to electrically gain control over the mechanical performance of the structure. Based on which property is utilized, MEMS devices can be electrothermal, electrostatic, piezoelectric etc. For this study a detail look at electrothermal and piezoelectric MEMS devices and their behavior is provided in the next sub-sections.

2.4.1 Electrothermal MEMS

Electrothermal MEMS takes advantage of Joule heating to control the temperature of the structure and utilizes its thermal properties. In many applications electrothermal MEMS are used for mechanical movement achieved by thermal expansion due to controlled heating of the device. Examples of electrothermal MEMS include micromirrors, microactuators such as microgrippers, temperature sensors etc. [58, 59, 62, 63].

Often in electrothermal MEMS devices a beam like structure is used that can be either unimorph or bimorph. In a unimorph structure, the device is made of a single material of high resistivity usually polysilicon or silicon nitride. The electrical current flows through the body of the device and generates heat due to resistive loss. Since the device is in micro scale, the resistance is high and produces enough heat to thermally expand the device body and cause deformation. Thus thermally caused deformation is utilized for actuation. In unimorph structures high current has to flow through the device to raise the temperature high enough to achieve sufficient thermal expansion to reach the desired level actuation. Very high temperature operation is involved in this case, and accordingly the device life is reduced.

In a bimorph structure typically more than one type of material is involved. In similar fashion to unimorph structure, Joule heating is used to increase the temperature of the device in desired places. Since different materials have different thermal expansion rates, their expanded length vary and if they are attached to each other a resultant deflection occurs in an attempt to balance the compressive and tensile forces experienced by the two materials thermally expanding at differential rate. In most cases the device involves a cantilever structure that actuates based upon the temperature increase and the deflection of the cantilever beam.

Electrothermal MEMS are also used as sensors where upon the absorption of heat the micro structures deform to produce an electrical signal [64]. Since the Joule heating process is non-reversible, deformation is converted to electrical signal by other forms of transducers, such as laser reflection or piezoelectric transducers. Because of its high sensitivity electrothermal MEMS are widely used for infrared imaging [21, 61, 65-70].

2.4.2 Piezoelectric MEMS

MEMS technology benefits itself tremendously by making use of the piezoelectric properties of material. The property of materials to deform upon application of electric field is largely used in MEMS technology to actuate micro devices and structures. Since this process is reversible, piezoelectric property is also utilized in MEMS based sensors, for example, in pressure sensors.

In microactuators fabricated using piezoelectric materials, electric potential is applied to deform the device structures in a desirable form to actuate micromotors, pump microfluidic channels, close microswitches, tune capacitors, adjust micromirror positions and so on[71-75]. Application of potential causes polarization in the lattice structure of the piezoelectric materials that displaces the position of the atoms in the structure causing deformation. Direction of the deformation is dependent on the piezoelectric coefficient and the direction of the applied voltage to the material.

Piezoelectric MEMS has also been widely researched and more recently commercially developed for energy harvesting from pressure and vibrations [37, 76, 77]. In piezoelectric energy harvesters a MEMS structure is allowed to pick up vibration or experience pressure which generates electric potential in the material. The generated potential is typically intermittent and requires conditioning circuit to rectify and store the harvested energy for use. The piezoelectric conversion efficiency needs to be higher for energy harvesting application.

Similarly for sensor application the piezoelectric material functions as transducer to convert pressure to electrical signals [65]. In this case low amplitude of converted electrical signal is acceptable for the purpose of analysis. Note that in comparison with electrothermal MEMS that controls the mechanical behavior with electric current, piezoelectric MEMS control the mechanical response with electric potential.

In light of the discussion presented in this chapter, the next chapter describes a novel MEMS based pyroelectric energy harvesting scheme and its working principle.

Chapter 3

PROPOSED MEMS DEVICE

This chapter describes the concept behind the proposed MEMS device that can be used to convert thermal energy from low grade waste heat to produce electrical energy by pyroelectric conversion. The first section describes the structure of the proposed MEMS device. The second section describes the working principle with detailed explanation of the physical phenomena utilized to realize the conceptual device. Performance criteria for successful energy harvesting are identified in the following section before concluding the chapter with a discussion on the advantages and disadvantages of the proposed scheme.

3.1 Proposed Scheme for Energy Harvesting

The proposed scheme is based on an energy harvesting system that features a microelectromechanical, or MEMS structure with an embedded pyroelectric capacitor structure that when heated and cooled causes current to flow in alternate directions, which can be used to generate electricity. The underlying concept of pyroelectricity is based on the use of pyroelectric materials embedded in a MEMS device that can thermally self-actuate and cycle temperature within it. The proposed MEMS device will use cantilever structures that are a few millimeter square in size. Thousands of these energy converters can be attached to a square centimeter sized hot surface such as computer chips, concentrated photovoltaic cell, or other devices that generate waste heat.

In the MEMS configuration, cantilevers are attached to an anchor that is affixed to a heat sink and the free end or tip of the cantilever is placed in contact with a heat generator surface. As the surface becomes hot, the cantilever also heats through the tip and bends and detaches from the hot surface because of the bimaterial effect, similar in principle to the bimetal switch used in room and oven thermostats. The cantilever is then cooled by dissipating the transferred heat through the heat sink. As the temperature of the cantilever decreases the cantilever moves back and makes contact with the hot surface. The cantilever then heats up again and cycles back to the cold heat sink. Upon contact the cantilever continues to oscillate between the heat source and the heat sink as long as there is a temperature difference between the hot and the cold surfaces irrespective of the value.

The high-efficiency thermal waste heat energy converter will be able to actively cool electronic devices, photovoltaic cells, computers and large waste heat-producing systems while generating electricity. Although the amount of electricity each device can generate is small, arrays of these devices can be used to generate sizable amounts of electricity that can power remote sensor systems or assist in the active cooling of the heat generating device, reducing cooling demands.

The principal challenge of the pyroelectric energy harvesting is maintaining a sustained temperature cycling. This is usually achieved by conventional method of heating and cooling that are typically bulky and consequentially slow. Since the rate of temperature change is directly related to the amount of the harvested energy, a microelectromechanical system is proposed to improve the rate of temperature cycling. The self-actuating device will house a thin film of pyroelectric material with metal contacts to extract the charge generated due to polarization from temperature cycling. A low power rectifying and storage circuit will be converting the alternating current to useful DC electrical storage. Different functional parts of this technology and their operating principles are discussed in this chapter.

3.2 Proposed MEMS Structure

The shortcomings of the previous pyroelectric energy harvesting approach can be overcome by taking a MEMS approach. Macroscale temperature cycling techniques were bulky and consequentially slow to respond. On the other hand MEMS devices are small and can respond at very high frequency. They also require very little energy input to operate. Therefore to address the problems affecting the energy conversion process a novel MEMS structure is conceptualized that is self-actuating from thermal energy to cycle temperature in an embedded pyroelectric film to generate electric current.

The proposed MEMS structure is basically a bi-material bimorph cantilever resting from the base of a cold heat sink that is at a temperature lower than the waste heat source. The bimaterial cantilever has the material with higher thermal expansion coefficient facing the hot surface. The pyroelectric element is embedded on the cantilever. A proof mass at the tip of the cantilever makes contact with the heated surface and transfers the heat from the source to the MEMS structure. The heat sink is kept as far as possible from the heat source to minimize radiative heat transfer. The detail structure of the MEMS device is shown in three dimensions in

Figure 3.1 and a cross-section is shown in Figure 3.2.

Dimensions of the cantilever structure were varied over a range to find optimal performance and are listed in Table 3-1 . The bimaterial combinations considered for the cantilevers are silicon dioxide-aluminum (SiO_2-Al) and silicon-gold (Si-Au). The material properties of interest for the bimaterial structures for the considered material are tabulated in Table **3-2**.

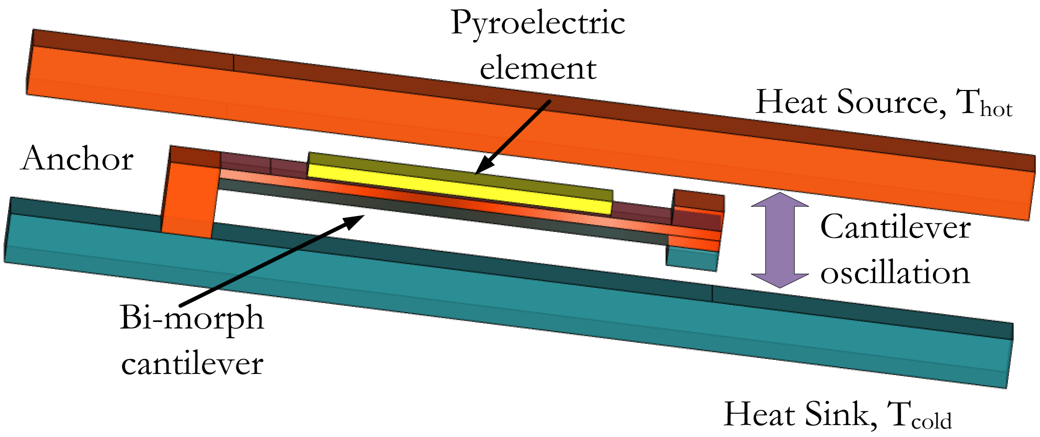

Figure 3.1: Three dimensional (3D) view of the proposed MEMS device.

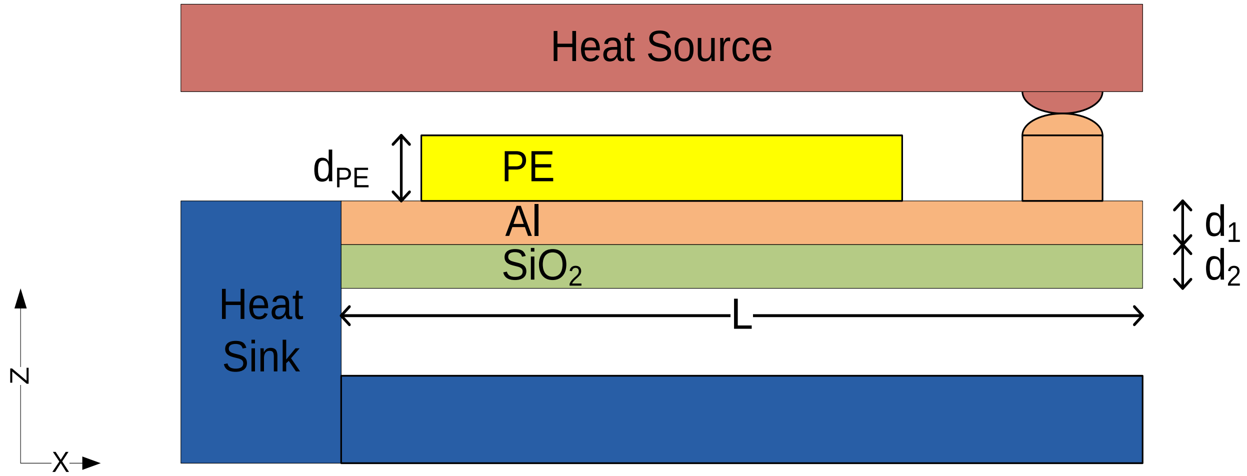

Figure 3.2: Two-dimensional (2D) view of the proposed system.

Table 3-1: Material dimension of the Bimaterial bimorph structure.

Dimension	Silicon di Oxide (SiO_2)	Aluminum (Al)	Silicon (Si)	Gold (Au)	PVDF
Length, L (mm)	0.5 – 7	0.5 – 7	5	5	0.25 – 6
Width, W (mm)	0.1 – 1.75	0.1 – 1.75	1	1	0.1 – 1.5
Thickness, t, (μm)	1-10	0.15-0.300	10	10	25

Table 3-2: Properties of Material of BiMorph Structure.

Property	Symbol	Silicon Di Oxide	Aluminum	Silicon	Gold	Unit (SI)
Thermal Conductivity	g	1.38	160	149	318	W/m-K
Specific Heat	C_P	703	900	329	129	J/Kg-K
Thermal Expansion Coefficient	α	0.55	23	2.6	14.2	μm/K
Density	ρ	2200	2700	2329	19300	Kg/m^3
Young’s Modulus	E	73.1	70	185	79	GPa
Poisson’s ratio	ν	0.33	0.33	0.28	0.28	-

The bimaterial combination used have differential thermal expansion coefficient and for the structure to self-oscillate, the material with higher thermal expansion coefficient in the combination is always placed to face the heated surface. The pyroelectric materials considered are polymeric PVDF that has higher thermal expansion coefficient than any other material in the bimaterial structure. Hence to maintain the self-oscillation after embedding the pyroelectric material, it is placed on the outermost surface. A proof mass is placed at the tip of the cantilever to make contact with the hot surface without conducting heat to pyroelectric element directly from the source.

The next section describes the working principle of the structure.

3.3 Working Principle

There are two parts of this energy harvesting: thermomechanical and electrothermal. The thermomechanical part involves cycling the temperature in the MEMS structure that is thermally self-actuated. The electrothermal part involves converting the thermal energy from the MEMS structure into electric current by pyroelectric conversion. The energy conversion cycle progresses by the following steps.

1) The tip of the bimorph cantilever is brought in contact with the hot surface by means of a proof mass. Heat flux flows from the hot surfaces through the proof mass and along the length of the cantilever, raising its temperature.
2) As temperature rises in the bimaterial cantilever beam, it bends downwards due to differential rate of thermal expansion. This phenomenon is discussed in detail in section 3.3.1. The bending causes the tip to lose contact with the heat source and the transferred thermal energy travels through the body of the cantilever towards the heat sink as it increases the temperature in the cantilever body.
3) The temperature increase causes change in the polarization of the embedded pyroelectric element, causing pyroelectric current flow. As the beam bends down, the PE also experiences mechanical stress and associated piezoelectric effect, since all pyroelectric material are subsets of piezoelectric materials. The piezoelectric effect produces further

polarization in the material which can be additive or subtractive. This indirect effect is further discussed in section 3.3.2 and 3.3.3.

4) The heat sink absorbs the heat flux transferred through the body of the cantilever beam and reduces the temperature back to initial temperature. As temperature falls, the cantilever beam is reinstated to its initial position, and the proof mass is back in contact with the hot surface.
5) The cantilever heats up again through the proof mass and the process starts repeating. Thus self-oscillation of the MEMS structure is achieved. Thermal actuation and self-oscillation is explained in section 3.3.4.
6) Due to self-oscillation of the cantilever beam, the temperature in the beam periodically rises and falls. The pyroelectric element produces alternating current with the temperature change.
7) The generated alternating and intermittent current is rectified and conditioned by additional circuit to store the energy in a battery and provide a fixed DC voltage for useful application. Possible current extraction, rectification and storage circuits are considered in section 3.3.5.

3.3.1 Thermal Response of BiMaterial Cantilever Structure

A bimorph cantilever is formed by joining two materials of different thermal expansion coefficients side by side with one end anchored to a fixed base. The tension between two thin film of materials joined side by side has been studied by Stoney in [78]. When heated the materials expand at different rates and results in bending with the less expandable material in the concave side. The forces in effect on the bimaterial structure are balanced by each other and the resultant

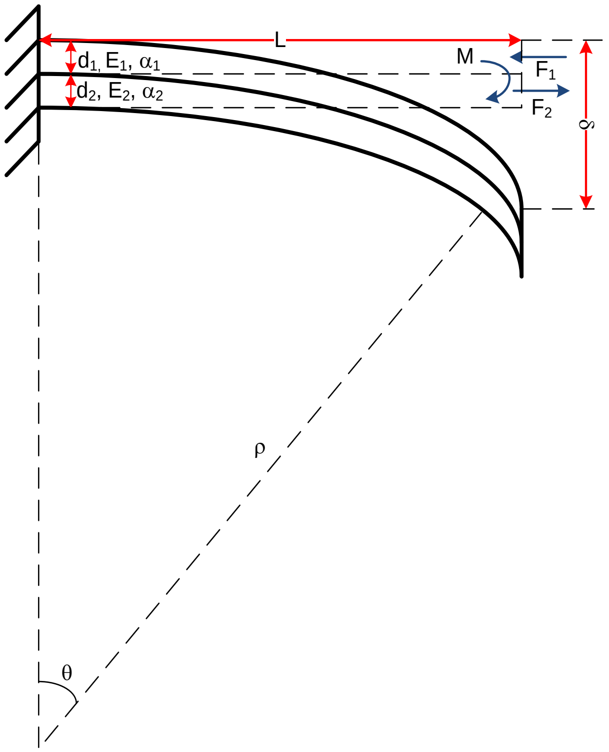

Figure 3.3: Curvature of a bimaterial cantilever with temperature change.

moment of the forces cause deformation of the structure. Timoshenko studied this phenomenon for simple beam structure in [79].

Let us assume a bimaterial structure with length L and thickness of material 1 and 2 being d_1 and d_2 respectively as shown in Figure 3.3. Thermal expansion coefficient and Young's modulus of the materials are α_1, α_2 and E_1, E_2 respectively. The reference temperature being $T = T_0$ and the increased temperature that causes deformation being $T = T_1$. Material 1 has a higher thermal expansion coefficient than material 2, i.e. $\alpha_1 > \alpha_2$. When the cantilever is heated to temperature T_1, material 1 and 2 expand at different rates. Material 1 expands more than material 2 and since they are joined at the surface material 1 exerts an expansion force F_2 on material 2. Since the forces are balanced, material 2 also applies a compressive force F_1 on material 1. At the neutral axis of the beam, the forces are equal and cancel each other out. Neutral axis is a horizontal line along the length of the cantilever beam where the forces are equal and no expansion or contraction takes place. If both materials had equal thermal expansion, then the neutral axis is at the common surface. In this case, the neutral axis is away from the common surface in towards depth of material 2. The beam experiences a flexural moment M at the neutral axis. This causes it to bend downwards. The radius of curvature of the bent cantilever beam can be found by solving the equation for balanced forces at the neutral axis. It is given by equation (3-1)

$$\frac{1}{r_c} = \frac{6(\alpha_1 - \alpha_2)\left(1 + \frac{d_1}{d_2}\right)^2 (T_1 - T_0)}{h\left\{3(1 + \frac{d_1}{d_2})^2 + (1 + \frac{d_1}{d_2}\frac{E_1}{E_2})\left(\left(\frac{d_1}{d_2}\right)^2 + \frac{d_2}{d_1}\frac{E_2}{E_1}\right)\right\}} \tag{3-1}$$

where ,

r_C= radius of curvature

$h = d_1 + d_2$, total thickness of the beam.

α_1, α_2 = thermal expansion coefficient of the materials and

T_1 = Temperature, T_0= Initial temperature.

If the ratio of thickness of two material layers is $m = \frac{d_1}{d_2}$ and, the ratio of Young's Modulus of two layer is $n = \frac{E_1}{E_2}$, then equation (3-1) reduces to

$$\frac{1}{r_c} = \frac{6(\alpha_1 - \alpha_2)(1+m)^2(T_1 - T_0)}{h\left\{3(1+m)^2 + (1+mn)\left((m)^2 + \frac{1}{mn}\right)\right\}} \tag{3-2}$$

From Figure 3.3 the tip deflection, δ at the free end can be found using tangent formula,

$$\theta = tan\theta = \frac{\delta}{L} = \frac{L}{r_{C-}\delta} = sin\theta \tag{3-3}$$

Since the deflection, δ is very small compared r_C equation (3-3) results in

$$\delta = \frac{L^2}{2r_C} \tag{3-4}$$

Replacing r_C in equation (3-4) we find,

$$\delta \ = \frac{3L^2}{h} \cdot \frac{(\alpha_1 - \alpha_2)(1+m)^2(T - T_0)}{\left\{3(1+m)^2 + (1+mn)\left(m^2 + \frac{1}{mn}\right)\right\}} \tag{3-5}$$

Here, the temperature T can be a variable that can be varied to control the deflection of the cantilever beam to obtain desired movement.

3.3.2 Pyroelectric Current Generation

The pyroelectric material is essentially a capacitor structure whose charge fluctuates with temperature and applied voltage. With two metal electrodes are connected to the surface of the material, this charge can be extracted as a current flow through a closed circuit. Application of potential causes additional polarization in the material and increases the flow of current.

Thermomechanical performance of the MEMS device cycles the temperature in the embedded PE in the cantilever beam. According to equation (2-6), the current generated from the PE capacitor varies following the slope of temperature change. For arbitrary values the generated current and temperature change behavior in the material can be estimated as shown in Figure 3.4. Voltage signal is also applied to increase the current. Pyroelectric material surface area is more important than its volume to generate more current. Therefore a thin film of the pyroelectric material film was used with the top and the bottom metal deposition for contact to form a capacitor-like structure.

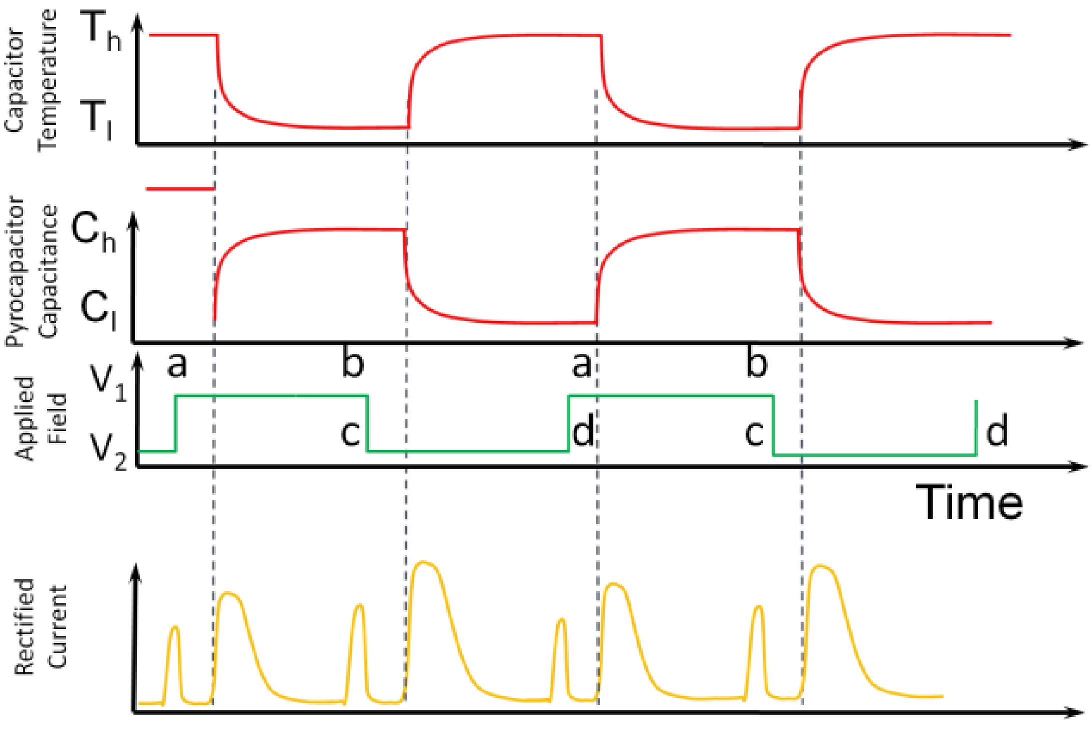

Figure 3.4: Pyroelectric capacitor temperature and current profile with applied voltage.

3.3.3 Piezoelectric Effect

As the cantilever undergoes a curvature due to the thermal expansion of the material, the embedded pyro/piezoelectric capacitor also experiences mechanical stress. Bending of the cantilever also causes flexural stress. Mechanical stress causes piezoelectric polarization in the material and the electric potential increase in the material that extracts charge from the material and contributes to the pyroelectric current. The piezoelectric response can be either additive or subtractive to the pyroelectric material and entirely depends on the electrode connection and crystal orientation of the material in the structure. When the cantilever structure is loaded with a force F, electrical energy W_{elec} is stored in the piezoelectric element, given by,

$$W_{elec} = \frac{1}{2} C \times U^2 \tag{3-6}$$

where, C is the capacitance of the piezoelectric element and U is the generated electric potential. The mechanical energy due to deformation can be expressed as [77],

$$W_{mech} = \frac{1}{2} T^2 \times s_{33}^{D} \times \forall \tag{3-7}$$

where, T is the mechanical strain, $\forall$ is the volume and s_{33}^{D} is the elastic constant. Therefore, the electrical energy W_{elec} and mechanical energy W_{mech} are related by,

$$W_{elec} = k_{33}^2 \times W_{mech} \tag{3-8}$$

where, k_{33} is the electromechanical coupling coefficient. The conversion from mechanical energy to electrical energy depends on the volume, the piezoelectric properties and both the magnitude and the direction of the mechanical excitation. Maximum energy output from mechanical energy can be extracted at cantilever's resonant frequency, whereas the maximum power output is available when the load resistance matches the output impedance of the PE. To calculate for the current output from piezoelectric conversion the produced charge needs to be calculated from the piezoelectric coefficient, d_{33} and effective force, F_{eff} working on the cantilever using the deflection measurement, δ. The produced charge, q_{piezo} can be accounted for by,

$$q_{piezo} = -d_{33\times}F_{eff} = -d_{33\times}\frac{SE}{\delta} \tag{3-9}$$

Here, SE is the strain energy stored in the cantilever. Vector of F_{eff} and d_{33} determines the direction of the current during the period of oscillation. The pyroelectric current is positive during heating and downward mechanical stress. If the material used produces positive piezoelectric current during downward motion, the piezoelectric and pyroelectric current is additive.

Since the deflection is very small, the resulting piezoelectric current is also small and has been omitted for the next level of modeling in this study.

3.3.4 Thermally Actuated Self-Oscillation of MEMS

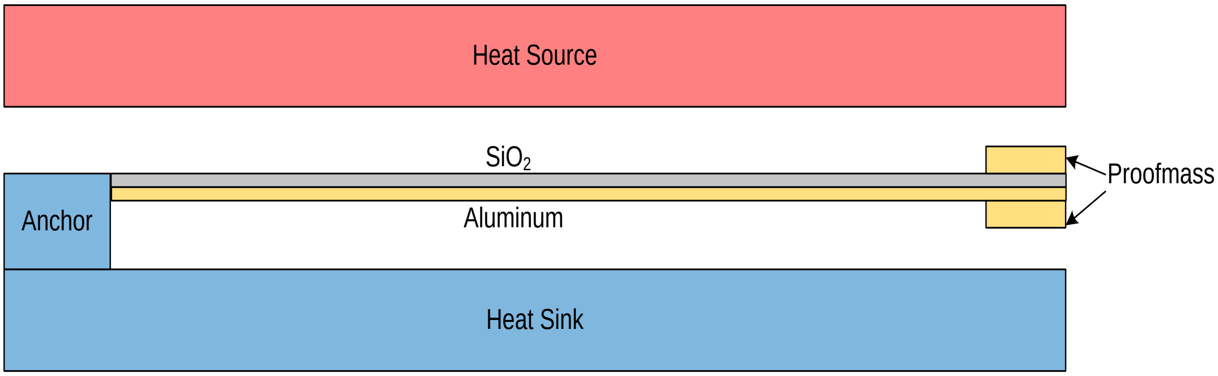

Figure 3.5: Cross-section of the MEMS device structure

The working principle of the MEMS structure depends on conductive heating, bimorph bending and ambient cooling technique. The cantilever is anchored to a heat sink which is at a lower temperature than the heat source surface. The cantilever is initially at uniform temperature with the heat sink. A proof-mass is placed at the tip of the cantilever to make thermal contact with the heat source. To initiate the actuation the proof-mass is brought in close proximity of the hot surface of the heat source and is allowed to touch the source. Depending on the thermal contact conductance a heat flux, Q passes through the contact to the body of the cantilever and increases its temperature, which can be mathematically expressed as,

$$Q = \mathrm{k} \times \nabla \mathrm{T} \tag{3-10}$$

where, T and k represent temperature and thermal conductivity, respectively. As the temperature rises in the cantilever beam, bimaterial deformation begins to take effect due to differential thermal expansion of the materials. Since the Aluminum is placed next to the heated surface and it has a higher thermal expansion coefficient, the cantilever beam deforms away from the hot surface and causes the proof-mass to lose thermal contact after time Δt_{heat}. The amount of thermal energy, W_{therm} transferred to the cantilever beam in this time is,

$$W_{therm} = \mathrm{Q} \times \Delta \mathrm{t}_{heat} \tag{3-11}$$

Temperature in the cantilever beam continues to increase as the transferred heat travels through the length of the cantilever before dissipating in the heat sink through the anchor. As the heat dissipates through Δt_{cool}, the temperature decreases in the cantilever body and the bimaterial deformation is removed to restore the cantilever to its initial position. With its return to initial condition the proof-mass regains contact with the hot surface and again conducts heat until bimaterial deformation causes detachment. Thus the cycle begins to repeat itself. The cycle continues perpetually once the device has been brought in contact with the heat source as long as there is a temperature difference between the heat source and the heat sink, irrespective of the magnitude. The base used as the heat sink needs to be at a lower temperature than the source and is assumed to be convectively cooled by ambient flow of air and does not require forced cooling. The frequency of the oscillation depends largely on the temperature difference, the thermal contact conductance and dimension of the cantilever.

The continuing temperature variation experienced in the body of the MEMS structure is also effective on the pyroelectric material housed within it. As the MEMS structure bends it also experiences strain and therefore displays additional piezoelectric response. Patterned metal contacts are used to collect the pyroelectric current generated from the thermal and the mechanical stresses experienced by the polymeric pyroelectric material.

3.3.5 Current Extraction, Rectification and Storage

The generated pyroelectric current is directly proportional to the rate of change of temperature, i.e. when the temperature change has a positive slope the current flows in one direction, and when the slope is negative, current flows in the opposite direction. Also the flow of current is not steady but fluctuating, intermittent, even random sometimes. To make this current supply into useful steady state voltage supply an interface circuit is required. Typically full bridge rectifier circuit or voltage doubler circuits are used for such intermittent energy harvesting interface circuit [80-83]. There are also novel concepts found in literature that uses switched rectifier circuits with inductors which

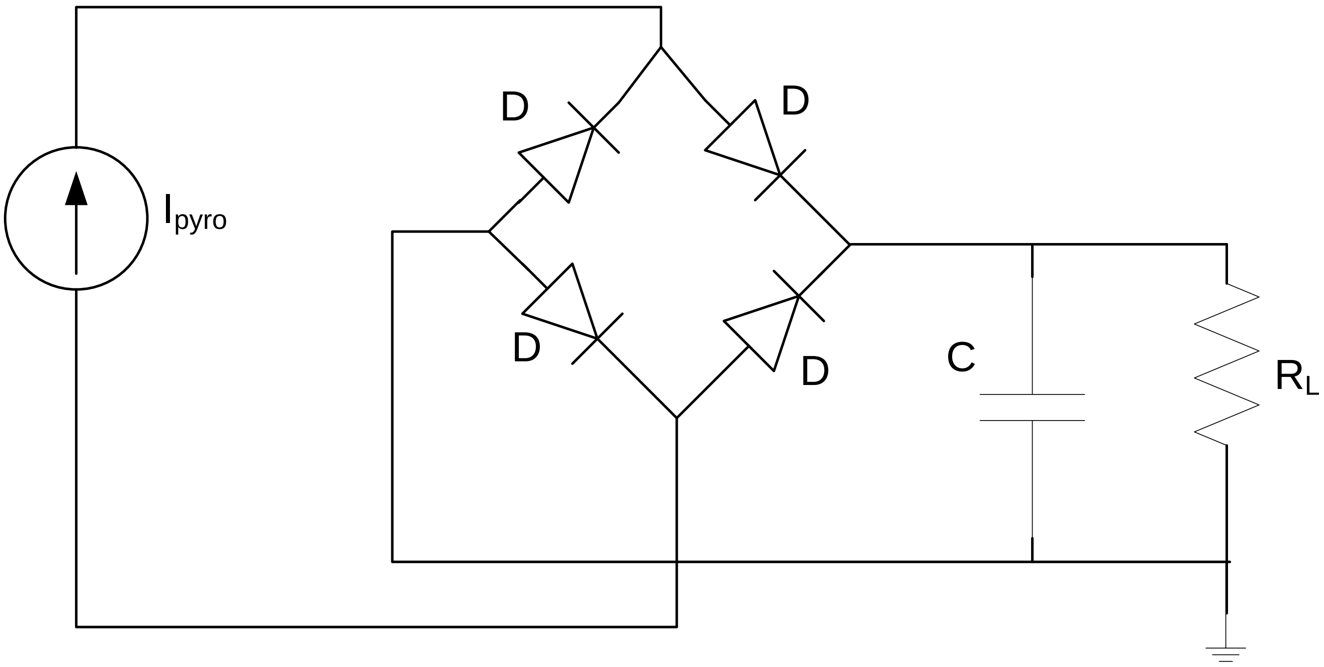

Figure 3.6: Full- bridge rectifier interface circuit for converting intermittent pyroelectric current to steady state voltage output.

achieve much higher output voltage [84]. An example circuit for interfacing pyroelectric energy harvester to conditioning and storage circuit is presented in Figure 3.6. For circuit expression, the pyroelectric current from the energy harvester can be represented with a low frequency sinusoidal current source. A large capacitor *C* is charged with the supplied current. The voltage magnitude is current times the load resistance, R_L.

3.4 Performance Goals

In order to successfully harvest energy from the proposed device some performance goals were identified. They can be separated intro two criteria: thermoelectric and pyroelectric. They are listed in the next two sub-sections.

3.4.1 Thermomechanical Response of the MEMS

1. Good thermal contact: Good thermal contact between the heat source surface and the cantilever tip proof mass needs to be established to ensure flow of large heat flux. The amount of heat transferred through this contact is going to be converted to electrical energy therefore it is important that the thermal contact transfers maximum heat possible. Surface roughness of the heat source as well as the proof mass is important to ensure maximum heat transfer area to maximize heat flux.
2. Large Bimorph deflection: The cantilever deforms to move away from the heat source. Once the cantilever tip moves away, a large deflection is desired to separate the cantilever from the heat source so that it solely dissipates the transferred heat through the heat sink and does not conduct heat between the heat source and the sink until the thermal contact is reestablished. Large deflection is also desired to maximize the piezoelectric effect.
3. Short thermal time constant: It is preferred that the cantilever body transfers the heat as fast as possible to increase the temperature change rate. With a short thermal time constant, the temperature cycling is faster and assists in generating more pyroelectric current. Short thermal time constant can be achieved by using material with high thermal conductivity and low specific heat capacity properties.
4. High capacity heat sink: The heat sink used for dissipating the heat should have a large thermal mass and high specific heat capacity so as to release the heat to air quickly and maintain its low temperature point. The low temperature maintenance is important since it determines the restoration point of the cantilever to repeat the oscillation periods.

3.4.2 Pyroelectric Response

1. High pyroelectric conversion coefficient: High thermal to electrical conversion coefficient is the most desired parameter in the pyroelectric material to most efficiently convert the transferred heat to pyroelectric current. High conversion coefficient increases the magnitude of the generated current and assists in the rectification and voltage conversion.
2. High thermal expansion coefficient: Since the pyroelectric material is embedded on top of the material with high thermal expansion properties it also needs to have either as high or higher thermal expansion properties compared to the cantilever material to comply with the thermomechanical performance of the MEMS structure. Low Young's modulus or flexural rigidity is also a desired property for this cause. Therefore, although ceramic pyroelectric materials have higher conversion coefficients, polymeric pyroelectric material are preferable as they meet the second requirement as well.
3. Large surface area: The magnitude of the pyroelectric current is related to the surface area of the material rather than the volume. Therefore a thin layer of pyroelectric material covering the most surface of the MEMS structure surface is desirable. A thin layer also ensures quick heating and cooling of the material, as well as high capacitance, both desired performance criteria for the proposed scheme.
4. Optimum load impedance: To extract maximum power from the pyroelectric energy harvester, the load impedance should be equal to the impedance of the pyroelectric material itself.

3.5 Advantage of Proposed Scheme

A microstructure assembly makes it possible to deploy with ease for on-the-field energy harvesting. A microstructure also facilitates quick heat cycling because of low thermal mass involved. Quick heat cycling results in more energy per volume and increased power density. Because of the basic cantilever MEMS structure used in the proposed scheme, fabrication of large array of these devices is feasible. In a large array the temperature cycling will occur at the same rate in every device because the thermal capacitances are in parallel rather than in series. Thus it can be used to generate a large quantity of power which will be equal to energy from a single device, directly multiplied by number of devices, without compromising fast temperature cycling. With the developing technology there is strong possibility of integrated CMOS-MEMS fabrication which would make the harvested energy instantly available for powering low power CMOS circuits embedded in the same system. Because of the self-oscillating structure used to cycle heat, the scheme also takes advantage of piezoelectric property to convert electrical energy from the vibration. Another advantage of pyroelectric property and a self-cycling heat pump is that there is not a fixed temperature requirement. As long as heat sink remains at a colder temperature than the heat source there is going to be continuous heat cycling. Absence of an external heat pump system reduces the auxiliary energy required to convert power, thereby increasing the efficiency significantly.

3.6 Disadvantage of the Proposed Scheme

The disadvantage of this scheme is the power output from a single device is very small because of the microstructure used in the design. Therefore a large array fabrication is almost inevitable to extract energy adequate enough to power even small electronics. Since the heat transfer between the heat source and the cantilever occurs very momentarily, the Carnot efficiency is not the best compared to other schemes. The power produced using the scheme is still expensive in terms of cost/kW-hr.

The concept must be theoretically tested and optimized before attempting realization. The physical phenomena discussed in this chapter can help develop a realistic model of the conceptual device to verify the possibility of realizing this device. The model development from basic physics concepts and optimization techniques are addressed in the following chapter.

Chapter 4

NUMERICAL SIMULATION

Advancement of computing technology and numerical analysis methodologies make it possible to build simulation model of a system and study its performances under simulated conditions. This allows for design correction and modification for desired performance with relative ease prior to its practical implementation. For a prototypical device as proposed in the previous chapter, a two dimensional model of the proposed structure has been developed in order to study the thermomechanical and pyroelectric performances and find key design and operating parameters to improve the power output and the efficiency of the device. This chapter reports on the methodology followed for developing a numerically simulated model as well as a simplified analytical model to calculate for device performance parameters. A SPICE model is also developed to simulate electrothermal response of the MEMS and its effect in an electrical circuit.

4.1 Analysis of the System

The operation of the prototypical device can be broken down in two physical sub systems for ease of analysis. One part includes the thermomechanical operation of the device to produce a temperature variation, and the second part is the electrical energy generation in response to the output of the first sub-system. In the following sub-section more detailed description of each sub-section is provided.

4.1.1 Thermomechanical Sub-System

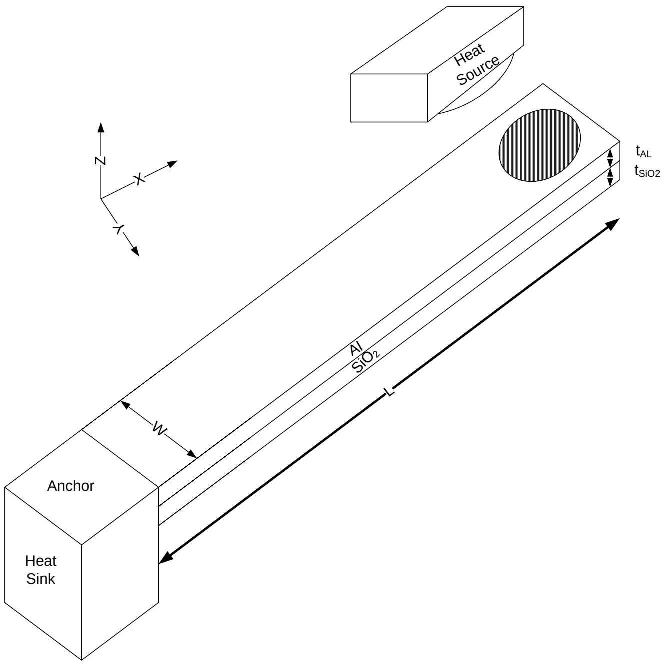

Figure 4.1: Three-dimensional (3-D) view of the electrothermal MEMS.

Figure 4.1 shows a three-dimensional (3-D) view of the simulated prototypical MEMS device and the associated co-ordinate system. The cantilever is made of two materials with different thermal expansion coefficients to achieve bimaterial effect. Initial choice of material is aluminum and silicon dioxide. The cantilever is anchored at the base to a bulk silicon wafer which also acts as the heat sink. In the simulation model the uneven surface of the cantilever and the heat source are represented with elliptical protrusion (bump). To initiate thermally actuated self-oscillation of the MEMS structure, it is brought in contact with the heat source by making contact between the two bumps to cause a flow of heat flux. The heat source temperature is denoted by T_{hot} and is varied in the numerical simulation to study the performance of the device. The heat sink is at room temperature and is denoted by T_{cold}. The length of the cantilever, L is varied for studying the performance response while the width, *w* is always taken as ¼ that of the length. In the 2-D approximation model used in the numerical simulation, heat propagation is assumed to be predominant along the length of the cantilever. Therefore the temperature distribution along the width of the cantilever is assumed to be minimal and the resulting curvature of the bimaterial structure due to thermal expansion to be negligible. Thickness of the materials is represented by d_{sub} where *sub* is replaced with Al, SiO_2 or any other material used for study purpose. Initially the thickness is taken to be 10μm.

Figure 4.1 shows a two-dimensional (2-D) cross-section of the simulated prototypical MEMS device. For studying the thermomechanical response, temperature and displacement of the cantilever at the tip are identified by the point A, located at co-ordinate $x = L$ and $z = d_{SiO2}$ (interface of the two materials). Thermal contact and heat transfer from the heat source to the cantilever is observed at point B in the epoch of the cantilever bump, and point E in the heat source bump. At points C and D located at 200μm and 300μm from point A, temperature is recorded to calculate for heat flux through the cantilever during self-oscillation.

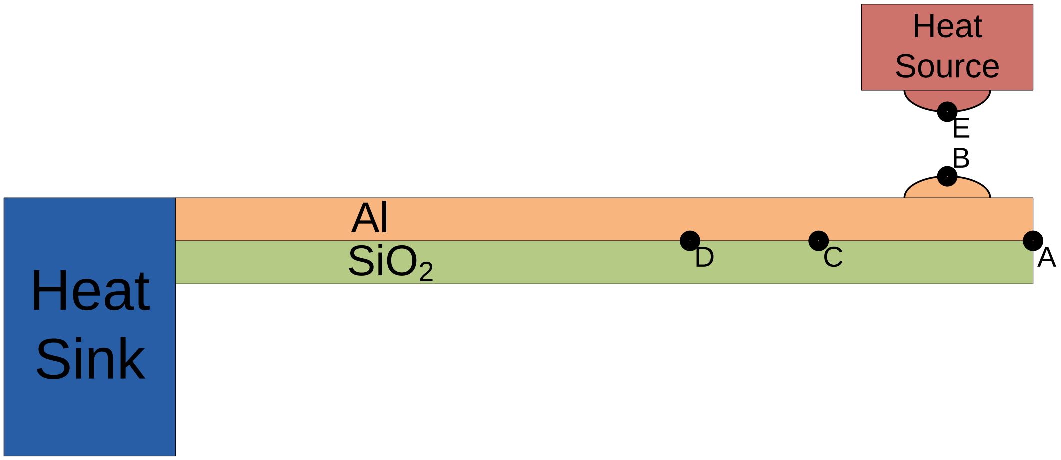

Figure 4.2: Two-dimensional cross-section of the electrothermal MEMS

4.1.2 Electrical Sub-System

The pyroelectric material and the measurement instruments constitute the electrical sub-system. The pyroelectric material of choice is polyvinylidene difluroethylene or (PVDF). The material is obtained from commercial source and is characterized to obtain dielectric constant and pyroelectric coefficient. These values are used in the numerical simulation. The response of the thermomechanical system determines the response of the electrical system. The temperature output from the thermomechanical sub-system is used as the input for the electrical sub-system, and the polarization and output current were observed at the materials surfaces.

4.2 Finite Element Modeling

Finite element method (FEM) is a numerical technique for solving partial differential equation (PDE) expressing a certain physical phenomenon in a geometrically defined domain. In this method the large domain is discretized into many sub-domains called mesh and is limited by boundary conditions. Using the boundary conditions and the physics-based equations, a continuous solution for certain parameters such as temperature, strain etc. at every point of the domain is found. Points between the mesh boundaries are interpolated.

A number of powerful software are available which allow the user to draw or import a geometrical structure and create a meshed sub-domain of the structure automatically or by customization. Meshing allows user to handle complicated geometry of a structure and to assign boundary conditions to them. The boundary conditions may define temperature, displacement, strain, applied force and other variables and are used as limiting conditions in the PDE to be solved.

4.2.1 Assumptions

In order to reduce the computational burden and to comply with software limitation some assumptions were made to simplify the numerical model. These assumptions are:

1. Heat source and heat sink are at respective constant temperatures. Thermal mass of the source and the sink are assumed to be much larger than that of the cantilever, so that the heat transferred between the source and the sink by the cantilever does not greatly affect their temperatures.
2. There is very low radiative heat exchange between source and the sink assuming the device is in vacuum.
3. Material properties are constant and isotropic.
4. Heat propagates along the length of the cantilever, and the heat flux distribution can be assumed 1-dimensional along x-axis only. Therefore temperature distribution along the width in y-axis is minimal and the thermal expansion of the material in y-axis is negligible. This assumption conveniently allows to approximate the model from 3-D to 2-D thereby greatly reducing the computational burden.
5. Pyroelectric material is embedded on top of the aluminum layer in the middle of the cantilever; therefore temperature recorded at 300 μm from the tip is taken as the temperature change experienced by the pyroelectric material to produce the pyroelectric current.
6. Electrodes connected to the pyroelectric sample have no effect on the heat transfer and provides low resistance path for the pyroelectric current.

4.2.2 Governing Equations

Temperature and displacement of the structure are calculated by solving for three-dimensional or two-dimensional (in the simplified form) thermal expansion strain equation coupled with heat equation. For heat conducting material with isotropic properties heat equation in Cartesian coordinates is expressed as,

$$\frac{\partial T}{\partial t} = \frac{k}{C_p \rho}\left(\frac{\partial^2 T}{\partial x^2} + \frac{\partial^2 T}{\partial y^2} + \frac{\partial^2 T}{\partial z^2}\right) \tag{4-1}$$

where, T is the temperature at time, t and k, C_p and ρ is thermal conductivity, specific heat capacity and mass density respectively. The heat transfer between the heat source and the cantilever is calculated by solving for the heat transfer equation,

$$Q = \frac{\Delta T}{{R_c}/{A}} \tag{4-2}$$

where, Q is the amount of the heat transferred, ΔT is the temperature difference between two surfaces, A the area of contact between two surfaces and R_c is the thermal contact resistance.

Thermal expansion of the material is calculated by solving for stress equation for linear expansion in one direction represented by,

$$\frac{\Delta L}{L} = \alpha_L \Delta T \tag{4-3}$$

where, $\Delta L/L$, is the stress experienced in a direction for temperature change ΔT in a material with thermal expansion coefficient α_L.

4.2.3 Initial and Boundary Conditions

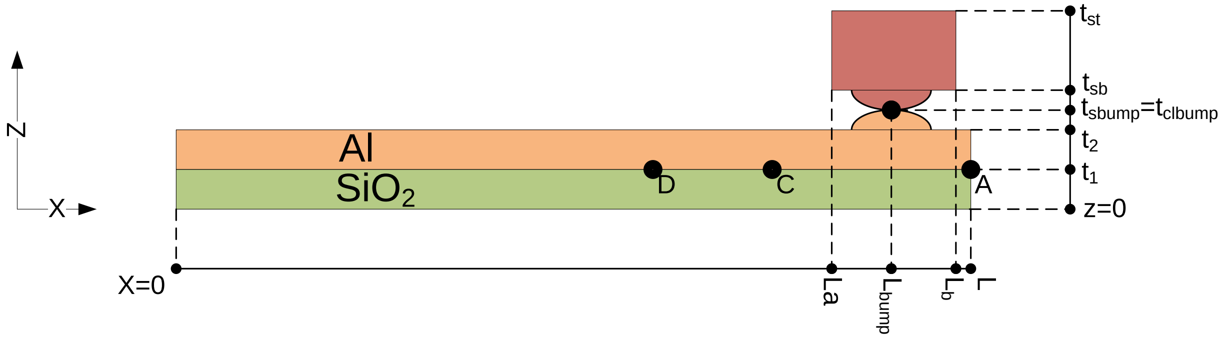

Figure 4.3: Dimensions of the MEMS structure for numerical simulation condition.

In numerical simulation the differential equation is required to be assigned with initial conditions to solve for the constants in the solution. For this particular problem initially the temperature is assumed to be at T_{low} in the heat sink and the cantilever and at T_{hot} for the heat source. The displacement, δ is initially assumed to be zero in all positions for all edges. This initial condition is mathematically represented as,

$$T = \begin{cases} T_{low}, & x = 0, \quad 0 < z < t_2 \\ T_{low}, & x = L_{bump}, z = t_{sbump} = t_{clbump} \\ T_{hot}, & L_a < x < L_b, t_{sb} < z < t_{st} \end{cases} \tag{4-4}$$

and

$$\delta = 0, \; 0 < x < L, 0 < z < t_{st} \tag{4-5}$$

The solutions of the PDEs are bounded by the boundary conditions. A fixed value or another equation defines the boundary relations. In case of the MEMS structure the anchored edge is maintained at T_{low} throughout the solution. The heat source boundaries are at T_{hot} except in the thermal contact boundaries where heat transfer equation is applicable. All other boundaries are considered thermally insulated. For deflection the anchored edge boundary is defined to have no deformation where all other boundaries are free to deform. The boundary conditions are mathematically expressed as,

$$T = \begin{cases} T_{low}, & x = 0, \quad 0 < z < t_2 \\ \dfrac{Q}{A/R_f}, & x = L_{bump,}\, z = t_{sbump} = t_{clbump} \\ T_{hot}, & L_a < x < L_b, t_{sb} < z < t_{st} \end{cases} \tag{4-6}$$

and

$$\delta(t,x) = \begin{cases} 0, & x = 0,\ 0 < z < t_2 \\ 0, & L_a < x < L_b, t_{sb} < z < t_{st} \\ equation\ \text{(3-5)}, & 0 < x < L, 0 < z < t_2 \end{cases} \tag{4-7}$$

4.2.4 Meshing

Finite element method simulation produces realistic results by breaking a large geometry into smaller domains and applying physics equations to the boundaries of these smaller domains. This procedure is known as meshing. Proper meshing is of great importance to achieving practical and realistic results. Large meshes can often provide inaccurate and misleading results. Meshes that are too small can be more accurate but requires large computational resource and sometimes becomes impossible to handle by software limitations. Therefore careful meshing techniques need to be applied to achieve optimized simulation results.

For the device to be simulated some areas are more important and prone to inaccuracy problems than others. Using a general mesh size for all areas is not sufficient to meet the computational accuracy limitations. Using software intelligence for meshing can sometimes fail to identify fine meshing requirements for specific physical equations being solved. Therefore a customized problem specific meshing steps have been adopted to create mesh for the said device.

The software used for simulation allows for different meshing geometries and techniques. Table 4-1 lists the domains with associated meshing geometries, dimension and techniques adopted. In the body of the cantilever, the simulation software solves for heat and tensile stress equations corresponding to thermal expansion. These equations can be satisfactorily applied to lumped geometries; therefore a coarse meshing in the bimaterial layers of the cantilever is sufficient. The temperature distribution in the heat source or the hot body is of less interest for the purpose of simulating self-oscillation and therefore a coarse meshing is also used for this domain. Using the software intelligence to define random mesh results in random mesh sizes to accommodate the minimal boundary length existing in that domain. Therefore using finer mesh element size using free triangulation technique in the above-mentioned domains generates large mesh elements (maximum 37 μm size) in the large domain of the bottom layer of the bimaterial and smaller mesh elements (minimum 0.125 μm size) in the small size domain in the bump present on the hot body. The top layer material of the cantilever body along with the contact bump is meshed separately to account for the finer mesh requirement associated with solving heat transfer equation.

Table 4-1: Mesh definition of the simulated device.

Domain	Meshing Geometry Type	Element size (μm)	Technique
Bottom material, heat source bump	Triangular	0.125 – 37	Free
Top material, hot body	Trapezoidal	0.125 – 37	Mapped
Cantilever bump	Trapezoidal	0.125 – 37	Swept

To maintain element size symmetry with the boundary of the adjacent domains, a mapped trapezoidal meshing technique is used in the body of the heat source and the top layer of the bimaterial cantilever. This results in mesh elements of comparable size in adjacent domains sharing a boundary, but not necessarily creates very fine mesh in mapped domain as the reference domain.

This technique saves computational burden as it reduces mesh numbers in less critical domain that the simulator has to calculate for. Although in domains that include boundaries where critical equations have to be solved a finer mesh is carefully defined. In the simulation of the proposed device the critical boundary equation is the heat transfer equation between the cantilever and heat source bump as the contact area in consideration is very small. Therefore, the boundary between these two domains is needed to be calculated with finer precision and requires the finest meshing achievable. In addition, the mesh sizes between these two boundaries should be comparable. Since the mapped meshing used for the top layer is a comparatively coarser mesh, the boundary specific swept mesh is used to split the mesh element adjacent to contact bump boundary to finer meshes. Meshing is characterized by a variable called mesh quality of elements that determine the symmetry of the mesh element. It is a number between 0 and 1 where 0.0 indicates a completely degenerated element and 1.0 represents a completely symmetric element. The goal of customized

(a)

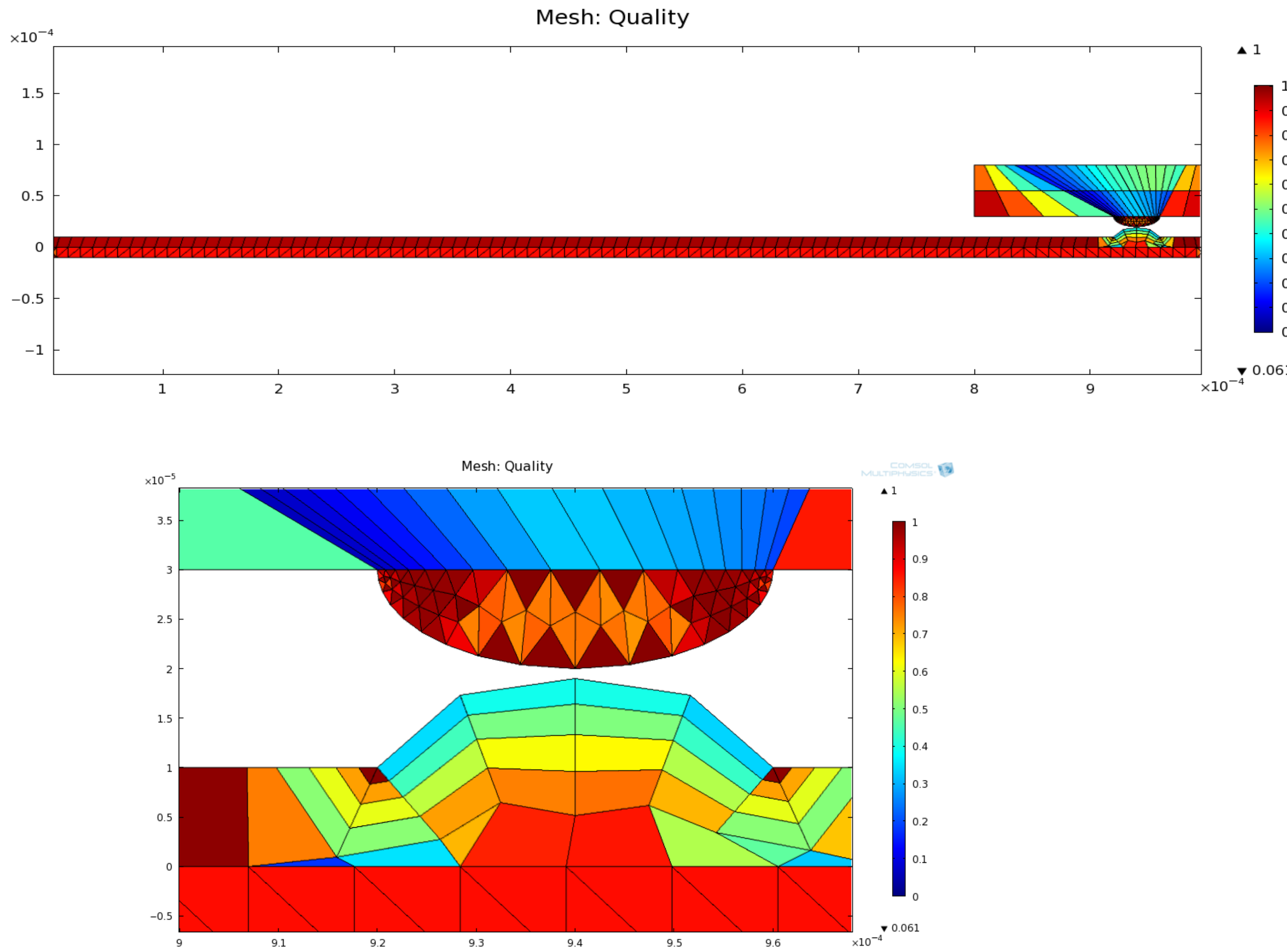

(b)

Figure 4.4: (a) Mesh definition of the proposed device. The color chart on the right represents the mesh quality where red indicates good and blue indicates poor mesh quality. (b) an enlarged view of the mesh definition in the contact bump area where heat transfer and contact equation is solved.

meshing is to remove degenerative or bad quality meshes from the geometry as much as possible and achieve a high quality overall mesh throughout the geometry. Figure 4.4 shows the mesh element quality of the geometry with a color bar where red indicates good and blue indicates poor quality mesh. The steps described above were followed to ensure the best achievable overall mesh quality in the device geometry.

The customized mesh used for simulation divides the 2-D geometric representation of the proposed device into total 467 elements of which 299 is triangular and 168 is quadrilateral. The worst mesh element quality is 0.06066 and average mesh quality is 0.8248. The worst quality mesh occurs in the heat source domain where the finite element solutions are not of interest.

4.2.5 Method of Solution

For this work COMSOL Multiphysics Version 3.5 through Version 4.1, a FEM software program, has been used for creating the geometry of the MEMS structure as well as for creating meshing and assigning boundary conditions and the PDE to be solved. The software program was separately executed in two machines, one of which is a DELL Latitude E6400 Laptop with Core 2 Duo processor and 4 GB of memory with Windows 7 OS, the second machine is a Macintosh with Intel Core i5 2.66 GHz processor and 4GB memory running Mac OS X version 10.6.6. The modeling began with simple most basic structures and the underlying physics with more complexities and interdependency were added in subsequent stages. Detailed procedure of creating a simulation model, definition of the physical equations, meshing and plotting and analysis of the results are provided in Appendix A.

4.3 Analytical Modeling

Although the finite element model is very accurate in predicting the behavior of structures under given conditions and circumstances they are time and resource consuming and require significant computational power. A simplified analytical model to calculate the parameters of design interest can greatly assist in design of the MEMS energy harvester. In this section attempt has been undertaken to express the parameters of interest using material properties and dimension as variables with physics based equations.

4.3.1 Time Dependent BiMaterial Thermomechanical Response

The analytical model is developed in steps, where the first step was to determine the temperature at the tip of the cantilever with time. It can be calculated if the thermal time constant of the structure in question is known. Thermal time constant is the time required for a certain volume of material at temperature T_1 to change the temperature by 63% of the temperature difference, when it is exposed to a temperature, T_2 , irrespective of the magnitude of the difference if the heat flux is unlimited. The thermal time constant of a structure is given by,

$$\tau_{therm} = \frac{C}{G} = \frac{mC_p}{\frac{wd}{L}g} = \frac{Lwd\rho C_p}{\frac{wd}{L}g} = \frac{L^2\rho C_P}{g} \tag{4-8}$$

where, C_P is the specific heat capacity and g is the thermal conductance of the material. For bimaterial structure the average of these values are considered. Temperature change in the material can be found by Newton’s law of cooling. It calculates the temperature change with time when the initial temperature difference and time constant are known.

$$\Delta T(t) = \Delta T(t=0)e^{\left(\frac{-t}{\tau_{therm}}\right)} \tag{4-9}$$

Now the temperature at time, *t* for an element that is uniformly heated can be calculated by,

$$T(t) = T_{hot} - \Delta T(t) \tag{4-10}$$

The deflection of the tip of a cantilever can be found from equation (3-5) for a given change in the temperature. Applying the value of *T(t)* from equation (4-10) to equation (3-5) will provide the time dependent displacement of the cantilever structure. This can be expressed as,

$$\delta(t) = \frac{3L}{h} \cdot \frac{(\alpha_1 - \alpha_2)(1+m)^2(T(t) - T_0)}{\left\{3(1+m)^2 + (1+mn)\left(m^2 + \frac{1}{mn}\right)\right\}} \tag{4-11}$$

However, equation (4-10) assumes that the material is being uniformly heated, whereas in the proposed scheme the cantilever beam being considered is heated through a point contact at the tip. As the heat propagates through the cantilever the temperature rises along the length with time. Therefore, the thermal time constant will be progressive for points along the length of the cantilever. For any point x along the length, the time constant can be expressed as,

$$\tau_{therm,x} = \frac{x^2 \rho C_P}{g} \tag{4-12}$$

Accordingly, since the beam is not uniformly heated, the effective length for the deflection at a time *t*, is the length *x*, i.e. up to the point the beam has been heated. If the cantilever is being heated from the free end then, deflection δ is given by,

$$\delta(t) = \frac{3L_{eff}^2}{h} \cdot \frac{(\alpha_1 - \alpha_2)(1+m)^2(T(t) - T_0)}{\left\{3(1+m)^2 + (1+mn)\left(m^2 + \frac{1}{mn}\right)\right\}} \tag{4-13}$$

where *T(t)* has been derived using equation (4-12) and (4-10). If the cantilever is being heated from the anchored end, then deflection is observed at point, x, and the deflection at the tip can be found by,

$$\delta(t) \ = \frac{\delta_{eff}}{L_{eff}} \times L \tag{4-14}$$

where δ_{eff} is the deflection calculated using equation (4-13). Effective bimorph length with time can be calculated the following way. Let us assume the initial temperature difference to be ΔT_0 and the effective length, L_{eff} and the corresponding thermal constant τ_1 at time *t*. At the thermal constant, the temperature difference reaches 63.2% of ΔT_0. Therefore L_{eff} can be calculated as follows:

$$\frac{\Delta T \times 0.632}{\Delta T} = 0.632 = e^{-\frac{t}{\tau_1}} \tag{4-15}$$

$$\Rightarrow \tau_1 = \frac{-t}{\ln(0.632)}$$

$$\Rightarrow \tau_1 = \frac{L_{eff}^2 \rho C_P}{g} = \frac{-t}{\ln(0.632)} = 2.18t$$

$$\therefore \ L_{eff}(t) = \sqrt{\frac{2.18t}{\rho C_P}} \tag{4-16}$$

In the self-oscillating bimorph structure as the heat propagates and the cantilever deforms, it loses contact with the heat source when the tip deflects a critical distance, $\delta_{critical}$. The cantilever is heated during the period until this deflection is attained. The heating period denoted by, $\tau_{heating}$ can be found by first calculating the critical displacement. For ease of calculation, it can be assumed that the temperature has to rise 63.2% of the difference in the cantilever body to cause critical displacement. Therefore, at $t = \tau_{heating}$, $\Delta T(t) = 0.367\Delta T_0$. The critical displacement can be found from effective deflection equation,

$$\delta_{critical} = \frac{3L_{eff}^2}{h} \cdot \frac{(\alpha_1 - \alpha_2)0.367\Delta T_0}{\left\{3(1+m)^2 + (1+mn)\left(m^2 + \frac{1}{mn}\right)\right\}} \tag{4-17}$$

$$\delta_{critical} = A \cdot L_{eff}^2 = \frac{2.18\tau_{heating}}{\rho C_P}$$

$$\tau_{heating} = \frac{A \cdot \delta_{critical} \cdot \rho C_P}{2.18} \tag{4-18}$$

During the heating period, the amount of thermal energy transferred to the cantilever body can be calculated by the following relation,

$$Q_T = \frac{\Delta T_0}{R_c/A} \times \Delta\tau_{heating} \tag{4-19}$$

where, R_c is the thermal interface resistance. It can be found from the equation and tables used by Yovanovich in [85] for aluminum surfaces.

The transferred heat increases the temperature in the cantilever body. For the amount of transferred heat, the temperature rise can be calculated by equation of heat conduction,

$$Q_T = K \times \Delta T \tag{4-20}$$

Considering the entire volume of the cantilever, the average temperature rise at the end of the heating period can be found by,

$$Q_T = K \times \Delta T_0 e^{-\tau_{heating}/\tau} \tag{4-21}$$

$$\frac{Q_T}{Ke^{-\tau_{heating}/\tau}} = T_{avg} - T_0$$

$$T_{avg} = \frac{Q_T}{Ke^{-\tau_{heating}/\tau}} + T_0 \tag{4-22}$$

The cantilever needs to dissipate this heat to return the temperature to T_{Low} to reinstate the cantilever beam to initial position or at less than $\delta_{\mathrm{critical}}$ displacement. Since it was assumed that $\delta_{critical}$ occurs at 63.2% of the temperature rise, it can be conveniently assumed that when the temperature decreases to 63.2% of the difference it reaches $\delta_{critical}$ displacement. If the time required for decreasing the temperature by $0.63\,(T_{avg}-T_{low})$ is $\tau_{cooling}$, then the cooling period can be found by,

$$\frac{\Delta T \times 0.632}{\Delta T} = 0.632 = e^{-\frac{\tau_{cooling}}{\tau}} \tag{4-23}$$

$$\Rightarrow \tau_{cooling} = -\tau \times \ln(0.632)$$

$$\Rightarrow \tau_{cooling} = 0.489\tau \tag{4-24}$$

Therefore, complete period of one oscillation, τ_{SO} is expressed by,

$$\tau_{SO} = \tau_{heating} + \tau_{cooling} \tag{4-25}$$

4.3.2 Pyroelectric Current Modeling

The pyroelectric current can be easily modeled using the theoretical equation 2-6 combining that with temperature variation found from the above section. The pyroelectric current for temperature cycling is calculated by,

$$I = \rho A \frac{\partial}{\partial t} T(t) \tag{4-26}$$

The temperature in the middle of the cantilever as experienced by the PE can be expressed as,

$$T_{middle} = \begin{cases} \Delta T_0 e^{-t/\tau_{middle}}, & 0 < x < \tau_{heating} \\ -\Delta T_0 e^{-t/\tau_{middle}}, & \tau_{heating} < x < \tau_{SO} \end{cases} \tag{4-27}$$

4.3.3 Harvested Power and Efficiency

The average power that can be harvested from the pyroelectric cycle can be found by integrating the energy over a period of time of the temperature cycle. Assuming that the period is equal to two thermal time constants,

$$P_{avg} = \frac{1}{\tau_{SO}} \int_0^{\tau_{SO}} I^2 R_{Load} dt \tag{4-28}$$

I is found from equation (4-26)**.**

R_{Load} = resistive load placed in series with the pyroelectric capacitance to ground.

Using maximum power transfer theory the optimum load impedance can be found by equalizing the power in the source and load. Since the impedance in the PE is purely capacitance, for a given frequency, *f* the optimum load impedance is found to be,

$$R_{Load} = \frac{1}{4fC_0} \tag{4-29}$$

where, C_0 is the impedance of the PE. The Maximum power harvested from the PE element can therefore be calculated using equation (4-32)

$$P_{max} = \frac{\rho^2 A^2 f \Delta T}{C_0} \tag{4-30}$$

where, f is the frequency of self-oscillation and ΔT is the maximum temperature difference.

4.3.4 Thermomechanical Response of Multilayer Cantilever Beam

The analytical model developed so far calculates bimaterial MEMS response characteristics. However, deposition of polymeric pyroelectric material also affects the response of the MEMS structure. For a multilayer cantilever the thermal response changes with the effect of thermal capacitance and conductance. For multilayer it can calculated as,

$$\mathrm{G}_{eff} = \frac{\sum g_i d_i}{\sum d_i} \cdot \frac{A}{L} \tag{4-31}$$

and $$\mathrm{C}_{eff} = \frac{\sum c_i d_i}{\sum d_i} \cdot L \cdot A \tag{4-32}$$

Although it has been designed to have PE on the outermost layer of the cantilever, it can also be embedded between bimorph layers. In such case the deformation will be greatly affected by the embedding of PE. An N-layer cantilever cross-section is assumed in this analysis as shown in Figure 4.5.

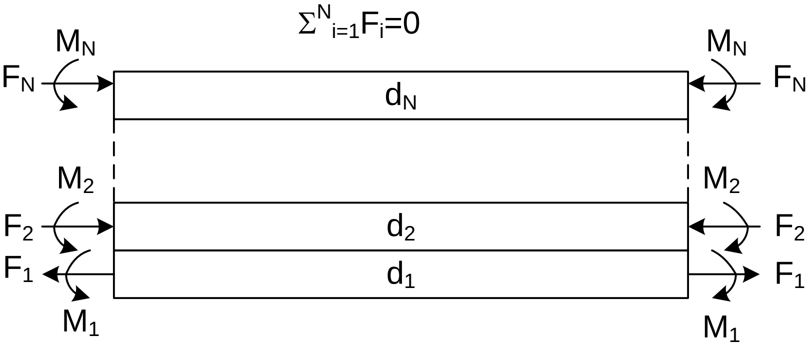

Figure 4.5: Distribution of force and momentum in part of a multilayer cantilever beam.

After deformation the cantilever is at static equilibrium, i.e. the summation of the forces acting upon it is zero and the strains in two materials at the interface are equal. Solving for the balanced force and the strain equation one can obtain the radius of curvature, r_C following the derivation method presented in [86],

$$\frac{1}{r_C} = -\frac{2\sum_{i=2}^{n} A_i C_i}{4\sum_{i=1}^{n} E_i I_i + \sum_{i=2}^{n} B_i C_i} \tag{4-33}$$

where,

$$A_i = \left(-\alpha_i + \frac{\sum_{i=1}^{n} \alpha_i E_i d_i w_i}{\sum_{i=1}^{n} E_i d_i w_i}\right) \Delta T E_i d_i w_i \tag{4-34}$$

$$B_i = \left(C_i - \frac{\sum_{i=2}^{n} C_i E_i d_i w_i}{\sum_{i=1}^{n} E_i d_i w_i}\right) E_i d_i w_i \tag{4-35}$$

$$C_i = -d_i + 2\sum_{j=2}^{i-1} d_j + d_1 \tag{4-36}$$

Here, *E* is the young’s modulus, *w* is the width of the beam and *I* is the moment of the layer. From the radius of curvature the deflection at the tip can be calculated as,

$$\delta(t) = \frac{L^2}{2r_C} \tag{4-37}$$

4.4 SPICE Modeling Of Thermoelectrical MEMS

For integration of the MEMS with CMOS circuit for further conditioning and electrical storage of harvested current, a SPICE model of the thermomechanical MEMS device along with the pyroelectric energy conversion is required. This will greatly assist complete design of the system from thermal to electrical part of the energy conversion system.

The first step towards developing a SPICE model of electrothermal MEMS is identifying their electrically analogous parameters. Electrical analog of thermal variables are listed in Table 4-2.

Table 4-2: Analogy between thermal and electrical parameters.

Property	**Thermal**	**Electrical**	Property
Temperature	T	V	Voltage
Heat Flux	Q	I	Current
Thermal resistivity	λ	ρ	Resistivity
Thermal capacitance	C_P	C	Capacitance

Effective thermal resistance and capacitance of the MEMS structure are found from equation (4-31) and (4-32). For a 1 mm long, 250 μm wide cantilever made of SiO_2 and Aluminum of 10 μm thickness, each thermal resistance and capacitance has been calculated to be,

$$\mathrm{R}_{th} = \frac{\sum d_i}{\sum \lambda_i d_i} \cdot \frac{L}{A} = 991.45 \times 10^6 \ {}^{K}\!/_{W} \tag{4-38}$$

and $$\mathrm{C}_{th} = \frac{\sum c_i d_i}{\sum d_i} \cdot L \cdot A = 4.975 \ \times 10^{-18} \, {}^{W.s}\!/_{K} \tag{4-39}$$

Thermal response of the structure can be found by calculating for the thermal time constant, τ_{th}, given as,

$$\tau_{th} = \mathrm{R}_{th} \cdot \mathrm{C}_{th} = 24.66 \, ms \tag{4-40}$$

For an electrical system analogous to the thermal system, an equivalent circuit with the same time response can be found. Using filter theory and Foster equivalent circuit such a network can be drawn [87-90]. The Foster equivalent circuit contains two poles and the equivalent circuit is represented by a two-stage and two R-C ladder networks. The poles and values of R-C in the two branches can be calculated following these equations [91],

$$\mathrm{P}_n = -\frac{\pi^2}{4} \cdot \frac{(2.n-1)^2}{\mathrm{R}_{th} \cdot \mathrm{C}_{th}} \qquad n = 1 \ldots \infty \tag{4-41}$$

Then, $$\mathrm{P}_1 = 248.87 \times 10^3 \ \rightarrow t_1 = 4.018 \mu s$$

$$\mathrm{P}_2 = 2.2398 \times 10^6 \ \rightarrow t_2 = 446.5 ns \tag{4-42}$$

Here, t_1 and t_2 are time constants. The corresponding magnitude of the R-C stages for these time constants are found by,

$$\mathrm{R}_{F_n} = \mathrm{R}_{th} \frac{8(-1)^{n+1}}{\pi^2 (2.\mathrm{n}-1)^2} \cdot sin\left(\frac{\pi}{2}(2n-1)\frac{x}{L}\right) \qquad n = 1 \ldots \infty \tag{4-43}$$

Then, $$\mathrm{R}_{F_1} = 2009 \, \Omega \ \rightarrow C_{F_1} = \frac{t_1}{\mathrm{R}_{F_1}} = 2 \, nF$$

$$\mathrm{R}_{F_2} = 223.23\ \Omega \rightarrow C_{F_2} = \frac{t_2}{\mathrm{R}_{F_2}} = 2\ nF \tag{4-44}$$

Foster equivalent circuit for the full length of the cantilever is shown in Figure 4.6. Foster network is a one-port network which is not most convenient to apply temperature inputs as voltage. Therefore, Cauer 1st order transformation is performed to convert it to a two-port R-C ladder network.

To perform Cauer transformation first equivalent impedance of the circuit is derived as,

$$\mathrm{Z(s)} = \frac{R_{F_1}}{1 + sR_{F_1}C_{F_1}} + \frac{R_{F_2}}{1 + sR_{F_1}C_{F_2}}$$

$$\therefore \quad \mathrm{Z}(s) = \frac{8.92s + 4464.44}{11.1 \times 10^{-6}s^2 + 11.1 \times 10^{-6}s + 1} = \frac{M(s)}{N(s)} \tag{4-45}$$

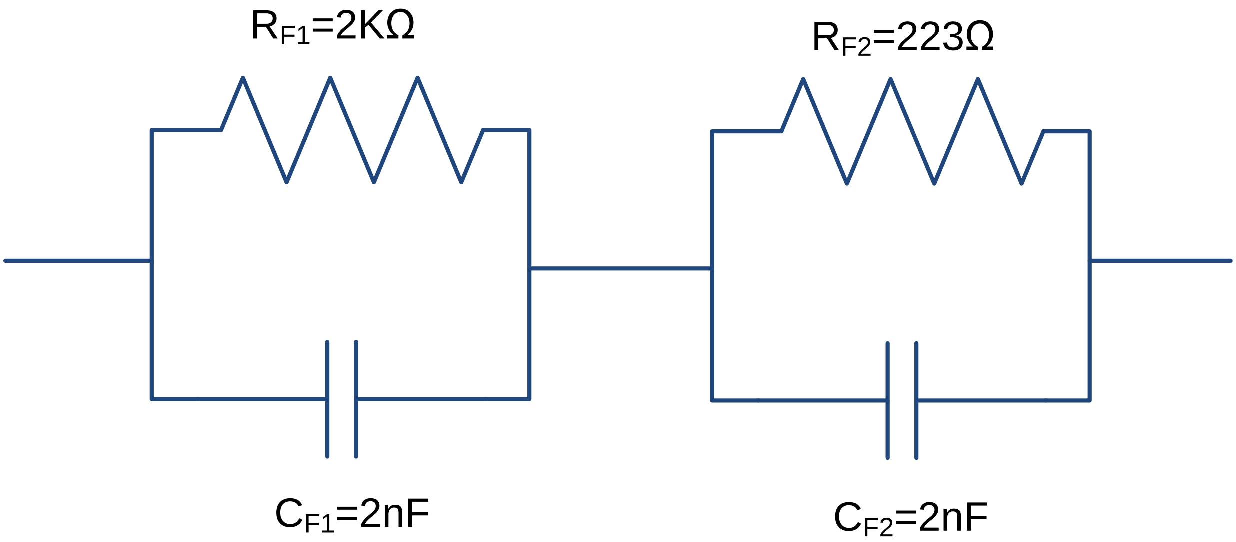

Figure 4.6: Foster equivalent circuit of a thermal MEMS structure.

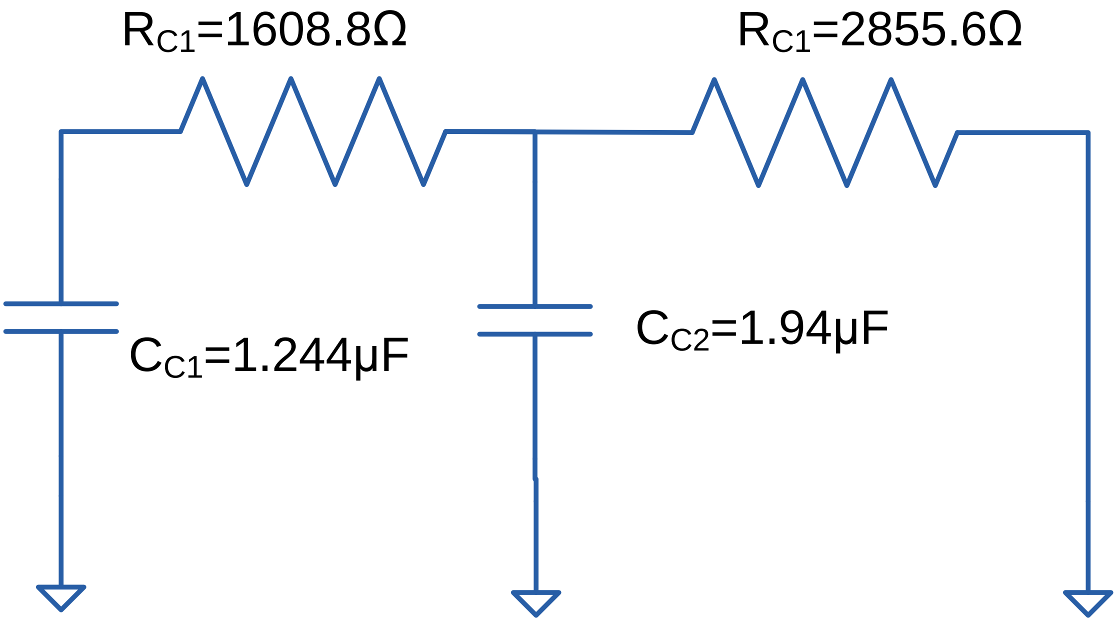

Figure 4.7: Cauer R-C ladder network representation of the thermal MEMS.

The Cauer R-C ladder is shown in Figure 4.7. The values for resistors and capacitors are found by expressing impedance Z(s) in the form presented in equation (4-46), [92].

$$\therefore \quad \mathrm{Z(s)} = C_{C_1}s + \cfrac{1}{R_{C_1} + \cfrac{1}{C_{C_2}s + \cfrac{1}{R_{C_2}}}} \tag{4-46}$$

Voltage at the right node represents the temperature at the tip of the cantilever when heated from the opposite end of the cantilever. To find temperature at any point, x, corresponding R_{F1} and R_{F2} have to be calculated to obtain the final R-C ladder network.

Assuming the cantilever is uniformly heated, the temperature at the tip is also experienced by the pyroelectric material. The PE can be necessarily modeled as a ferroelectric capacitor [93], whose charge is dependent on temperature. In [94], Wei et al. presents ferroelectric capacitor as a capacitor whose charge is dependent on the voltage across it. In the analogous circuit the capacitor charge is dependent on the voltage across it. The current flowing in the capacitor is proportional to rate of change of voltage, i.e. temperature. A current controlled current source that supplies a current proportional to the current flowing through the pyroelectric capacitor is representative of the pyroelectric current. The thermal and electrical equivalent circuit for the SPICE model is presented in Figure 4.8. The value of the pyroelectric capacitor can be found by,

$$\mathrm{C} = \frac{\varepsilon A}{d_{pyro}} = \rho A \tag{4-47}$$

where, ε is dielectric constant of the pyroelectric material. The complete thermomechanical system can be modeled in SPICE using more complex parts such as amplifiers and comparators. A possible model of the complete system is presented in Figure 4.9.

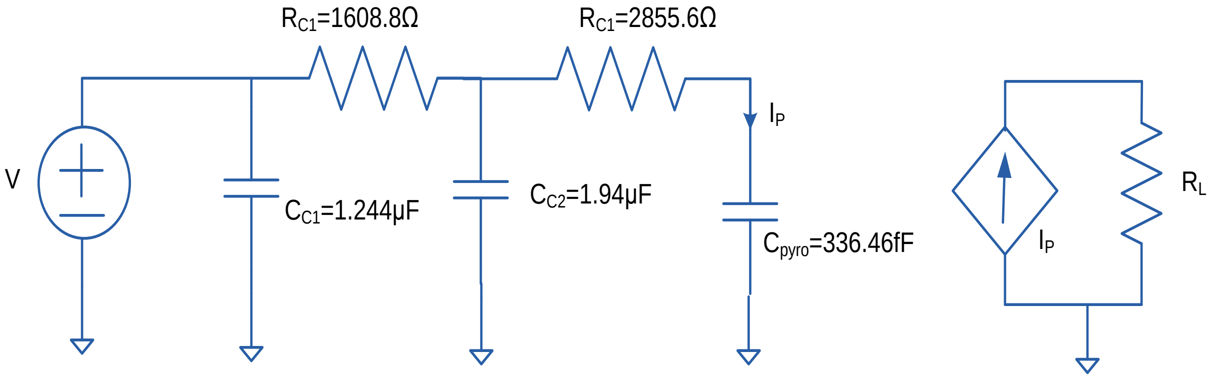

Figure 4.8: SPICE model of the thermal and pyroelectric MEMS device.

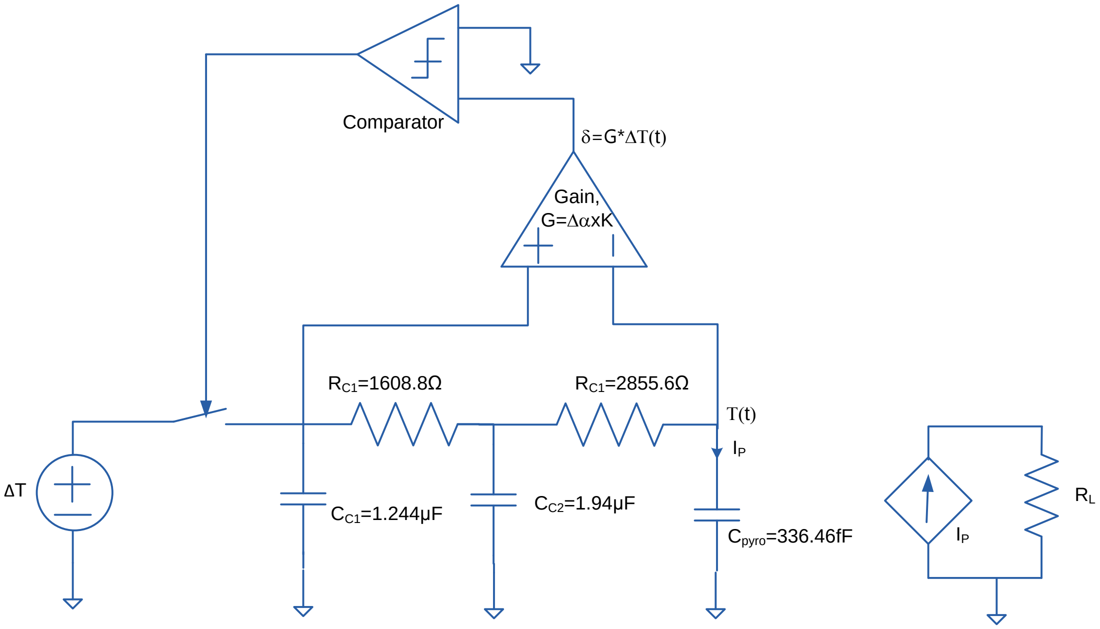

Figure 4.9: SPICE equivalent of the thermomechanical-pyroelectric self-oscillating MEMS.

SPICE netlists of the models are provided in appendix C.

4.5 Results and Discussion

4.5.1 Finite Element Solutions

4.5.1.1 Heat conduction and bimaterial behavior study

To begin with finite element modeling of the MEMS device, most basic part of the structure i.e. a bimaterial cantilever structure was studied. The physics involved in this MEMS device is the heat conduction and the mechanical stress strain distribution. In the first step the thermal response of the structure was studied. The geometric parameters or the dimension of the structure was varied over a feasible range to observe its effect on the thermal response time. Thermal response of interest was the thermal time constant, i.e. the time required by a structure to reach approximately 63.2% of the set temperature. Since the thermal response is dependent on the thermal capacitance and the

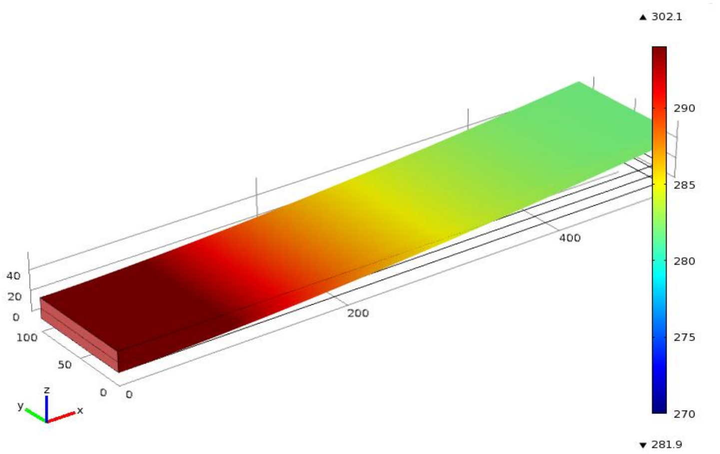

Figure 4.10: FEM 3-D Model of the bimaterial MEMS cantilever structure and its temperature distribution.

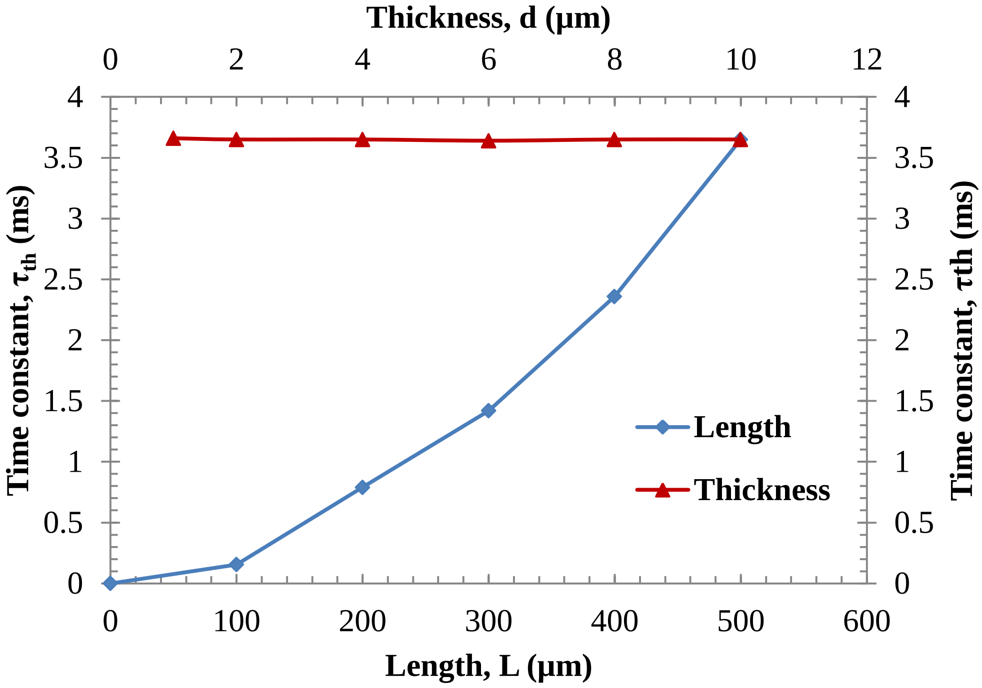

Figure 4.11: Bimaterial thermal response from FEM model with variable length and thickness.

conductance of the material, with increasing length the thermal time constant suffered a reduction and vice versa. Varying the thickness or the width of the structure did not affect the thermal response by far. Figure 4.10 shows the model of a bimaterial (SiO_2/Al) cantilever with fixed temperature at the boundary located near the origin of the graph and the temperature distribution across the length of the cantilever. Figure 4.11 reports the effect on thermal time constant with variable length, width and thickness of the cantilever structure. In the subsequent stages, mechanical stress and strain analyses in response to thermal expansion are included. The thermal expansion variable is linked to the time varying temperature change occurring due to the heat conduction. The thermal as well as the mechanical responses are observed over a range of geometric parameters to determine the desired range of the dimension for the MEMS structure. Another variable of interest is the elasticity of the materials in use and these values were varied over a range of theoretical values to observe the mechanical response. Mechanical strain and the deformation due to the thermal expansion are identified by the deflection of the tip of the cantilever from its original position in the z-direction. Figure 4.12 looks at the tip deflection, δ with varying length and thickness. It is evident from this plot that because of the lever like structure, the deflection at the tip is due to strain experienced at the base of the cantilever amplified by the length of the structure. In addition, the thicker the cantilever, lesser is the strain and the expansion of the structure in the x-direction, therefore less deflection in the z-direction. Figure 4.13 looks at both thermal and mechanical responses of the cantilever as the thickness ratio of the two materials used in the bimaterial structure is varied. Since Aluminum has higher thermal conductivity, increasing the thickness of Aluminum reduces the time constant. This response is observed because with increased aluminum thickness more heat is transferred to the bimaterial structure and the deflection increases up to an optimum point. The advantage begins to suffer as thickness increase leads to stiffness increase of the bimaterial structure. Figure 4.14 also looks at the thermomechanical response of the cantilever with variable ratio of elasticity between the two materials in the structure. The time constant remains constant irrespective of the change in Young's modulus. Tip deflection response improves as the material with higher thermal expansion coefficient becomes more rigid and until it is on par with the less expansive material. Higher rigidity of expanding material curtails the deformation.

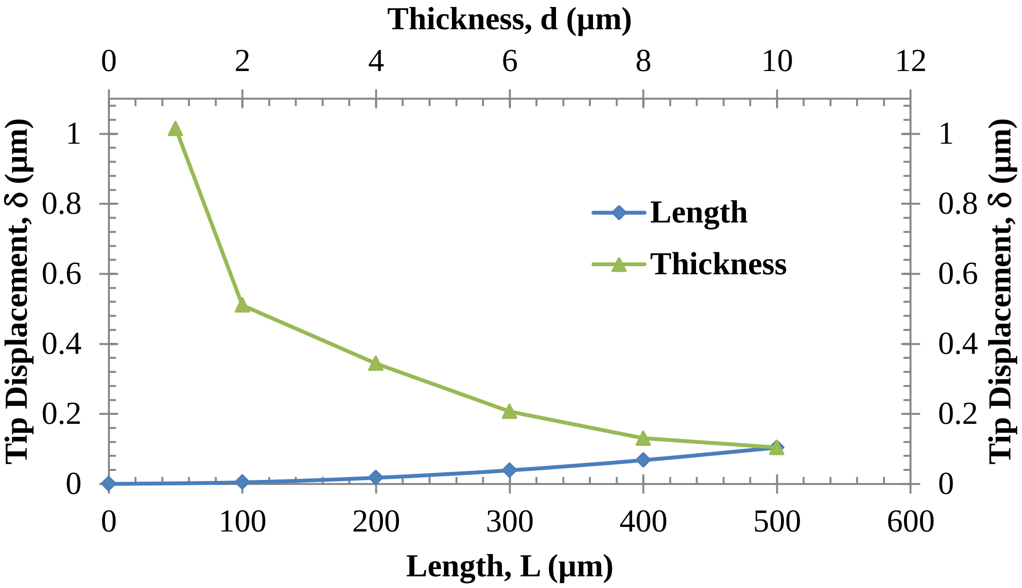

Figure 4.12: Bimaterial mechanical response from simulated FEM model with variable length and thickness.

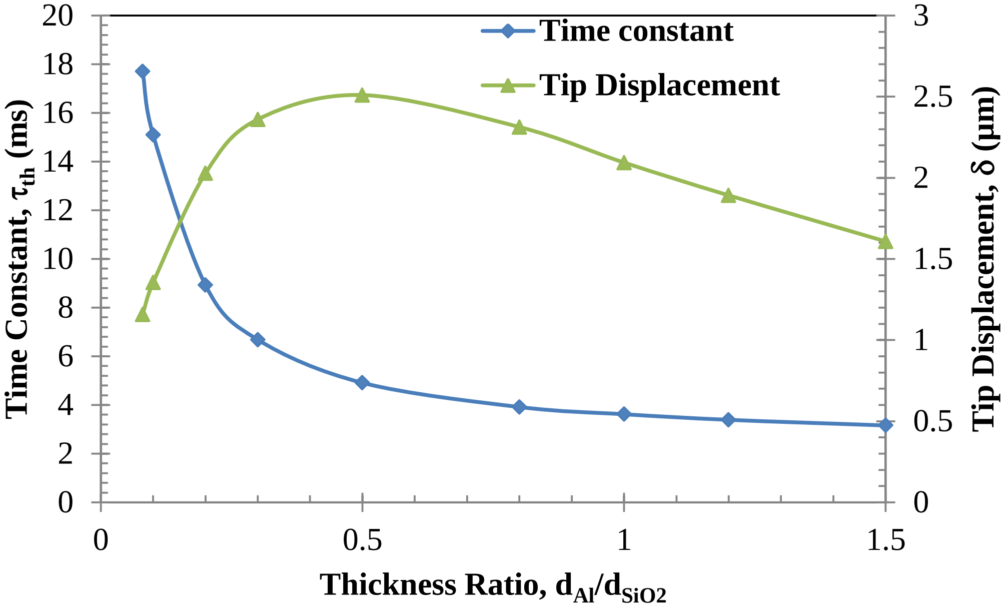

Figure 4.13: Bimaterial thermomechanical response with variable thickness ratio of Al and SiO_2.

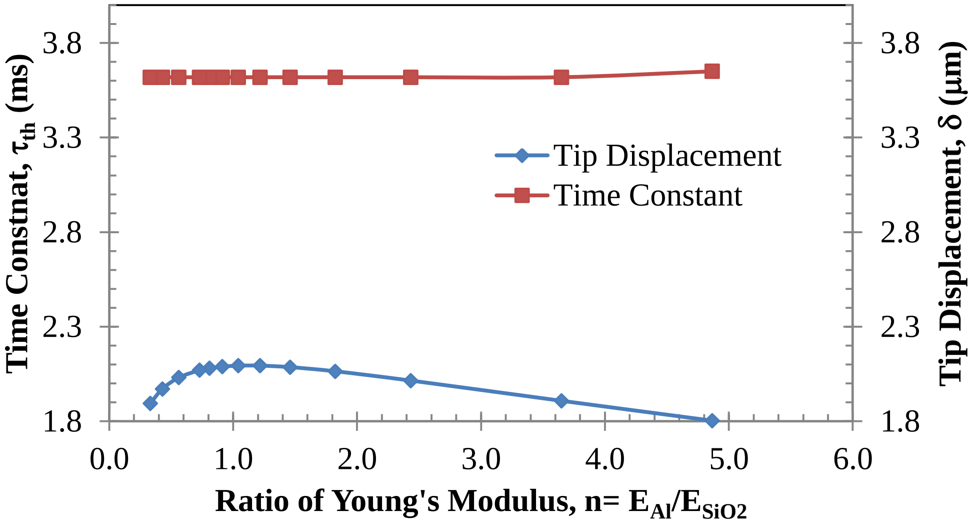

Figure 4.14: Bimaterial thermomechanical response with variable elasticity of material.

4.5.1.2 Temperature Cycling Study

Once a convincing finite element model of the bimaterial cantilever is developed, its performance with temperature cycling was studied to determine the optimum frequency for temperature cycling and fatigue and the hysteresis effects with the mechanical stress and the strain. Figure 4.15 shows the thermomechanical response of the bimorph cantilever during a low temperature point in the temperature cycle. The temperature was varied from 273 K to 313 K over 35 ms time period. This period was found to be agreeable with the thermal time constant of the structure to reach the set point value of the temperature. The input temperature was varied at the anchored boundary (base) of the structure. Figure 4.16 shows the time varying output temperature at the tip of the cantilever as well as the set point temperature at the base of the cantilever. The set point temperature is altered between 20K above and below the room temperature (RT = 293K). The cantilever is assumed to be flat and at zero displacement at room temperature which is used as reference temperature for thermal expansion calculation. Decreasing the temperature below RT results in bending of the cantilever in one direction and, increasing the temperature results in deformation in the opposite direction.

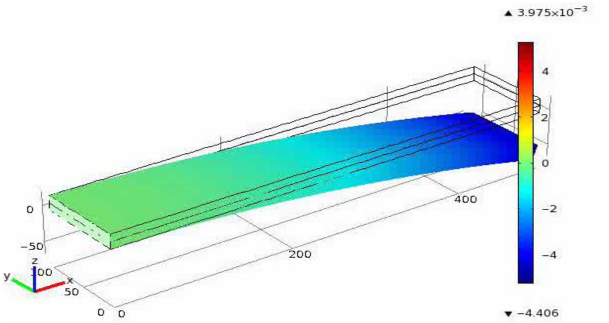

Figure 4.15: Thermomechanical response of the bimorph structure with time simulated using the FEM .

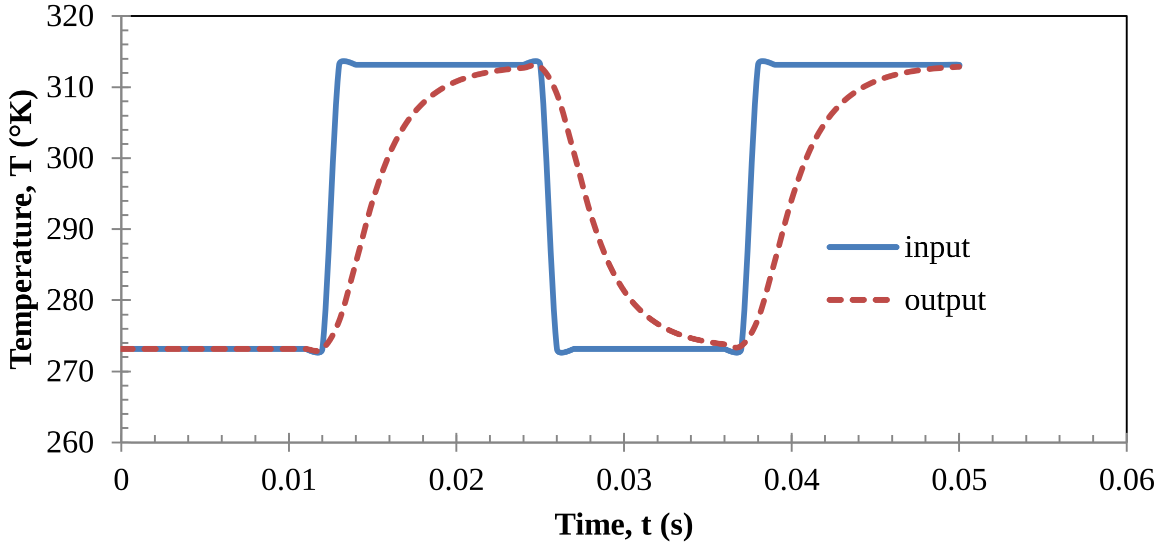

Figure 4.16: FEM modeling of thermal response of the bimorph structure with time

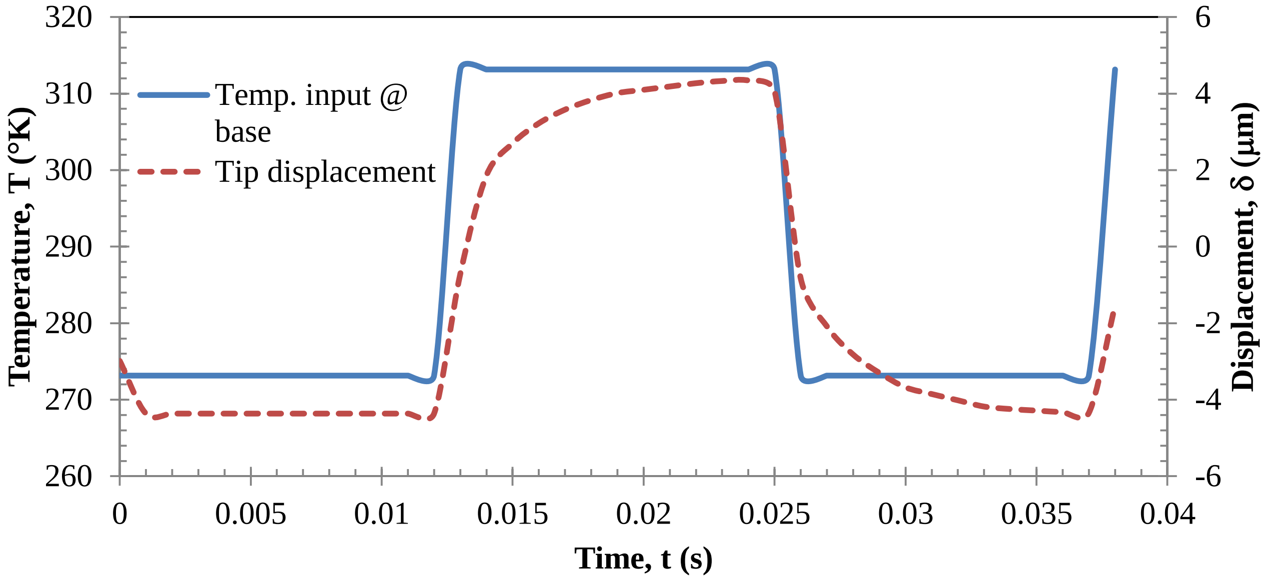

Figure 4.17: FEM modeling of mechanical response of the bimorph structure with time.

4.5.1.3 Self-Oscillation Study: Criteria for Self-Oscillation

After a satisfactory model of a temperature cycling bimorph cantilever is achieved, the criteria required for a self-oscillating structure is researched. In the previous step the oscillation observed was by means of forced temperature cycling. In the modified simulation, the cantilever base is connected to the heat sink and the tip of the cantilever is brought into contact with the heat source. Figure 4.18 shows the two-dimensional finite element model of the self-oscillating cantilever structure and the temperature distribution at the initial condition. As the proof mass makes thermal contact, the cantilever is heated up from the tip as seen in Figure 4.19. With heat propagating through the body of the cantilever, the bimaterial deflects away from the heat source as pictured in Figure 4.20. Small but sufficient entropy of heat is transferred to the cantilever body that increases the temperature and causes thermal expansion before it deflects away from the heat source. The strain in the cantilever body mostly occurs at the tip and to the right of the midpoint of the structure due to the temperature increase. Hardly any strain occurs at the base since it is kept at the heat sink temperature. The transferred heat is dissipated through the base connected to the heat sink. Figure 4.21 shows the heat flux being absorbed by the heat sink as the cantilever cools down and returns to its initial position. Once the cantilever is cooled to the initial temperature, it returns to its previous position and reestablishes thermal contact with the heat source which is pictured in Figure 4.22. The process begins to repeat itself at regular period. Thus self-oscillation of the MEMS perpetually continues.

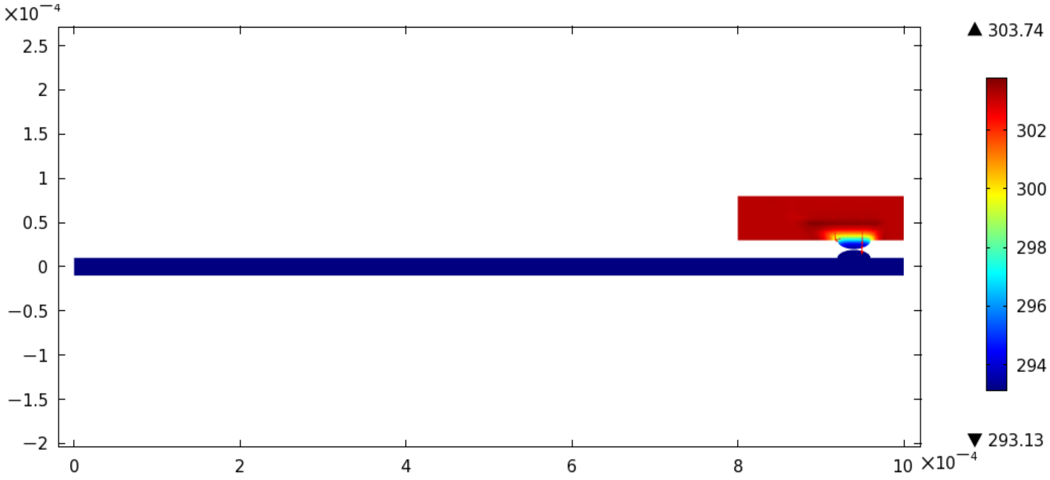

Figure 4.18: Starting self-oscillation at t=0ms. To initiate self-oscillation the cantilever proof mass is brought in contact with the heat source surface which is at 10K higher temperature than the cantilever body. The colored scale on the right represents temperature data. X and Y axis represents dimension and position in meters.

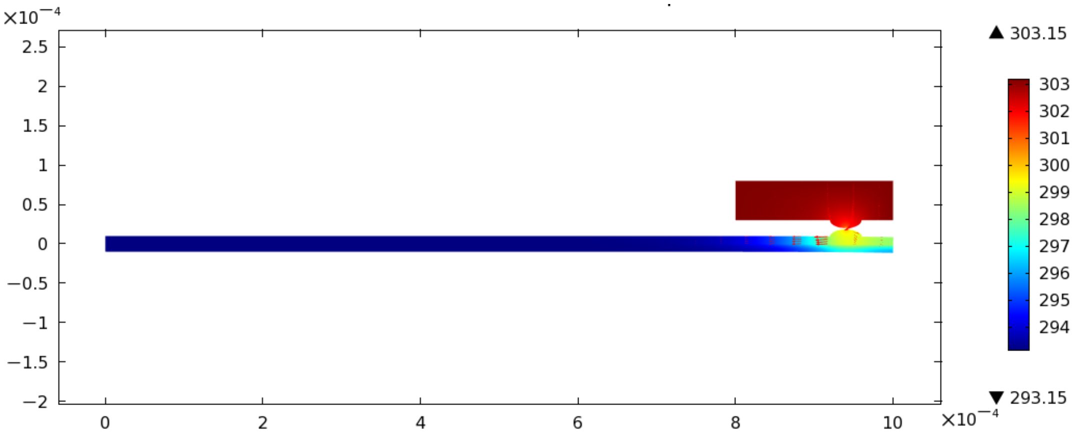

Figure 4.19: At t =0.1ms heat conducts from the source to the body of cantilever through the contact area between the cantilever proof mass and the heat source surface. The colored scale on the right represents temperature data. X and Y axis represents dimension and position in meters. Small red arrows in the body of the cantilever represent heat flux magnitude and direction.

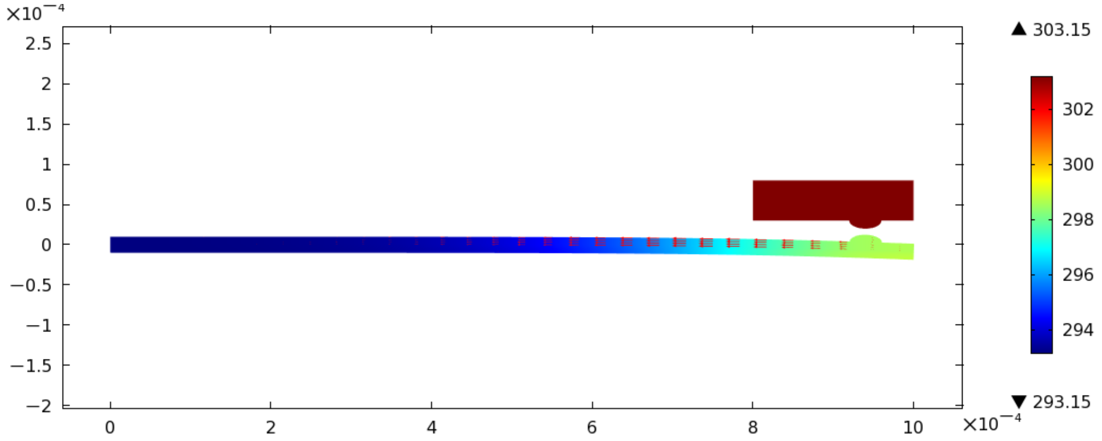

Figure 4.20: At t = 1ms due to temperature increase deformation of the cantilever beam is observed as heat propagates. Contact between heat source and cantilever is lost and the cantilever begins to cool down. The colored scale on the right represents temperature data. X and Y axis represents dimension and position in meters. Small red arrows in the body of the cantilever represent heat flux magnitude and direction.

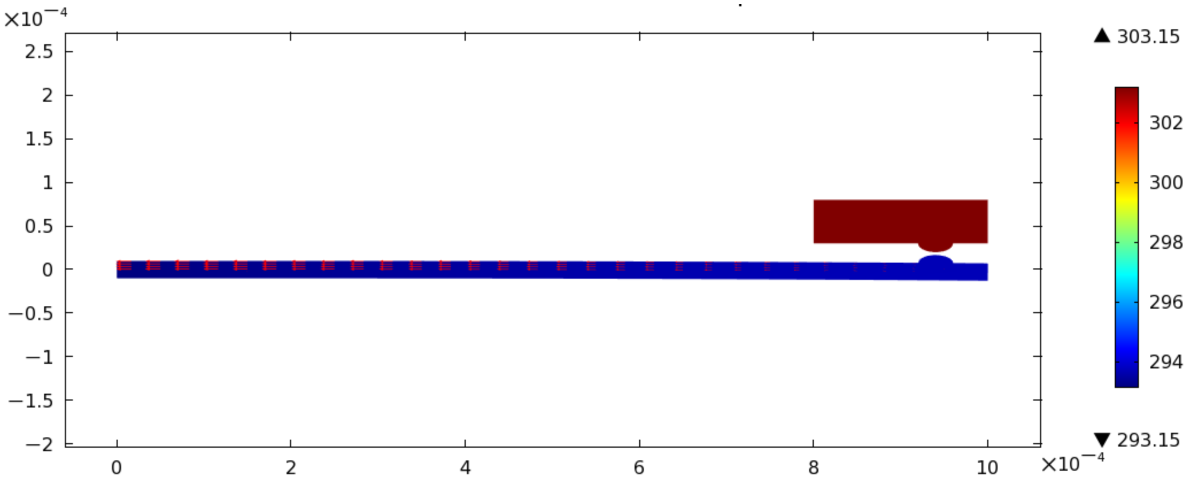

Figure 4.21: Heat flux transferred to the body of the cantilever is absorbed by the heat sink, as seen by the red arrows representing heat flux. As the cantilever temperature decreases it reverts back towards its initial position.

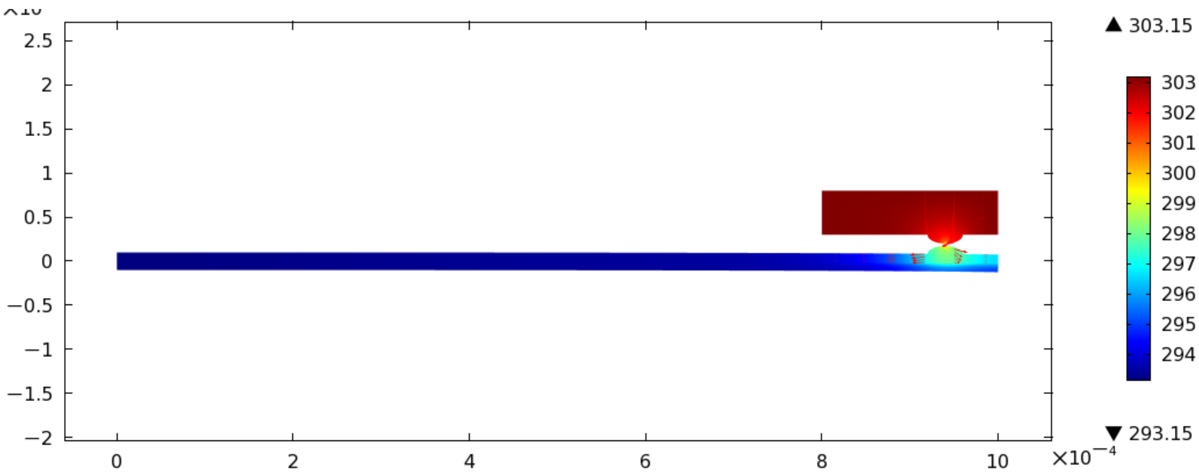

Figure 4.22: Heat flux dissipated through the heat sink and cantilever return to initial position and resumes contact with the heat source. Heat flux from the source is transferred to the cantilever through the surface indicated by red arrows representing heat flux.

Figure 4.23 illustrates the temperature variation at the tip of the cantilever structure and Figure 4.24 shows the deflection of the tip with temperature cycling. The period of oscillation for the cantilever in this case is approximately 33 ms. Dimension of the cantilever was 1 mm in length, 10 µm in thickness for SiO2 and 10 µm for Al layer. The heat source was at 150 K higher temperature than the heat sink. Ambient room temperature of 293 K is assumed for the initial condition and the radiative or the convective heat transfer was not accounted for the vacuum condition. Thermal contact conductance depends on contact surface, area and roughness, materials and their thermal conductivity. Since these parameters, especially contact area and roughness is not a variable parameter in the COMSOL simulation tool, the thermal contact conductance has been mimicked by a thermally conducting layer with variable thermal conductivity and continuous heat transfer between this layer and the cantilever bump.

Using the software to solve for thermal conduction problem, parameters such as contact layer thermal conductivity (to mimic change of thermal contact conductance), heat source temperature, device aspect ratio and different material with different thermal conductivities and expansion coefficients were varied and the effect on the resonance frequency, tip deflection of cantilever, the amount of heat cycled per period and the overall thermal power flow data have been collected. It was observed that the frequency increases with reduced contact conductance and reduced heat source temperature (Figure 4.25). This is because conductance and temperature allows more heat flux to be transferred to the cantilever. With a given thermal response the cantilever requires longer time to dissipate this heat to the heat sink, thereby increasing the cooling time, τ_{cooling}. Therefore the period of oscillation increases with increased contact conductance and heat source temperature.

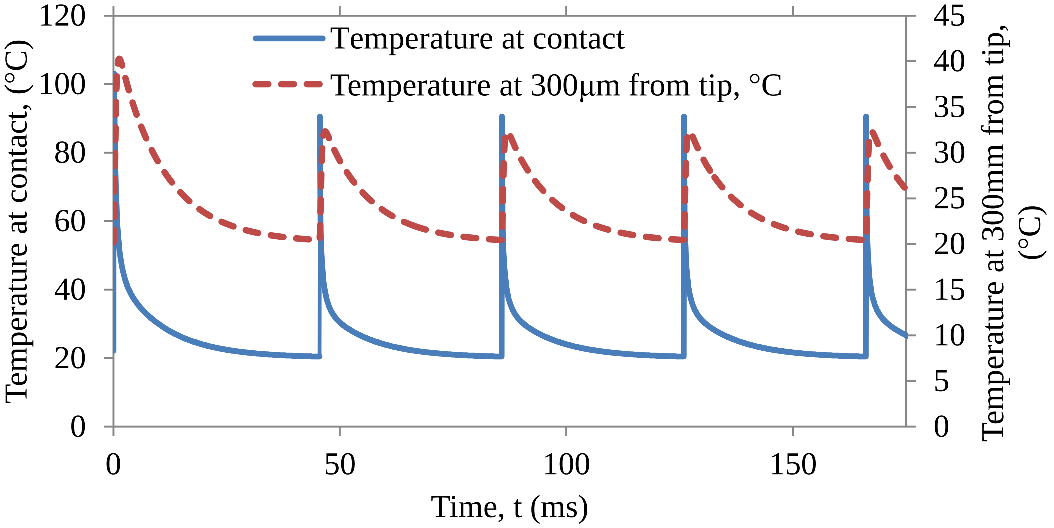

Figure 4.23: Temperature at the heat source-cantilever contact point and at 300μm away from the tip.

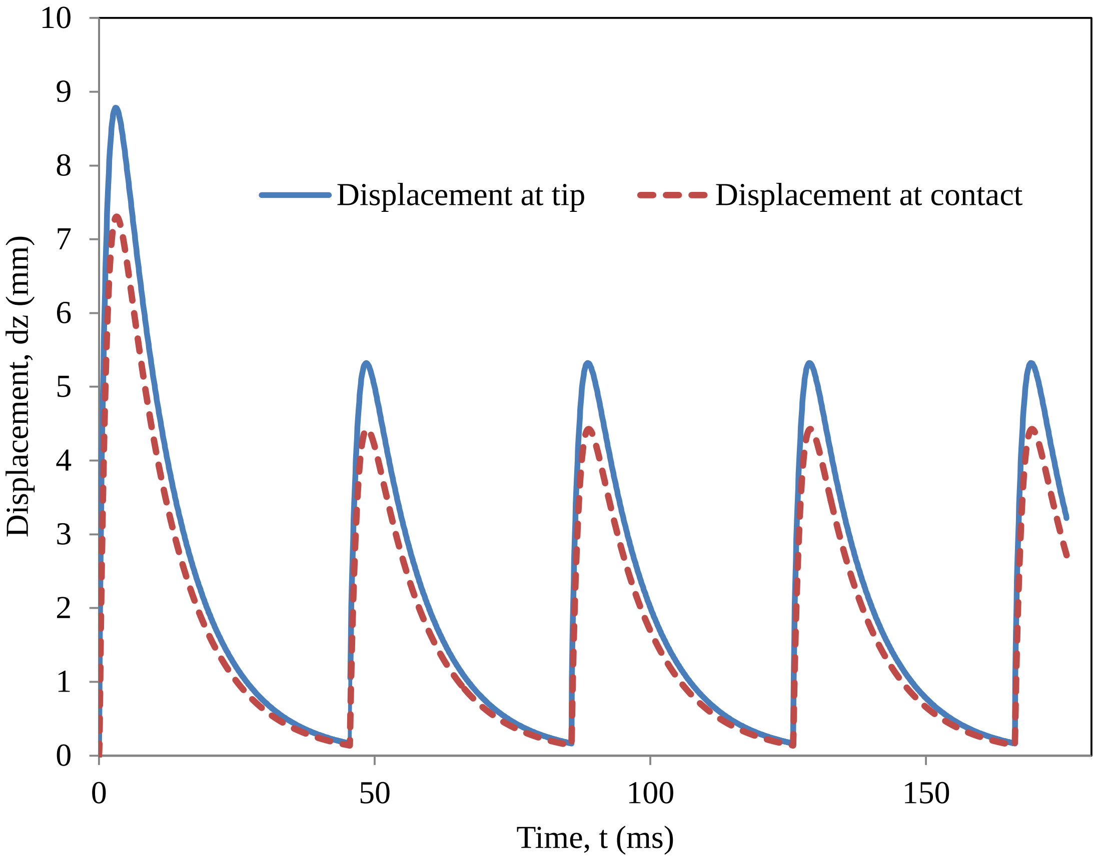

Figure 4.24: Deflection of the tip of the cantilever and the spatial displacement at the heat source-cantilever contact point.

Aspect ratio also effects the period of oscillation. It can be observed in Figure 4.26a that with increasing length the period of oscillation also increases. This is because the heat has to travel a longer distance before being dissipated at the heat sink. Since increasing length increases the thermal response time, it affects the period. Different materials with different thermal conductivity can also affect thermal response time and therefore the period of oscillation. Among the four

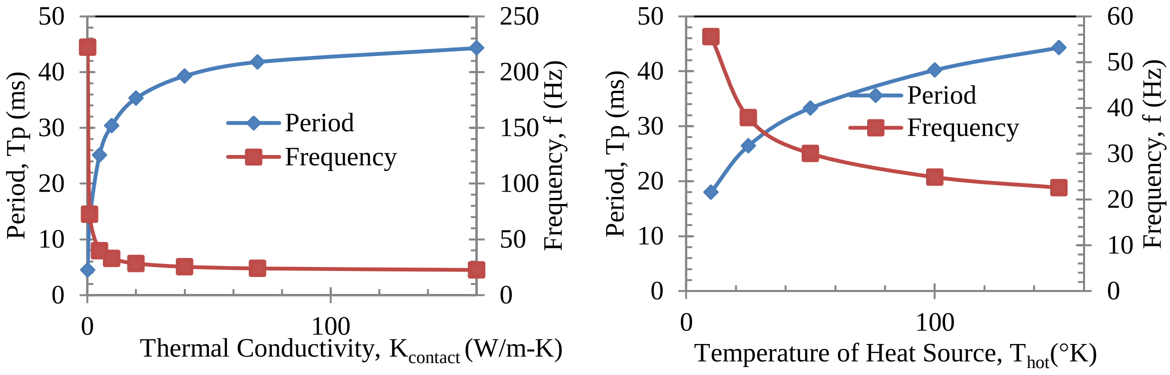

Figure 4.25: Period and frequency of resonance with variable thermal conductivity of the contact layer (left) and heat source temperature (right).

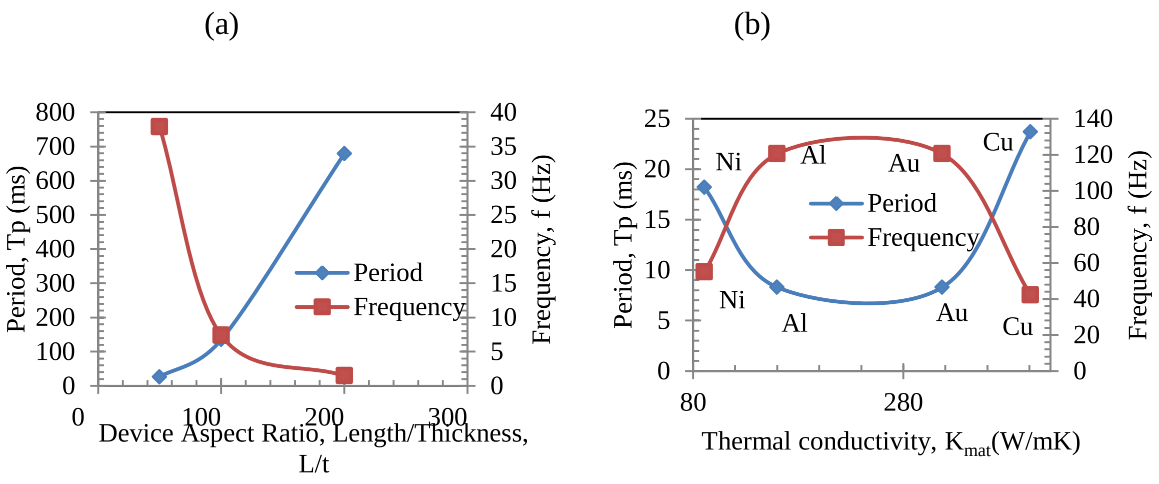
(a)

(b)

Figure 4.26: (a) Period and frequency of resonance with variable device aspect ratio, (b) and various materials.

materials considered for bimaterial combination aluminum and gold are more suitable as material of choice for reduced period (Figure 4.26). Although nickel and copper have largely different thermal conductivities their period of oscillation is similar, because nickel has higher Young’s modulus than copper. Therefore nickel has less tip deflection and has to dissipate less heat to

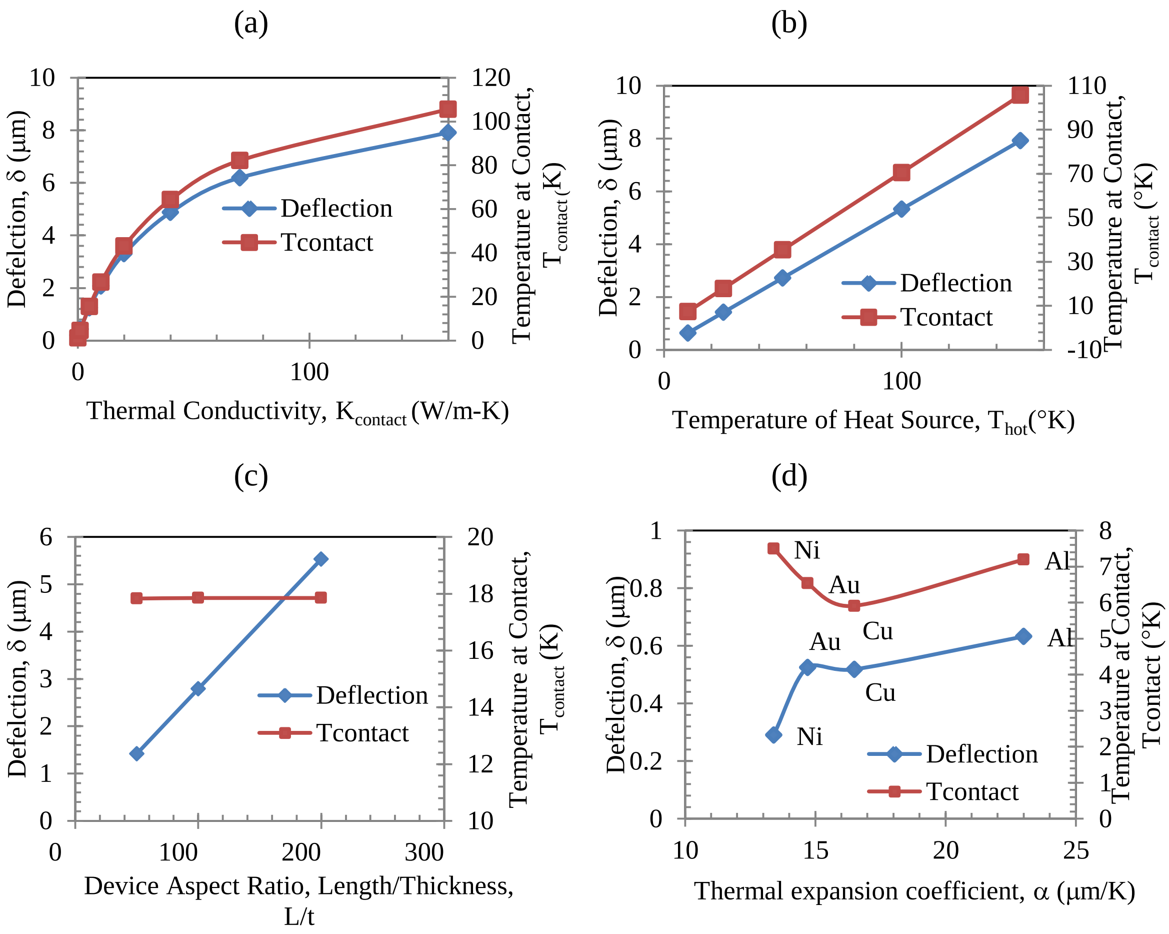

Figure 4.27: Tip deflection and temperature at contact with variable (a) thermal conductivity of the contact layer (b) heat source temperature (c) device aspect ratio (d) material.

overcome the critical distance, $\delta_{critical}$. On the other hand copper has higher deflection due to lower Young's modulus and has to dissipate more heat before returning to original position. Deflection of the cantilever determines the furthest distance the heat sink can be placed to minimize radiative heating. Simulation results reveal that the deflection increases with increased contact conductance, heat source temeprature as larger heat transfer results in greater deformation and higher aspect ratio (longer cantilevers) causing more deflection at the tip since deformation closer to the base are multiplied.

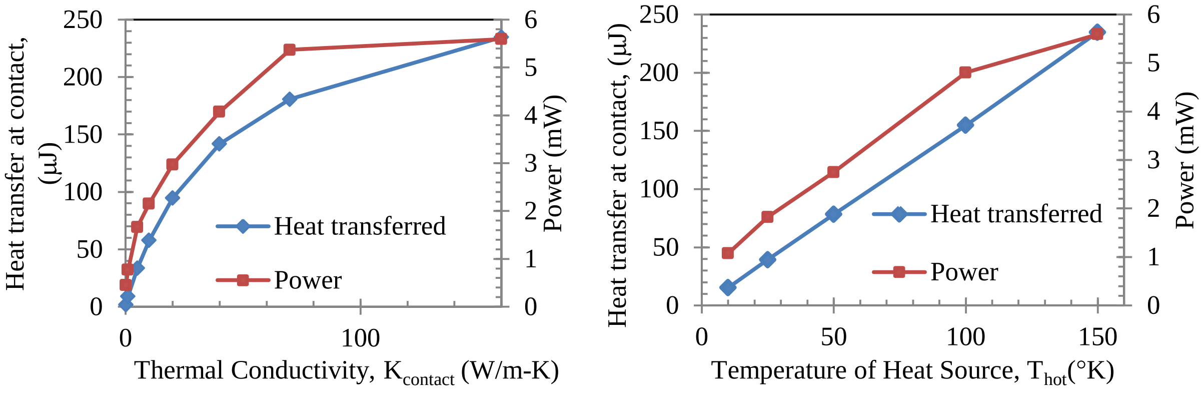

(a) (b)

Figure 4.28: (a) Heat energy transferred during a contact and overall thermal power flow in the cantilever with varying thermal conductivity of the contact layer, (b) heat source temperature.

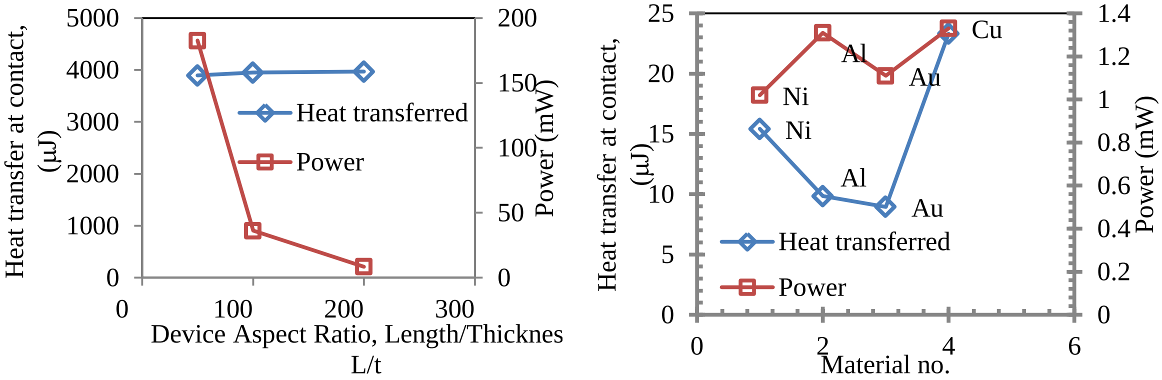

Figure 4.29: Heat energy transferred during a contact and overall thermal power flow in the cantilever with varying device aspect ratio and (left) material (right).

Since the purpose of this device is to harvest thermal energy from waste heat, parameters related to the amount of heat energy scavenged from the heat source and the overall power flow in the cantilever that can be converted to electrical power are of most interest.

Figure 4.29 shows that increased thermal contact conductance greatly increases the amount of transferred heat energy and power flow. Similarly an increase in the source temperature translates to more energy in the heat source which is transferred to the cantilever. Device aspect ratio does not affect the amount of energy transferred but the low frequency of thermal cycling at higher aspect ratio minimizes the power flow in the structure as cacntilevers become longer (

Figure 4.29a). Among the possible materials that dominate the heat conduction in the structure such as nickel, gold, copper and aluminum , the last two metals provide the best results in terms of power flow and thermal cycling mostly due to their higher thermal conductivities.

4.5.1.4 Optimization of the MEMS Structure

Although the bimaterial cantilever structure was studied in the previous section, it did not address how the structure would behave with the pyroelectric material housed in it. The thermomechanical properties of the pyroelectric material would affect the response of the MEMS device. To find the optimized design for the MEMS housing, the optimal design dimensions for the pyroelectric material were researched. Since the main objective is to have a fast temperature cycling, one of the optimization criteria was the lowest possible thermal time constant. Another optimization criterion was to have the maximum deflection of the cantilever tip so the heat source and the sink can be placed as further apart as possible to avoid radiation of heat and maintain a high temperature difference as well as maximize the piezoelectric effect. In summary, the goals for multilayer cantilever optimization were: shortest thermal response time and maximum displacement of the tip of the cantilever.

Table 4-3: Starting Parameters of Fabrication Limitation.

	Thickness, d	Density, ρ	Specific heat, Cp	Thermal conductivity, g	Young's Modulus, E	Thermal Expansion Coefficient, a
Unit	μm	Kg/m^3	J/Kg-K	W/m-K	GPa	μm/K
SiO_2	0-8	2200	703	1.38	73.1	0.55
Aluminum	0-0.3	2700	0.9	160	70	23
PVDF	0-25	1777	1.2	0.2	0.35	120

The range of dimension where to look for optimized values was limited by fabrication feasibility. Table 4-3 lists the range of the dimension for the three materials in the structure and their material properties that will govern their thermomechanical responses. The most contributing variable was the thickness of each material.

In the first optimization sequence, the thickness of SiO_2 and polymer were kept constant while the thickness of the aluminum was varied. Since the desired low thermal constant was achieved with higher value of thickness, the highest feasible thickness was chosen for Aluminum. Figure 4.30 shows the cantilever response varying with the aluminum layer thickness.

In the next sequence, the thickness of the aluminum was fixed and SiO_2 thickness was varied and the response is shown in Figure 4.31. In the last stage aluminum and SiO_2 thickness were fixed and the polymer thickness was varied. Since the polymer has very low elasticity at higher thickness, it dominates the deflection of the structure, but when the thickness is too low, the deflection is dominated by the bimaterial structure. The thermal time constant diminishes as the thickness is reduced and correspondingly reduces the thermal mass. Figure 4.32 plots this behavior and decides on 10μm as optimal polymer layer thickness for best responsivity.

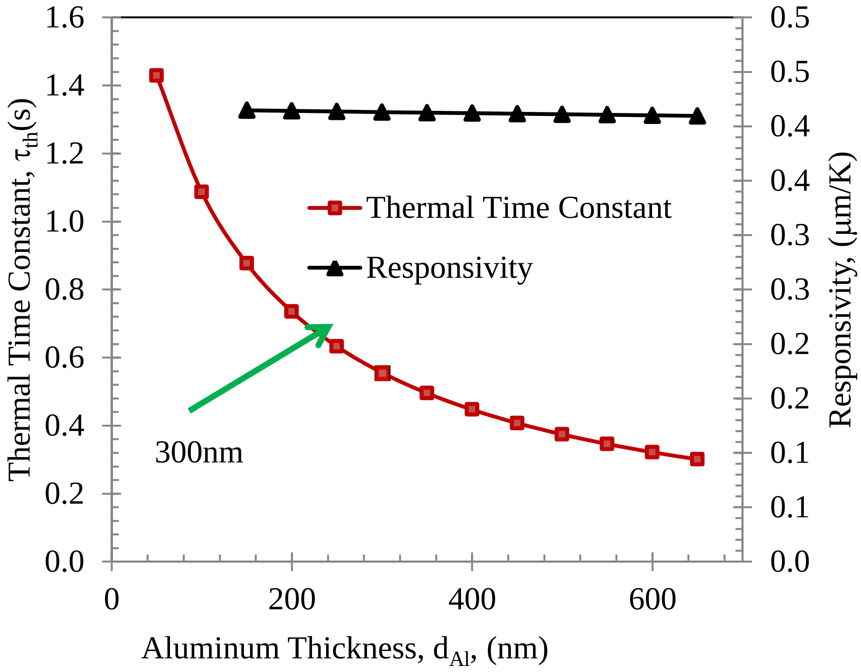

Figure 4.30: First optimization sequence decides thickness of aluminum layer. d_{al}= 300nm.

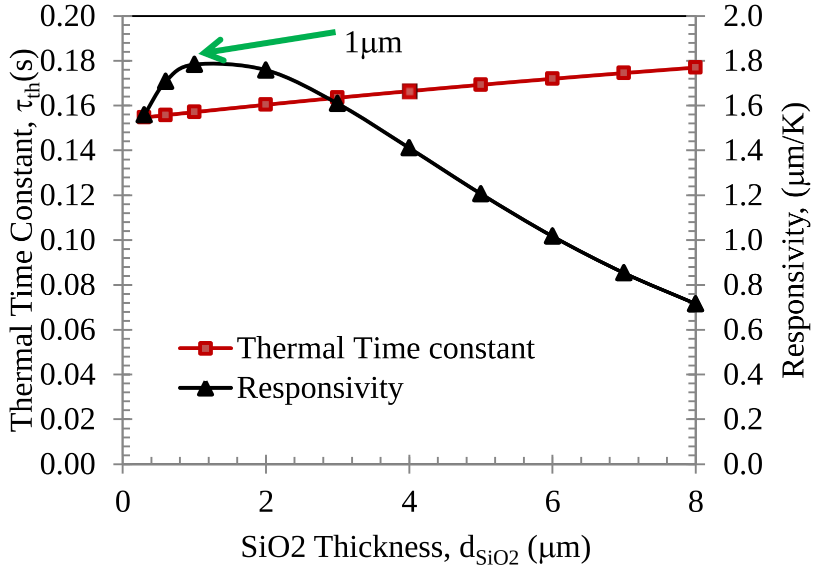

Figure 4.31: First optimization sequence: Decide thickness of aluminum layer. d_{SiO2}=1μm.

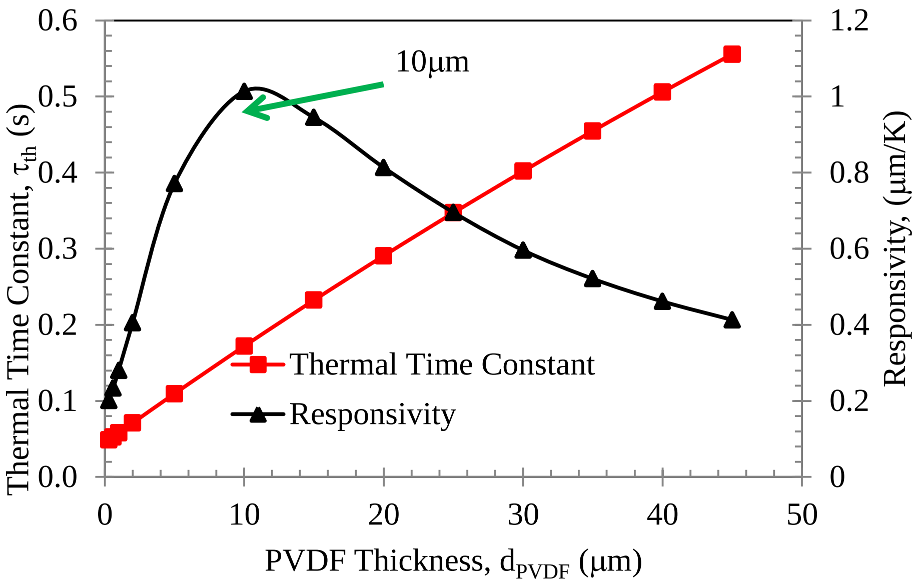

Figure 4.32: First optimization sequence: Decide thickness of polymer layer. d_{PVDF}= 10µm.

In a fashion similar to that described above, the optimal thickness of SiO_2 was also found which provides an idea about the ratio of the thickness to look for in search of optimization. Therefore a second batch of optimization sequence was performed to determine the best performance that can be achieved for the thicknesses listed in Table 4-4.

Table 4-4: Optimized Design Parameters

Set	Length	Width	Thickness		
	L	w	PVDF	Al	SiO2
	mm	mm	µm	nm	µm
1	0.5	0.125	10.00	300.00	1.00
	1	0.25			
	1.5	0.375			
	2	0.5			
	2.5	0.625			
	3	0.75			

For the given thickness, a batch of cantilever was fabricated with different lengths and widths for the experimental characterization purpose. The finite element model helped save resource before going to fabrication by providing optimum device dimensions and material choices that will be functional with a desired response.

4.5.2 Results of Analytical Model

The finite element response of the cantilever was found from previous section. The temperature at the tip of the cantilever was calculated using equation (4-10) and it is compared with the simulated data in Figure 4.33. Equation (4-11) was used to calculate the deflection at the tip of the cantilever and was compared with that found from the finite element modeling. The comparison is shown in Figure 4.34. Both figures confirm good agreement between simulated results and analytical models

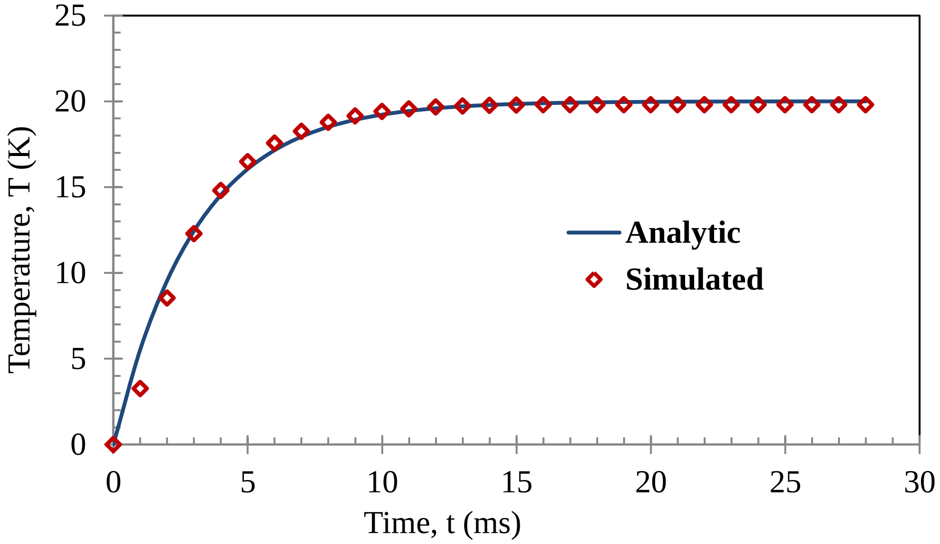

Figure 4.33: Comparison of FEM and analytical response for thermal response of the bimorph cantilever.

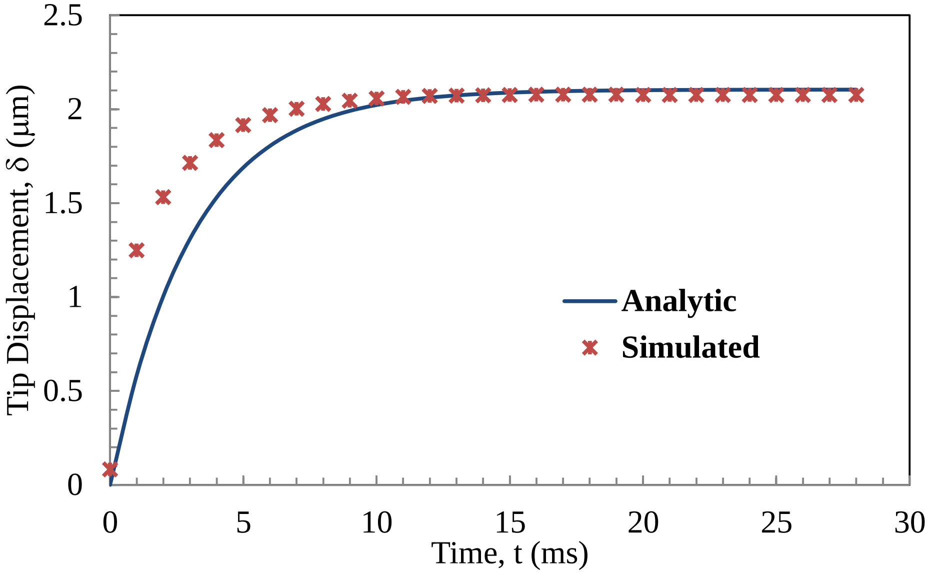

Figure 4.34: Comparison of FEM and analytical response for mechanical response of the bimorph cantilever.

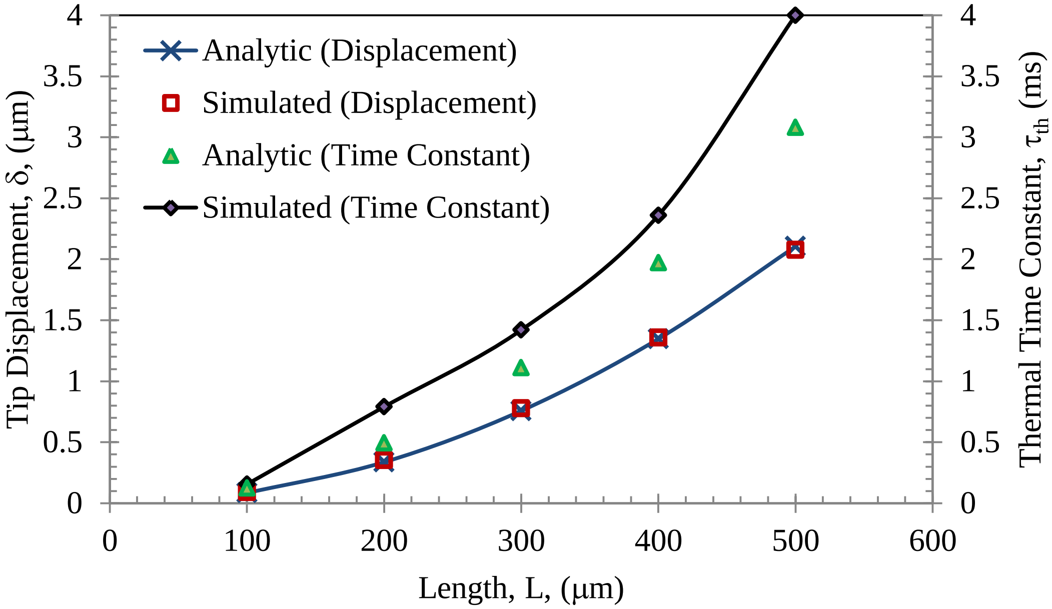

Figure 4.35: Mechanical response of the cantilever structure calculated from FEM and analytical model.

To verify the validity of the model, the thermomechanical response was compared with different parameters varied in both analytical and FEM models and the comparison are shown in Figure 4.35.

To verify the analytical model of the thermomechanical response of a multilayer cantilever, the tip deflection has been calculated for a group of sample cases. The sample cases are cantilevers of same length and width, but three layers of different materials with variable thickness. The dimension of the sample cantilevers are provided in Table 4-5. The tip deflection using equation (4-37) has been calculated using a MATLAB code provided in appendix B. The same structures have been modeled and simulated for FEM solution using the software COMSOL. The tip deflection found from both approaches is plotted in Figure 4.36. The percentage difference between these two results is also plotted for each case and does not exceed 3%. The analytical method and simulated FEM solution shows good agreement.

Table 4-5: Sample multilayer cantilever dimensions.

case	Length	width	Thickness		
			PVDF	Al	SiO2
	Mm	mm	μm	nm	μm
1	0.5	0.125	7.50	50	1.00
2			25.0	100	2.00
3			22.5	150	3.00
4			30.0	200	4.00
5			37.5	250	5.00
6			45.0	300	6.00

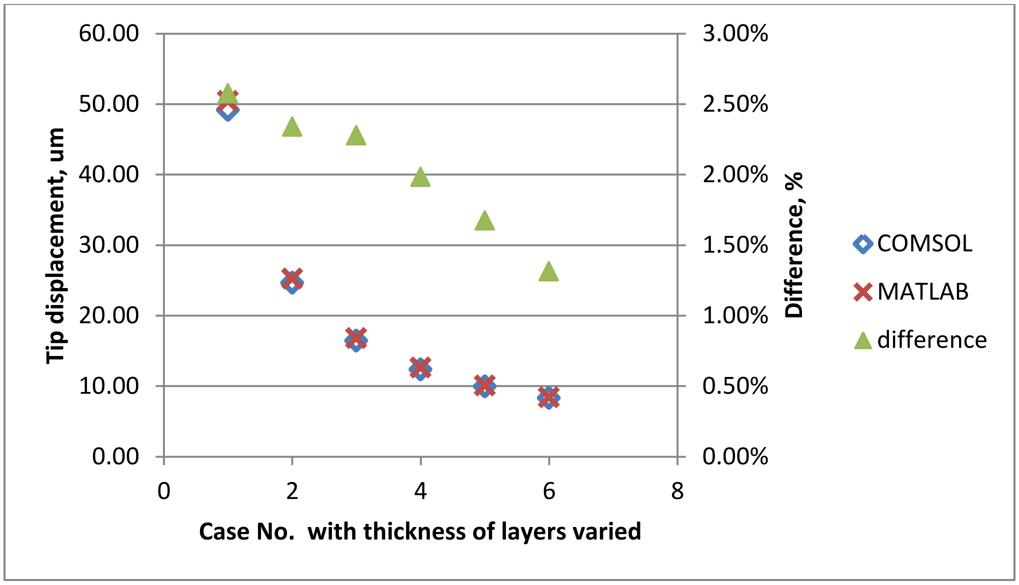

Figure 4.36: Tip displacement for varying multilayer thickness in sample cantilevers as calculated using MATBLAB (analytical model) and from COMSOL (simulated model). Percentage difference between obtained values from both methods is less than 3%.

4.5.3 SPICE Modeling Results

SPICE model has been simulated for a temperature difference of 20 K at one end of the cantilever. The thermal response of the MEMS structure has been derived for the opposite end, i.e. full length of the cantilever with dimensions of 1mm in length, 250μm width and 10μm thickness of aluminum and silicon di-oxide layers. Thermal response time is found to be 25 ms which agrees with the result found from numerical analysis and analytical model. Thermal response of the SPICE model as found from the simulation is shown in Figure 4.37.

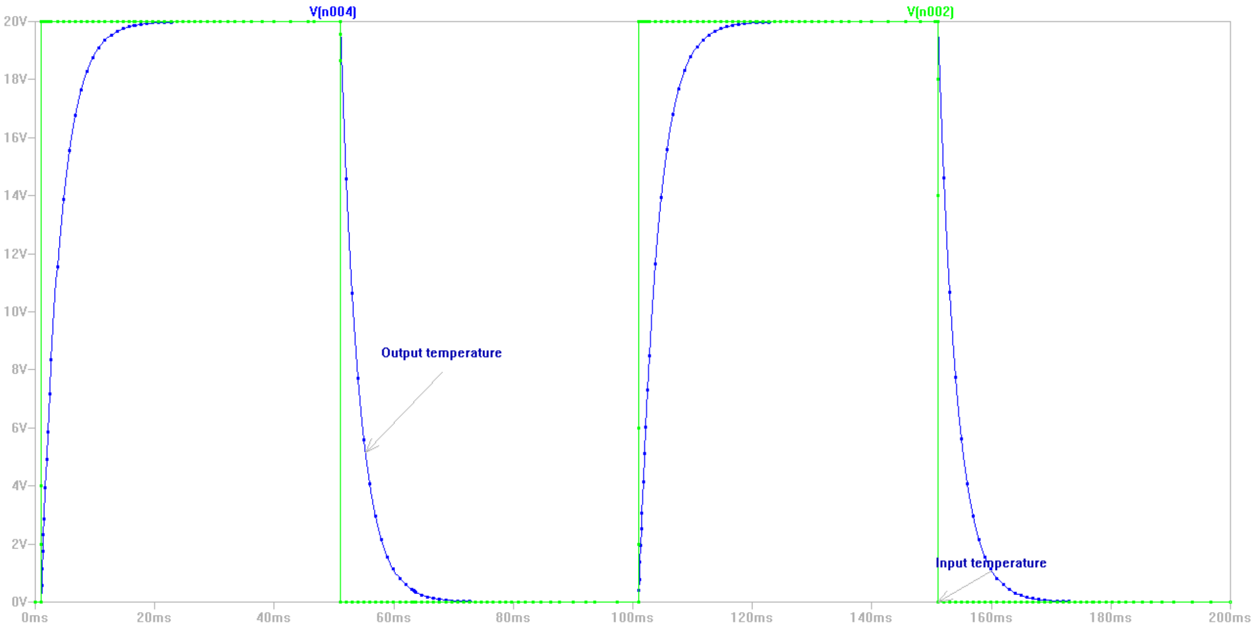

Figure 4.37: Applied temperature change and thermal response of the MEMS structure calculated by the SPICE model.

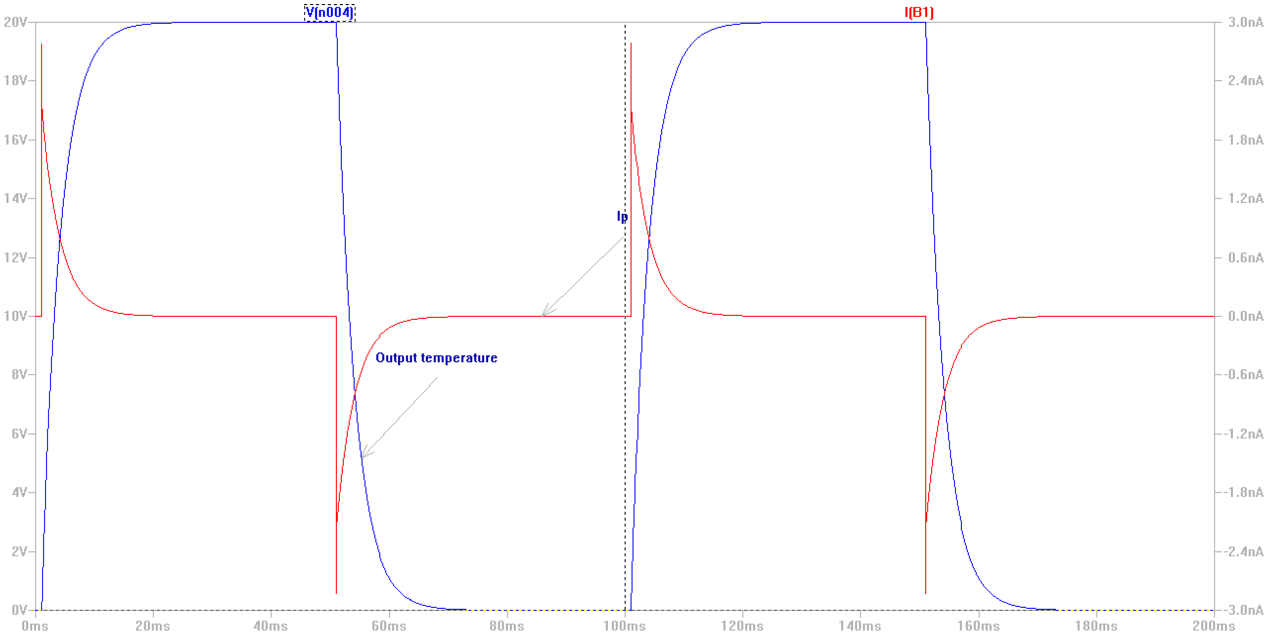

Figure 4.38: Temperature change and corresponding pyroelectric current calculated from the SPICE model.

The pyroelectric current calculation using the MEMS model is achieved and shown in Figure 4.38. For the applied temperature change the peak current is found to be 1.5 nA in magnitude for a pyroelectric element with 1mm×250μm×10μm volume.

4.6 Conclusion

Finite element, analytical and SPICE models of the device have been presented in this chapter. The models present a complete analysis of the proposed scheme and studies different design parameters to realize the device. Studies presented in this chapter greatly enhance the design of an efficient device. It also assists in determining the experiment techniques and identifies criteria of greater importance. With the knowledge of the models developed in this chapter, the next chapter presents the experiments undertaken to realize the proposed device.

Chapter 5

EXPERIMENTS

Following the optimized design parameters the cantilever structures were fabricated. Their bimorph behavior and thermomechanical response were characterized and the self-oscillation was also observed. Additionally the pyroelectric capacitor structures were also fabricated and characterized in the laboratory. Following sections highlight the experimental setup and the observed and measured data and provide brief analyses.

5.1 Pyroelectric Material Characterization

Pyroelectric materials that have been considered include aluminum nitride (AlN), zinc oxide (ZnO) and polymeric PVDF. Since PVDF is commercially available and less expensive compared to the others, it has been chosen as the pyroelectric material for device fabrication. Also its thermomechanical properties are compliant with the operating conditions of the MEMS structure.

5.1.1 Pyroelectric Film Synthesis

Commercially obtained polymer material (PVDF) has been characterized to specify the exact value of different properties. Commercially PVDF is available as a thin film of polymers which cannot be directly used for characterization experiments. Therefore the thin film polymer has been synthesized for experimental measurement. One surface of the film has been deposited with a very thin layer of aluminum. On the opposite surface circle shaped dots of 2 mm radius have been patterned with chromium. The patterned dots define capacitor areas of a pyroelectric capacitor. They also serve as metal contact for probing during experiment. Figure 5.1 depicts the cross-sectional view of the synthesized pyroelectric film and the top view of the patterned dots.

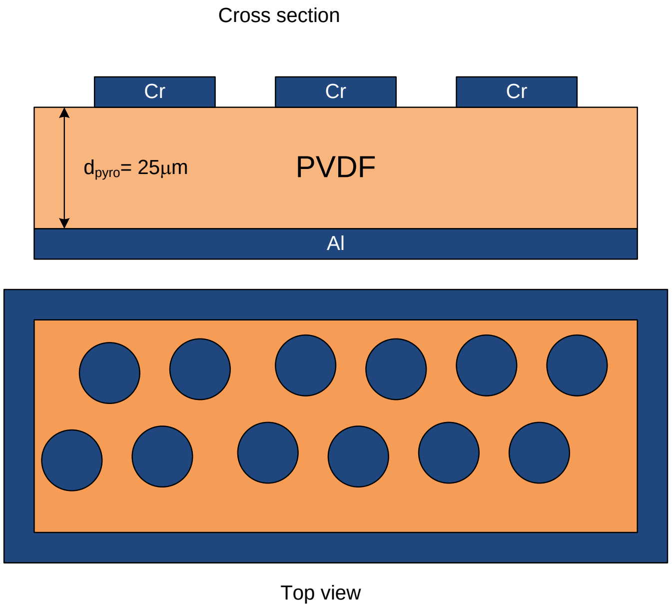

Figure 5.1: Cross-section and top view of the synthesized pyroelectric PVDF film.

5.1.2 Dielectric Properties

The synthesized PVDF film has been used for characterizing the dielectric properties of the pyroelectric material in use. This characterization also helps to define the pyroelectric coefficient of the material as the charge stored by the capacitor is generated due to temperature change. The capacity of the charge containment depends on the capacitance and therefore on the dielectric property of the material.

5.1.2.1 Experimental Setup

To find the dielectric property of the pyroelectric material the capacitance of a pyroelectric material was measured at different spots. Each patterned dot on the pyroelectric film along with the bottom metallization represents a capacitor. Measuring the capacitance of a material with known area and thickness reveals the dielectric constant of the material. To measure the capacitance at various frequencies, the pyroelectric dot capacitors were interfaced with a low impedance amplifier sweeping a sinusoidal voltage signal from low to high frequency. Current was measured at each step frequency to calculate for the impedance. The capacitance value was found by,

$$C = \frac{V}{I \times 2\pi f} \tag{5-1}$$

where, V is the amplitude of the signal, I is measured current at frequency f. The schematic drawing of the experimental setup is shown in Figure 5.2 and probe contact with the pyroelectric film is shown in Figure 5.3 .

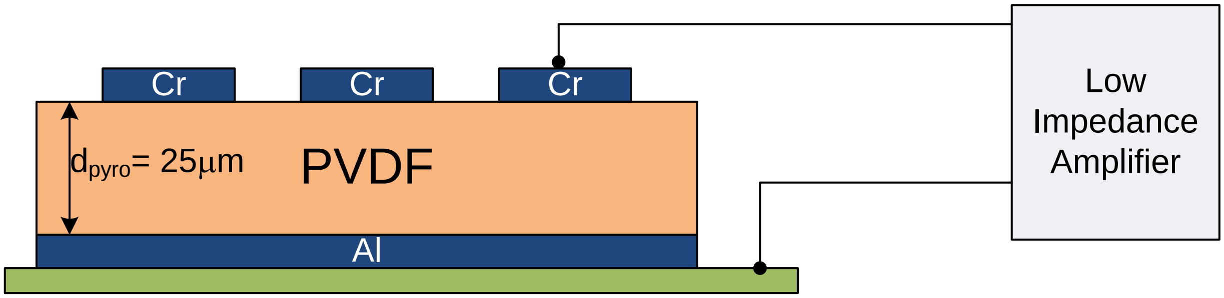

- **Measurement settings:**

Input: Source = I (Current)
Current Gain= 1M
Grounding= Ground, Coupling : DC
Line Notches= Out
Ref/Phase: Internal Sweep (logarithmic)= 50Hz to 50KHz
Sine output= 0.01V (10 mV)
Gain/TC: Sensitivity =500nA Time constant = 1ms

Figure 5.2: Experimental setup and measurement settings for dielectric characterization of PVDF film.

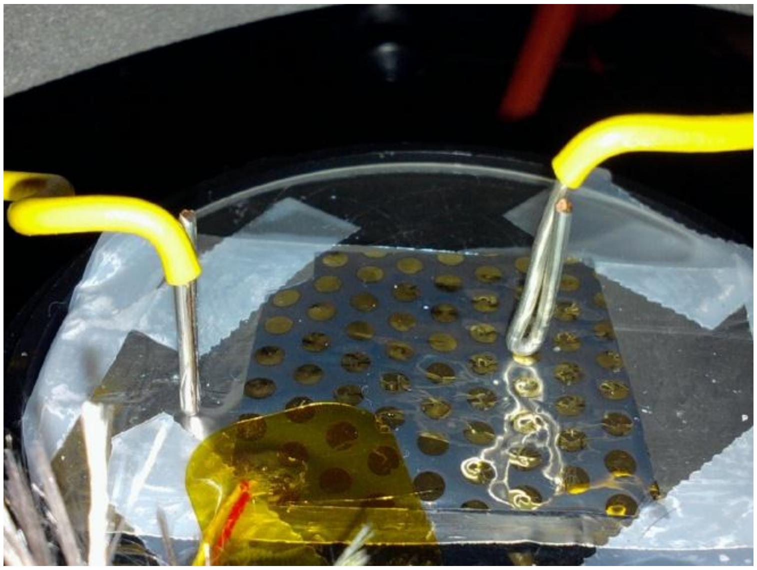

Figure 5.3: Experimental Setup for making contact to thin film pyroelectric capacitor for current measurement.

5.1.2.2 Results and Discussion

Capacitance has been calculated from measured current using equation (3-5) and averaged for a particular capacitor. Capacitance has been measured in 21 different capacitors and the average value of these measurements is taken as the average capacitance of a capacitor with area of π mm^2 (Figure 5.2). The average capacitance value is found to be 8.58 pico-Farad. The thickness of the film is 25 μm and the area is known. Therefore the dielectric constant is calculated to be 7.72 which is close to the value of 7.6-10 provided in the manufacturer datasheet.

5.2 MEMS Fabrication

A bimaterial cantilever is the basic structure of the MEMS device. For the study two different bimaterial combinations were tested. First combination consists of a cantilever with thin layer of Aluminum on SiO_2 surface. The second combination is a layer of gold on bulk silicon wafer of micrometer thickness. The fabrication techniques of both cantilevers are discussed below. The fabrication was carried out at the Center for Nanophase Materials Sciences (CNMS) facility at Oak Ridge National Laboratory (ORNL) by Dr. Nicolay Lavrik.

5.2.1 Silicon Dioxide and Aluminum Cantilever

The fabrication of a silicon dioxide- aluminum cantilever follows the steps below.

i. The process begins with a sacrificial layer of bulk silicon wafer. By PECVD deposition a thin layer of SiO_2 is grown on the silicon wafer.

ii. SiO_2 growth is followed by Electron beam deposition of thin aluminum layer.

iii. On the front side of the wafer photolithographic pattering is done to pattern opening to the bulk silicon wafer.

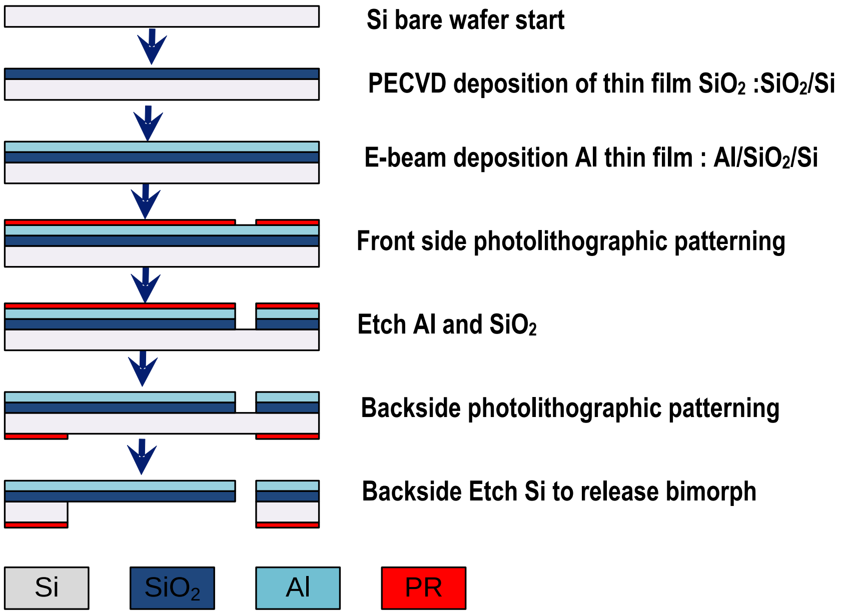

Figure 5.4: Fabrication of SiO_2-Al bimaterial cantilever MEMS structure.

iv. In the following step aluminum and SiO_2 on the patterned opening is etched away by reactive ion etching. This creates an opening for chemical etchant to access the bulk silicon wafer.

v. Then the backside of the wafer is patterned to the shape of the cantilever. The patterned photoresist protects the bulk silicon area from being chemically etched.

vi. Next the wafer is exposed to selective chemical etchant which dissolves the exposed silicon in the wafer. As the patterned silicon is etched away the SiO_2-Al cantilever is released.

vii. In the final step, the photoresist is removed from the backside of the wafer to finish the fabrication of the MEMS device.

Due to internal stress often the cantilevers are bent in concave shape once released from the wafer. Special care needs to be taken to control the deposition to obtain cantilevers that are horizontal. Although for the operation of the self-oscillating MEMS a concave cantilever with the tip pointing upward is beneficial. Figure 5.5 shows photograph of the fabricated SiO_2-Al MEMS cantilever arrays.

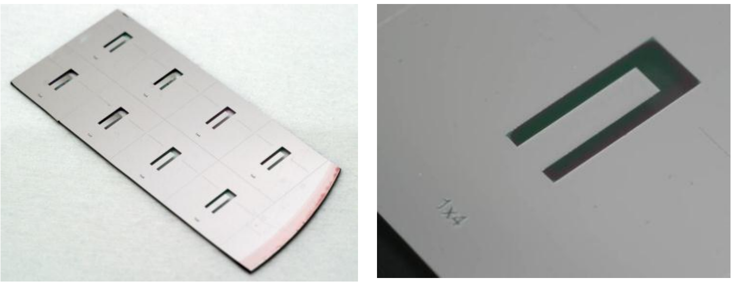

Figure 5.5: Fabricated SiO2-Al MEMS cantilevers.

5.2.2 Silicon and Gold Fabrication

Fabrication of the silicon-gold cantilever involves the following steps,

I. A bulk silicon wafer is deposited with 10 μm layer of gold (Au).

II. The backside of the bulk wafer is then chemical mechanically polished to decrease the depth of the bulk. Polishing is done until the wafer is only 10μm in thickness. Thus a thin bimaterial film is created.

III. The thin film can be cut with a sharp knife to any dimension and size desired. The cut beam can be attached to a small piece of bulk wafer with thermal glue such as silver paint to anchor the cantilever and also to serve as heat sink.

The fabrication processes is depicted in Figure 5.6.

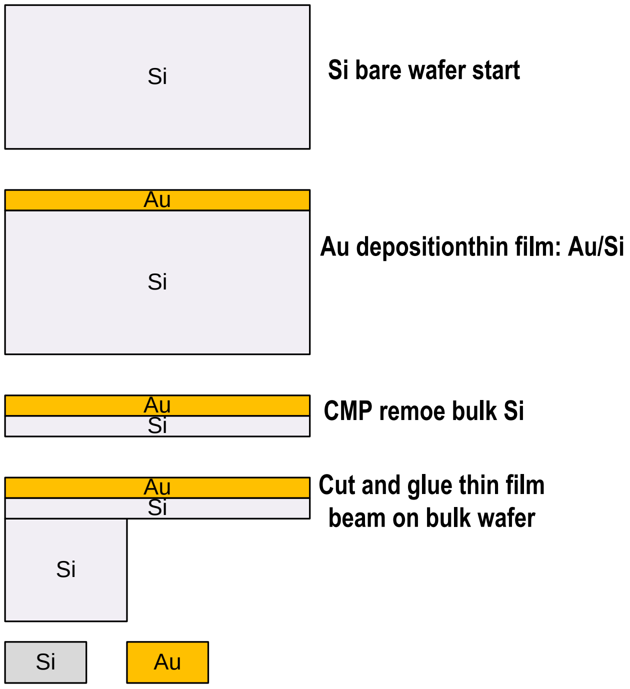

Figure 5.6: Fabrication of Si-Au MEMS cantilever.

5.3 MEMS Thermomechanical Characterization

Thermal response of the MEMS cantilever is studied in two steps for both combinations of bimaterial cantilevers. In the first step the thermal and mechanical responses with controlled temperature change are studied to characterize their behavior. In the second step, the self-oscillation condition and performance are observed.

5.3.1 Thermal and Mechanical Response

The responsivity of the fabricated cantilevers has to be characterized to predict the self-oscillation performance of the cantilever and to compare with simulated or analytical models. Characterization involves measuring the deflection of the cantilever in response to a controlled temperature change. Time dependent thermal response of the cantilever can also be monitored in this process by measuring the temperature change in the cantilever body.

5.3.1.1 Experimental setup

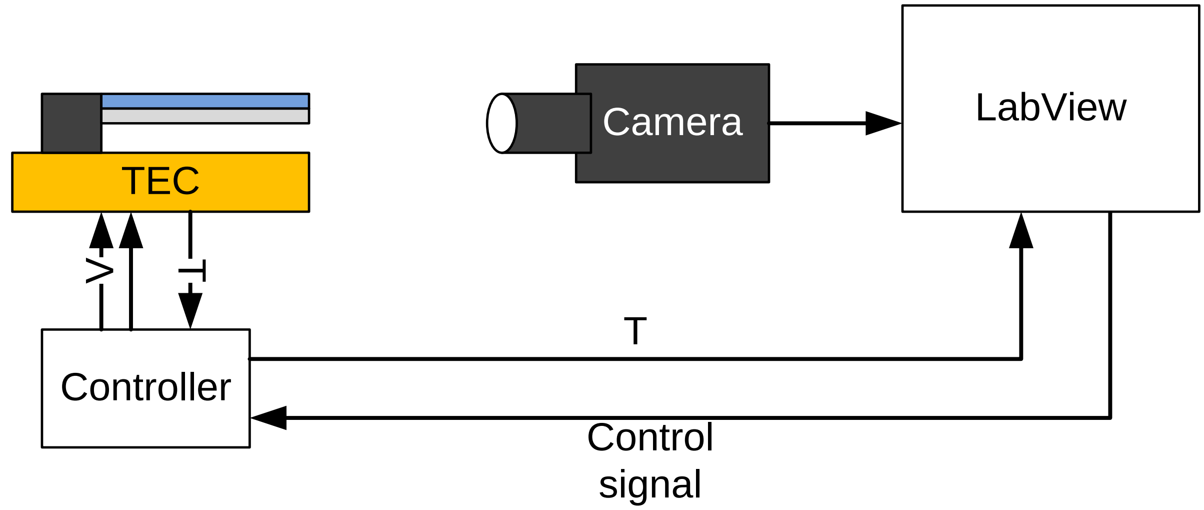

Figure 5.7: Experimental setup for measuring thermomechanical response of bimaterial cantilever.

The bimaterial cantilever is anchored to the wafer chip which was mounted on a thermoelectric cooler (TEC). The Series 800 TEC control from Alpha-Omega Instruments is used to control the temperature at the base of the device. The controller controls the temperature by applying voltage and derivative (PID) control to the input of the TEC to change the temperature. It maintains a tight control over the temperature by using reads feedback data read through a thermocouple. A Labview© program was used to interface the TEC controller for data acquisition and remote control. A fire wire camera is also interfaced with the Labview© program to capture video of bimaterial cantilever deflection while the program controls the temperature of the TEC and the cantilever mounted upon it. The program stores temperature data against time and collects screenshots at every 200 ms time step.

5.3.1.2 Results and Discussion

Thermocouples placed on the TEC measure the temperature and sends feedback to the controller and to the Labview program for control and acquisition. The cantilever itself is too small and fragile to support the placement of thermocouple, therefore the thermal time response of the cantilever cannot be measured accurately. However the bimaterial deflection can be derived from the captured video. If the cantilever length is known it can be used as reference to find length per pixel from the captured screenshot. When the cantilever deforms due to thermal expansion the displacement can be calculated from the change in pixel location of the tip of the cantilever and the knowledge of length per pixel scale. This is the method followed to find the tip deflection for silicon di-oxide/aluminum and silicon/gold cantilevers. The thermomechanical response is characterized by the term, responsivity, which indicates displacement per degree kelvin change of temperature and is denoted by R.

5.3.1.2.1 SiO_2-Al cantilever

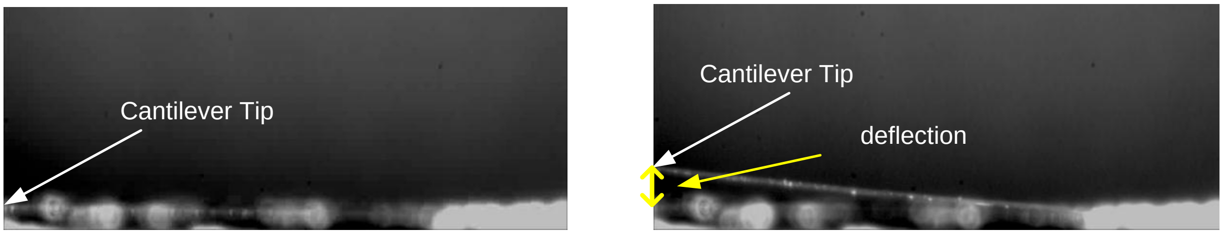

Figure 5.8: Video capture shots used to determine the deflection of bimaterial cantilever.

SiO_2-Al cantilevers have been fabricated as arrays. A single cantilever has been separated from the wafer and used for this measurement. Care was taken to choose a cantilever that has been released as a horizontal beam during fabrication. The cantilever was placed on the TEC with the aluminum layer in the bottom so when heated the cantilever bends up.

Initially the responsivity of the cantilever was studied for 1°K temperature variation and from the video it was found to have 150μm/ K responsivity for a 2mm long cantilever. Figure 5.8 shows the captured screenshots captured by the camera at initial temperature and after temperature increase.

5.3.1.2.2 Si-Au cantilever

A 7 mm long, 1 mm wide strip of silicon gold film was cut and glued to a silicon wafer with electrically and thermally conductive silver paint to create a 5mm long cantilever with the gold surface facing upward. Since gold has higher thermal expansion coefficient, increasing the temperature causes the cantilever to bend downwards. The TEC temperature was increased from 10°C to 50°C to observe the responsivity of the cantilever. Figure 5.9 shows the camera captured screenshots of the cantilever at 10°C and 50°C.

From this screenshots the actual displacement was derived by the following method. First a scale was established to account for length represented by each pixel in the picture. This is shown in Table 5-1.

Table 5-1: Scale establishment for presenting length per pixel.

	Pixel location	Pixel count	Actual length	Scale
Cantilever	(68,373) to (568,356)	500	5mm	1px=10μm
Anchor	(151,372)	(568-151)=417	4.17mm	

The displacement of the tip is identified from changed pixel location. Using previously established scale the actual deflection is calculated in Table 5-2.

Table 5-2: Calculation of bimaterial deflection.

Time (s)	Tip location (px)	Temperature (K)	Displacement (px)	Displacement (μm)
0.0	548,342	299.73	-	-
31.37	545,318	261	24	240

Responsivity can be found by, R= 240 μm /38K= 6.31μm/K

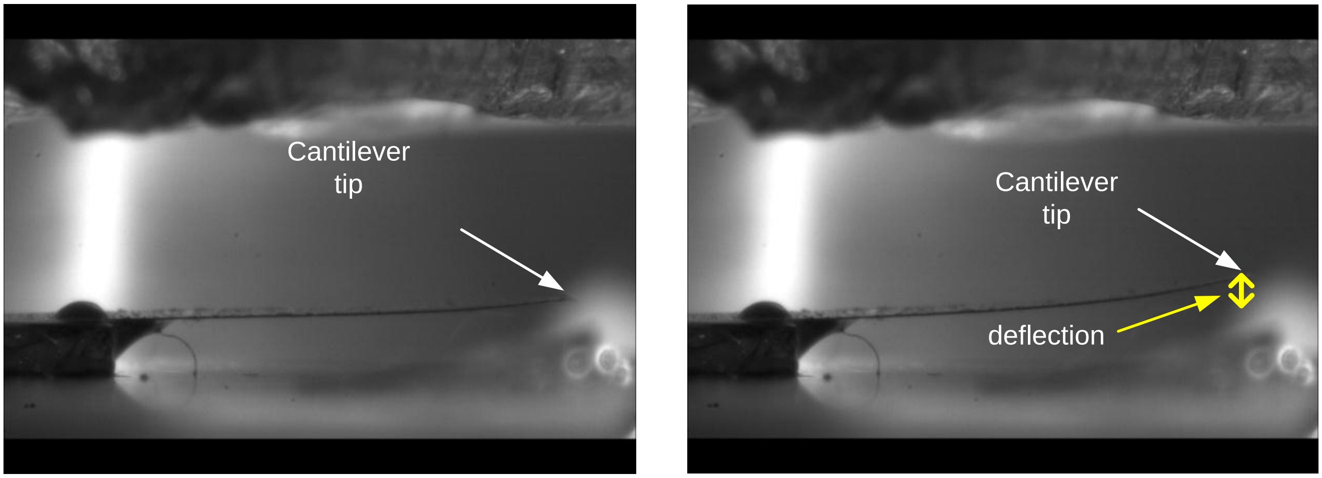

Figure 5.9: Video capture shots used to determine bimaterial response of a Si/Au cantilever.

5.3.2 Thermally Actuated Self Oscillation

Thermal actuation and self-oscillation of cantilever MEMS is possible under certain operating conditions. These conditions must be maintained to achieve self-oscillation.

5.3.2.1 Experimental Setup

To self-actuate the cantilever device its base must be anchored to a constant temperature. The cantilever needs to be heated through its tip so that the cantilever deflects away from the heat source and cools through the base. For the SiO_2/Al cantilever the base was maintained at room temperature 21°C with the help of the TEC controller. A 25 μm thick tungsten wire is used as heater by applying small voltage across it, utilizing Joule heating to increase the temperature. The cantilever tip is brought in contact with the tungsten wire heater with the help of a micromanipulator to initiate the self-oscillation process. The experimental setup schematic is shown in Figure 5.10.

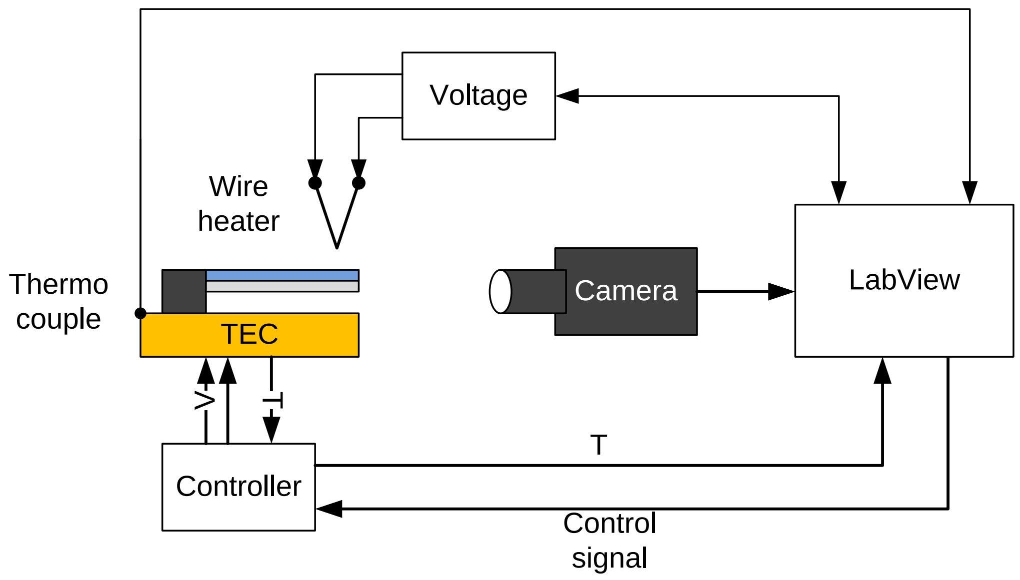

Figure 5.10: experimental setup for measuring self-oscillation response of MEMS cantilever.

In a practical commercial device the cantilever may be housed in a hermetically sealed system with the cantilever proof mass used to initially maintain contact with a top surface that is thermally conductive. The top surface will be attached to a heat source to increase its temperature and conduct heat to the cantilever through the proof mass.

The entire TEC, cantilever and heater have been placed inside a vacuum chamber to remove the probability of radiative heat transfer between heater and cantilever. A video camera captures the cantilever deformation at 200 ms intervals. The wire heater has been characterized beforehand to know temperature for applied voltage value. A Labview© program maintains the temperature at the TEC, acquires temperature data from a second thermocouple measuring TEC temperature, collects voltage data from the voltage supply to the wire heater and captures video from a video camera.

For the Si/Au cantilever the experimental setup is similar, except that an indium wire is used for heater with zero voltage applied to it, so that the wire maintains ambient room temperature, i.e. 21°C. Since the temperature decrease causes the cantilever to bend upward, initially the temperature was lowered to -20°C to deform the bimaterial and bend upwards to make contact with the indium wire heater. Figure 5.11 displays the Si/Au cantilever mounted on the TEC, housed inside the vacuum chamber. The image is used with permission from the Nanosystems and Structures group, in the Measurement Science and Systems Engineering division of Oak Ridge National Laboratory.

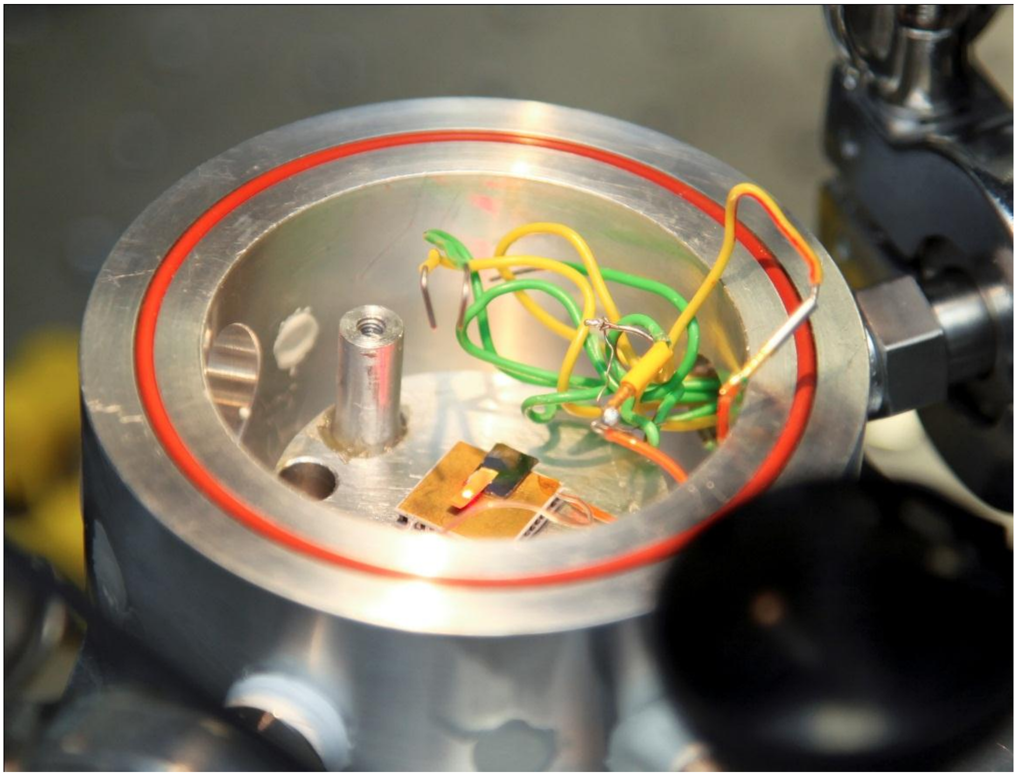

Figure 5.11: Vacuum chamber housing the cantilever, TEC and wire heater.

5.3.2.2 Results and Discussion

The SiO_2/Al cantilever responded with aperiodic intermittent oscillation and period of sub-seconds (video is attached in the digital version of the document). Figure 5.12 shows the tungsten wire point heat source and the bimorph behavior of the cantilever structure.

For the Si/Au at initial contact there is one self-oscillation detected, but subsequent oscillations are either not detectable in the camera or absent. Screenshots are collected from the recorded video and pixel location at the tip of the cantilever was recorded to calculate for the deflection. The following captured video screenshots. Therefore a scale of 10 μm per pixel was established to calibrate the deflection measurements. A self-oscillation incidence was observed at approximately 40 s of the recorded video. Subsequent screenshots saved from 40s onwards were analyzed for the change in the tip location and in one screenshot the tip location was moved by 2 pixels which indicate a deflection of 20 μm. Since the silicon/gold cantilever has higher rigidity and corresponding lower responsivity the deflection is expected to be very small and also the frequency of oscillation should be much higher. The major concern is the time intervals at which the screenshots were taken as the interval is most likely longer than the period of oscillation. Therefore the measured frequency of oscillation is not accurate.

Table 5-3 lists the pixel and time lapse calculation used to detect the self-oscillation of the cantilever. The measured length of the cantilever was found to be 5mm and 500 pixels in the

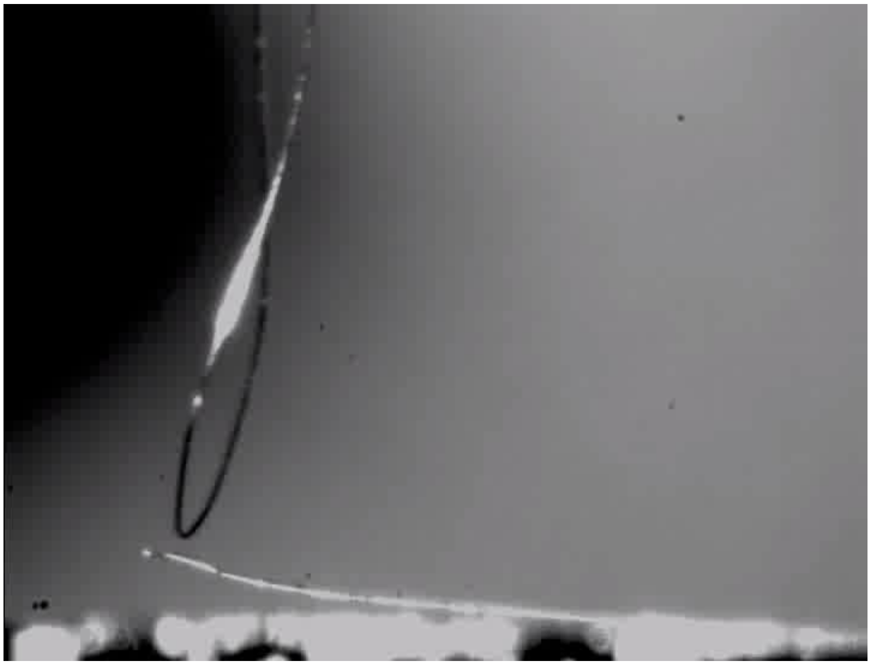

Figure 5.12: Self oscillation using a tungsten wire as point heat source.

captured video screenshots. Therefore a scale of 10 μm per pixel was established to calibrate the deflection measurements. A self-oscillation incidence was observed at approximately 40 s of the recorded video. Subsequent screenshots saved from 40s onwards were analyzed for the change in the tip location and in one screenshot the tip location was moved by 2 pixels which indicate a deflection of 20 μm. Since the silicon/gold cantilever has higher rigidity and corresponding lower responsivity the deflection is expected to be very small and also the frequency of oscillation should be much higher. The major concern is the time intervals at which the screenshots were taken as the interval is most likely longer than the period of oscillation. Therefore the measured frequency of oscillation is not accurate.

Table 5-3: Pixel point measurement of the cantilever tip location from the captured screenshots.

Time (s)	Tip location (x,y)	Displacement (pixel)	Displacement (μm)
40.00	545,318	24	240
40.04	545,318	24	240
40.26	545,318	24	240
40.28	545,318	24	240
40.34	545,320	26	260
40.47	545,318	24	240

5.4 Pyroelectric Current Generation

To characterize pyroelectric current generation, temperature needs to be varied in the pyroelectric material while the current output is being measured. Temperature has been varied in two methods. In an attempt to find maximum magnitude of pyroelectric current from the material, very fast temperature change was performed. In the second experiment, temperature was varied with more precise control over frequency and magnitude to characterize for energy harvesting parameters.

5.4.1 Fast Temperature Change

Temperature change rate with the help of the TEC controller is limited by the amount of power the controller can deliver. Therefore to increase the temperature at a very fast rate, a halogen lamp flash was used. The halogen lamp gives a very short 1 ms duration pulse with enough power that raises the temperature of the pyroelectric capacitor for a very short period.

5.4.1.1 Experimental Setup

To study their behavior at very high frequency temperature cycling, JTL Versalight 160 photographic flash was used generate short duration light pulse of approximately 1 ms. At full-scale power the flash discharges 160 Watt energy per second. This light energy is converted to thermal energy and is absorbed by the metal contacts on the pyroelectric film raising the temperature within. The quick rise in the temperature during that short time frame gives a very high value of *dT/dt*. The top of the thin-film capacitor was probed with folded wire probe so that the thin film is not punctured. The bottom of the thin film was uniformly metal coated and a contact was made with aluminum foil extending out from the bottom of the PVDF film. The current during this short period was measured by using the trigger mode in a Tektronix 3034 Oscilloscope. The experimental setup schematic is shown in Figure 5.13.

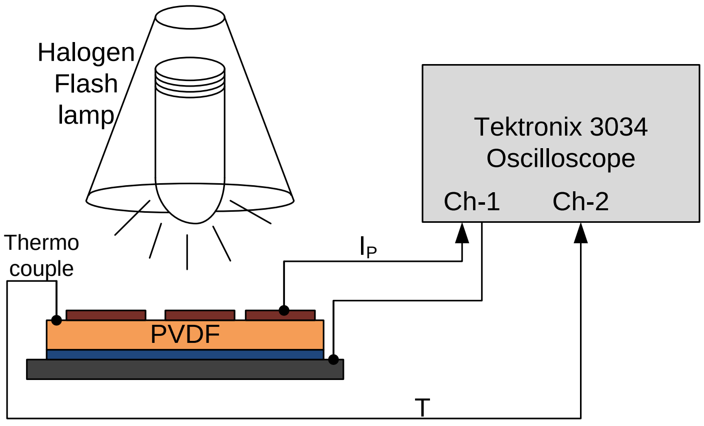

Figure 5.13: Experimental setup for pyroelectric current measurement.

5.4.1.2 Results and Discussion

The current was measured using a TDS3034 Oscilloscope with a 1 Mega-Ohm input load so as to drop the pyroelectric current across the input resistor and to take voltage reading from the channel. Input mode triggering was used to capture the data at the instant of the flash of the lamp. Figure 5.14 shows the pyroelectric current response from the oscilloscope measurement during the flash. Thermocouple based instant temperature measurement is plagued by electrical discharge picked up by the metal wires from the flash lamp and shows false readings. Therefore a thermocouple sampling data at 1 sample/second is used to allow the electric noise to disappear and settle the temperature change. The highest temperature increase measured during the flash was found to be ~5K. For a small area capacitor of approximately 3.15 mm^2 and a temperature change rate of about 5000K/s, the pyroelectric current is found to be about 750nA.

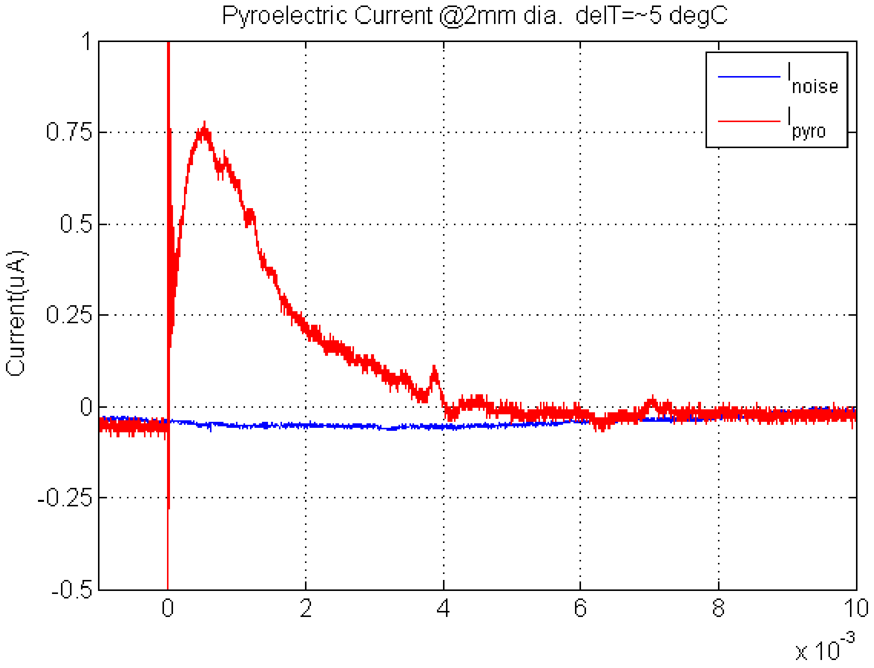

Figure 5.14: Fast thermal response of pyroelectric material.

5.4.2 Controlled Temperature Change

To study the effect of temperature change under various conditions a temperature of the pyroelectric capacitor was varied in a more controlled way. The frequency of temperature change, change rate, magnitude of temperature difference was controlled using the TEC controller and the current output as well as power was calculated for.

5.4.2.1 Experimental Setup

To standardize the pyroelectric current generation with rate of temperature change the temperature in the pyroelectric capacitor was varied periodically in a controlled way using a TEC controller operated with a LABVIEW program. The pyroelectric current was amplified using a pre-amplifier SRS M570 from Stanford Research System with 1nA/V gain before collecting the data using a National Instrument's standard DAQ card. The temperature at the pyroelectric sample was also measured using a standard J-K thermocouple using the DAQ card and conversion tool inside the LABVIEW Program. Figure 5.18 shows the measured polymer temperature and the pyroelectric current measured from this setup. The period of temperature cycling was 30 seconds and adequate time was given for the sample to reach a steady state set point temperature as controlled from the thermoelectric heater/cooler. The temperature difference was ~50 K ranging from 10 °C to 60 °C. The TEC controller has a fixed step response, i.e. the temperature change is achieved within the given response time irrespective of the temperature difference. Therefore, for a large temperature difference, the temperature change rate is higher. A higher voltage input or power delivery is supplied by the controller to maintain this time response if the temperature difference is higher.

5.4.2.2 Analysis of the Data

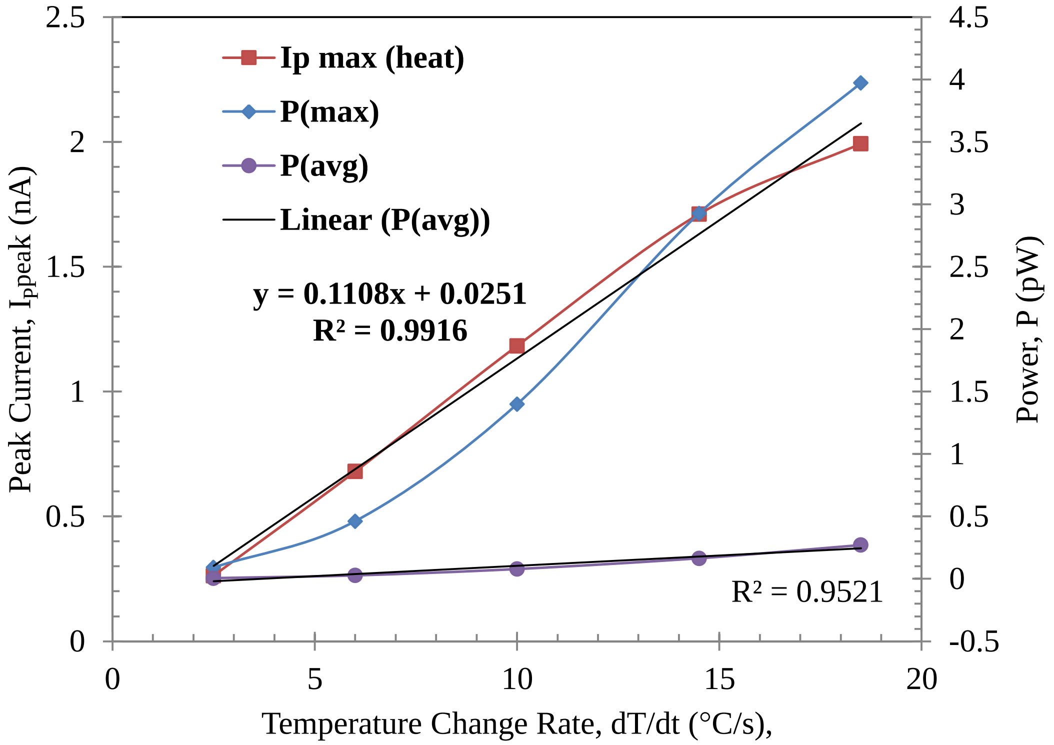

Figure 5.15: Increase in harvested power with increased temperature cycle rate.

The average power was calculated by integrating the power over a period of temperature cycling and dividing by the time period. For a given range of temperature swing, increasing the frequency of the temperature cycling yields better average power production. The reason is that the pyroelectric material only produces current while the temperature is changing and it is proportional to the change rate. Highest current is produced initially when the temperature rises fast to reach the set value and diminishes as the temperature is settling to final value after the thermal time constant. Therefore when averaging the power over a period the value is reduced due to dividing total power with a longer time period. To mitigate this issue, the temperature needs to be changed at a fast rate during most part of the period. This can be achieved by following a time period close to the thermal time constant without concerning whether the temperature reached set-point or not. This would give a better average power rating. Attempt was taken to cycle the temperature at up to 5 Hz frequency. But due to the limitation of the thermoelectric cooler/heater only up to 0.21 Hz can be successfully achieved. Beyond this frequency the temperature in the mount/sample could not follow the set periods and temperature cycles at a much lower rate of *dT/dt*. The temperature range between which the sample cycles itself becomes very small. Figure 5.16 provides the picture of average power and the average current during a single cycle time period, *T* as the frequency of the temperature cycling is varied.

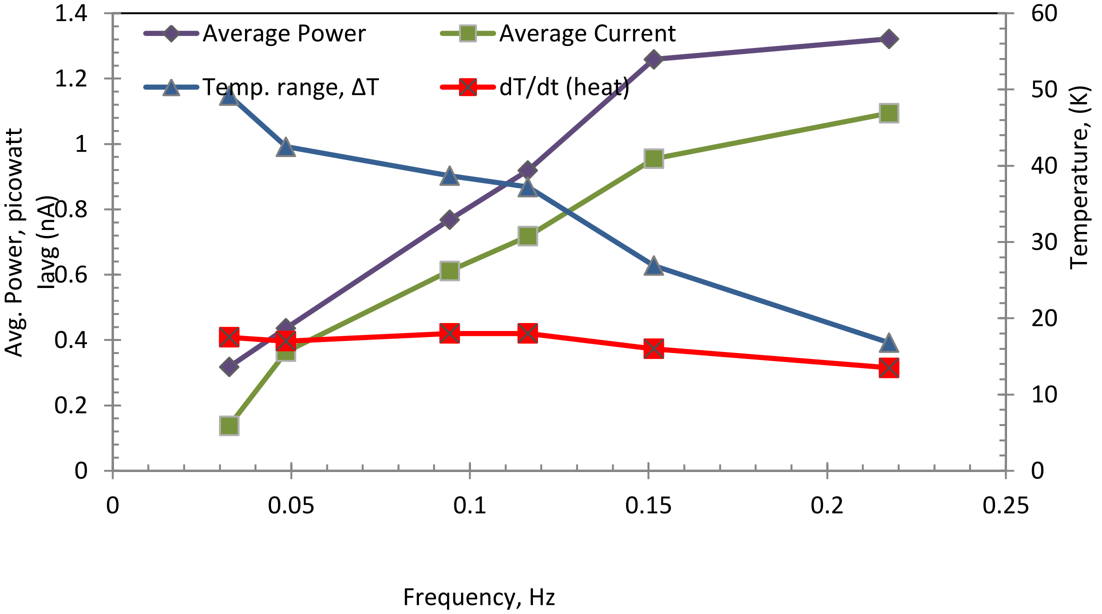

Figure 5.16: Average power and average power with increasing frequency. Optimal frequency is 0.2Hz at the given instrumental setup.

There is an optimal point where frequency is too fast for the temperature to reach the set point and the temperature change rate suffers. At this point the power harvested is calculated for power density.

Power harvested= 1.3 Pico-Watt

Area= 3.14159×10^{-6} m^2

Thickness= 25μm

Volume= 78.5×10^{-12} m^3 = 78.5×10^{-9} L.

Power density = 16.6μW/L.

Although the value found from initial measurement is very unattractive at this point, this is not the best case scenario or optimum frequency. The optimum frequency where the duty cycle is 50% should have a period close to the thermal time constant of the pyroelectric capacitor. In practice that frequency is far above 0.15 Hz and beyond the limit of the thermoelectric heaters temperature cycling capability. It is also to be noted the pyroelectric polymer used in this measurement is as found commercially and not processed to optimize the sample to have higher pyroelectric coefficient. Also it was operated at temperature far below the Curie temperature (~ 85°C) where polarization is found to be the maximum. This measured power is obtained for non-optimal load condition. Under matched load impedance the maximum power that can be harvested can be calculated using equation (4-30) and results in a 220W/L energy harvested per dot. The same equation can be used to calculate for power generated under ideal conditions where temperature can be cycled at 70K difference at around 50Hz frequency as deemed possible from the simulated performance. Figure 5.17 plots the predicted maximum energy harvested from a 5mm long device

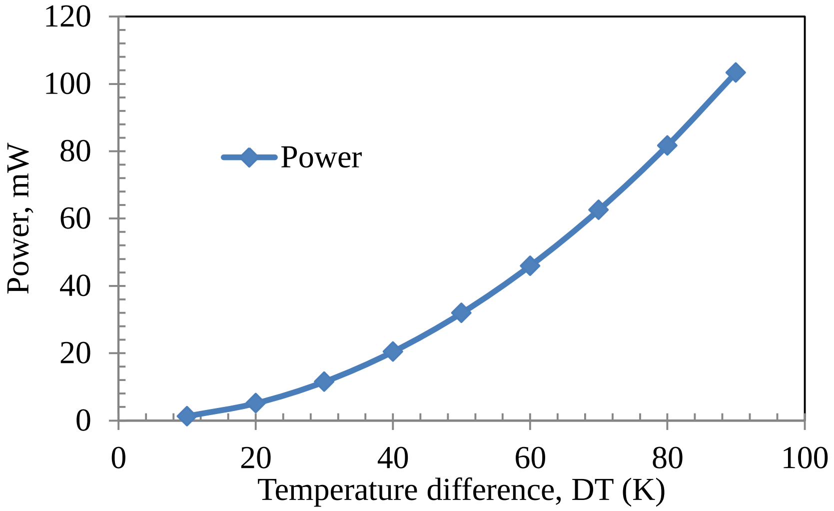

Figure 5.17: Theoretically calculated maximum harvested power, for 50Hz frequency temperature cycling.

that cycles temperature at 50Hz frequency for different temperature difference. At 70K difference, the generated power per device is calculated to be 62.53 mW. This translates to an energy density of 400,000W/L.

5.4.2.3 Results and Discussion

To achieve variable temperature change rate the range of temperature was varied which changed how fast the thermoelectric cooler was increasing or decreasing the temperature as it has a fixed time constant within which it operates. The period of the temperature cycling was also varied so that time varying temperature plot becomes almost sinusoidal. Figure 5.19 plots the temperature and the current data from a faster temperature cycling with sinusoidal behavior. Faster cycling or short periods results in the thermoelectric heater falling short from reaching the set-point value

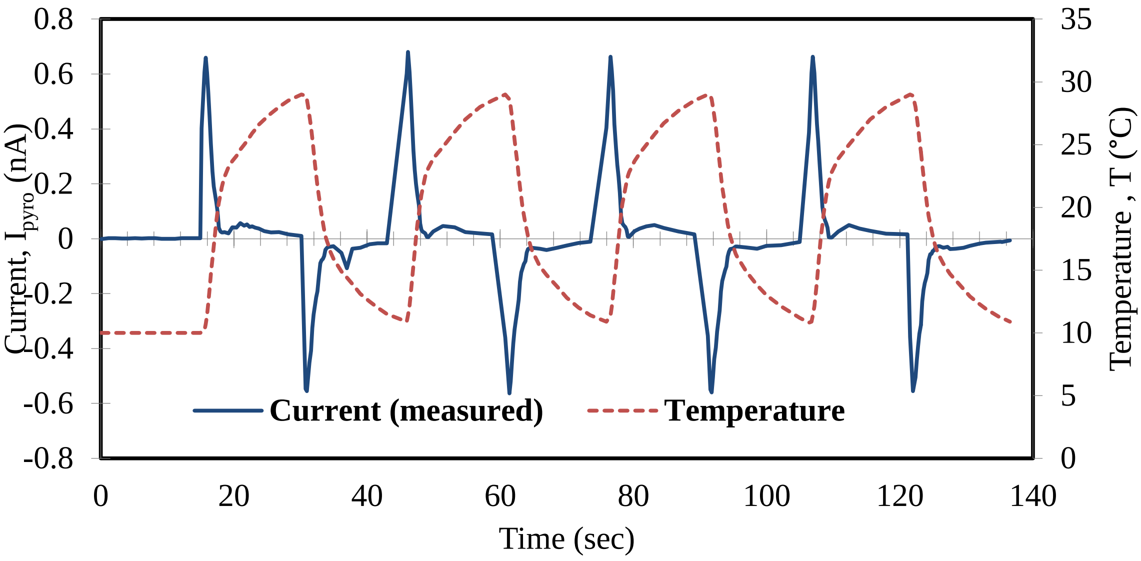

Figure 5.18: Pyroelectric current with temperature change.

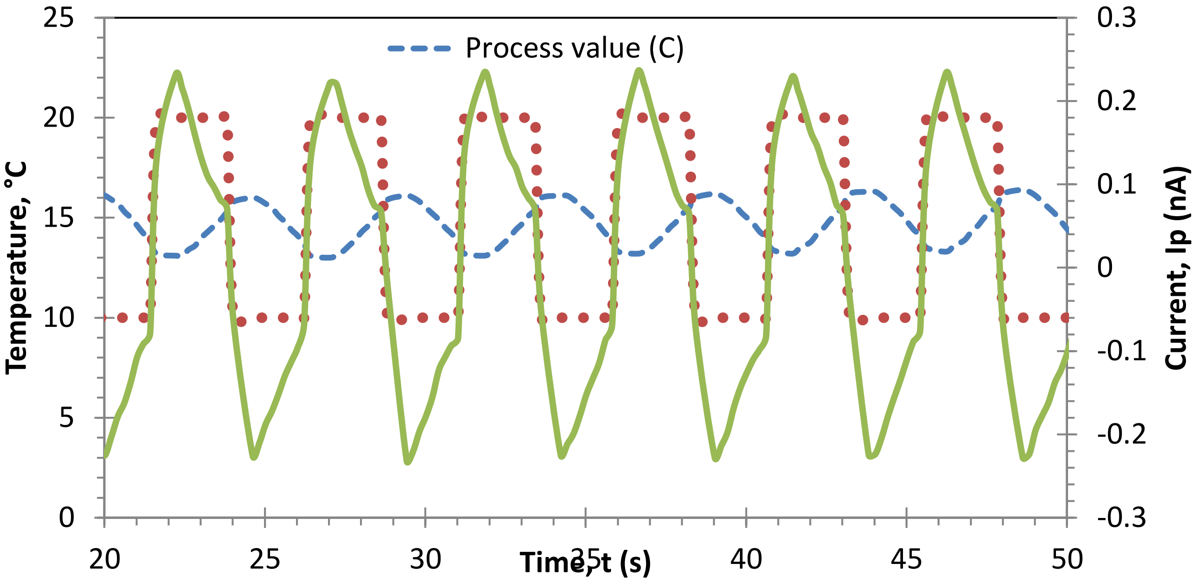

Figure 5.19: Faster temperature cycling gives sinusoidal temperature variation but reduced peak current.

over a wide range of temperature swing and thereby results in smaller temperature change rate, giving a reduced peak current for this case. Since the thermoelectric heater has a built-in thermal time constant, by setting the temperature value the instrument had to reach in that time, the temperature change rate was varied and the resulting peak current was measured.

Figure 5.15 shows the increase in peak current with increase in temperature change rate. From the current measurement data power was also calculated assuming a 1 MegaOhm input resistance of the pre-amplifier as resistive load. The peak power also increases with temperature change rate increase.

5.5 Conclusion

The experimental results show progress and promise towards realizing the proposed device. Characterization and measurement data project a picture of the possible output from the energy harvester. But there are still more steps to undergo before a final finished product can be launched. The next chapter focuses on the future works towards completion of this proposed energy harvester to a successful goal which was not possible to undertake in the given time frame.

Chapter 6

CONCLUSIONS

This research looks at establishing a new and innovative way to scavenge energy from low grade waste heat sources in an efficient and cost-effective manner. It employs MEMS technology to take advantage to self-governed system and pyroelectric property of material to convert heat to electrical energy.

6.1 Summary

6.1.1 Self-oscillating bimaterial MEMS cantilever

The building block of the energy harvesting device proposed in this research is the thermally actuated self-oscillating bimaterial MEMS cantilever. The criteria for a bimaterial cantilever to respond to thermal excitation for cycling heat from a heat source to a heat sink and thereby vary temperature within itself has been researched and identified. The thermal and mechanical responses of such a cantilever with variable physical properties have been studied and characterized. Numerical and analytical models have been developed to simulate and predict these responses of the aforementioned device. A SPICE based equivalent model has been developed to calculate for pyroelectric and thermomechanical MEMS response in a combined simulation.

Based on the response obtained from the simulations, optimized design properties have been recognized and practical device fabrication is pursued guided by this knowledge. Simulated model response suggested that in the bimaterial cantilever equivalent thickness of the layer and equivalent stiffness gives the best mechanical response. Thermal response is better when cantilever length is small and the cross-sectional area is large. The self-oscillating device model also indicates that for greater amount of heat cycling and thermal power transfer higher thermal conductance is preferred, albeit frequency compromise. The calculated numbers promise self-oscillating frequency up to 222 Hz with transferred thermal power as high as 5.6 mW for a device that is 0.25 mm^2 in size.

The simulated model for bimaterial cantilever was extended to account for embedding of pyroelectric element layer. Optimized properties for best thermomechanical response were researched. It was noticed that a 10:1 thickness ratio for the embedded layer and bimaterial layers provides best thermomechanical response. The fabricated devices responsivity has been characterized with measured mechanical response with controlled temperature change. The measured responsivity for a 7 mm long silicon di-oxide/aluminum cantilever is 300 μm/°K and 6.31 μm/°K for silicon/gold cantilever.

6.1.2 Pyroelectric energy harvesting

The goal of this research work is to harvest energy from a heat source using pyroelectric material. The aforementioned MEMS device is used to cycle temperature in the pyroelectric element to generate current. To comply with the performance of the MEMS device polymeric PVDF is chosen as the energy harvesting pyroelectric material. Pyroelectric current generation formula in relation with MEMS device performance has been developed and power harvesting equation been developed. Commercially collected PVDF material has been characterized for pyroelectric coefficient and current generation capacity. In the laboratory setup temperature change of 30K at 0.2 Hz frequency generates maximum 16.6 μW/L power density.

6.2 Future Plan

Modeling:

- FEM Modeling of the pyroelectric behavior: The finite element model of the pyroelectric model has to be developed using multiphysics simulation tool. This can be achieved by solving electrical charge distribution equation where similar to modeling a capacitor model. Temperature change rate has to be used instead of voltage input. Temperature change rate data can be extracted from the self-oscillation temperature cycling model and used as input. A preferred and advanced method would be to couple electric current model with heat conduction and solid mechanics model so that the software can use the temperature data automatically.
- MATLAB CODE for analytical model: MATLAB code solving for time and space dependent temperature distribution and corresponding response of the bimaterial structure will be helpful to calculate for device performance and design.
- Electronic circuit: A circuit for rectifying and storing the current output from the pyroelectric sample can be simulated using SPICE. Combining the rectification circuit with the SPICE model will give a complete simulation system of the energy harvester.

Experimental:

- Optimum load resistance: The pyroelectric current extracted from the sample is maximum when the load resistance is equal to the output impedance of the sample itself. Finding output impedance matching for pyroelectric sample to extract maximum power output is important for maximizing efficiency of energy harvester.

- Integration: A pyroelectric capacitor sample has to be integrated with the self-oscillating cantilever. The pyroelectric material must contain top and bottom contacts to extract current from the sample.
- To implement the rectifying and storage electronic circuit and demonstrate operating a low-power electronics with the stored power.

Appendix A

COMSOL Modeling Instructions

Model Wizard

1. Go to the Model Wizard window.
2. Select space dimension as 2D.
3. Click next icon.
4. In the Add Physics tree, select Heat Transfer> Heat Transfer in Solids.
5. Click '+' to add to selected physics.
6. In the Add Physics tree, select Structural Mechanics>Solid Mechanics (solid).
7. Click '+' to add to selected physics.
8. Click next icon.
9. In the Studies tree, select Preset Studies>Time Dependent.
10. Click Finish.

Geometry

1. In the geometry settings window select Length Unit as m for meters, Angular unit in Degrees.

   Keep Default relative repair tolerance as 1.0E-6.

Rectangle 1 (r1)

1. In the Model Builder window, right-click Geometry 1 and select Rectangle.
2. Go to the Settings window for Rectangle.
3. Locate the Size section. In the Width edit field, type 1e-3.

4. In the Height edit field, type 10e-6.
5. In the position section select Base as Corner and type 0 and 0 for x and y.
6. Click Build Selected icon.
7. Right click Rectangle 1 and Rename. Type Aluminum-10um in the New name field.

Rectangle 2 (r2)

1. In the Model Builder window, right-click Geometry 1 and select Rectangle.
2. Go to the Settings window for Rectangle.
3. Locate the Size section. In the Width edit field, type 1e-3.
4. In the Height edit field, type 10e-6.
5. In the position section select Base as Corner and type 0 for x and -10e-6 for y.
6. Click Build Selected icon.
7. Right click Rectangle 2 and Rename. Type SiO2-10um in the New name field.

Rectangle 3 (r3)

1. In the Model Builder window, right-click Geometry 1 and select Rectangle.
2. Go to the Settings window for Rectangle.
3. Locate the Size section. In the Width edit field, type 200e-6.
4. In the Height edit field, type 50e-6.
5. In the position section select Base as Corner and type 800e-6 for x and 30e-6 for y.
6. Click Build Selected icon.
7. Right click Rectangle 3 and Rename. Type Heat Source in the New name field.

Ellipse 1 (e1)

1. In the Model Builder window, right-click Geometry 1 and select Ellipse.
2. Go to the Settings window for Ellipse.
3. Locate the Size section. In the a-semiaxis edit field, type 20e-6.
4. In the b-semiaxis edit field, type 9e-6.
5. In the position section select Base as Center and type 940e-6 for x and 10e-6 for y.
6. Click Build Selected icon.
7. Right click Ellipse 1 and Rename. Type contact bump in the New name field.

Union 1 (uni1)

1. In the Model Builder window, right-click Geometry 1>Boolean Operation>Union.
2. Go to the Settings window for Union.
3. In the Graphics window click r1 and right click to select.
4. Click e1 and right click to select.
5. In the Relative repair tolerance edit field type 1.0e-8.
6. Click Build Selected icon.

Ellipse 1 (e1)

1. In the Model Builder window, right-click Geometry 1 and select Ellipse.
2. Go to the Settings window for Ellipse.
3. Locate the Size section. In the a-semiaxis edit field, type 20e-6.

4. In the b-semiaxis edit field, type 10e-6.
5. In the position section select Base as Center and type 940e-6 for x and 30e-6 for y.
6. Click Build Selected icon.
7. Right click Ellipse 1 and Rename. Type contact bump in the New name field.

Rectangle 4 (r4)

1. In the Model Builder window, right-click Geometry 1 and select Rectangle.
2. Go to the Settings window for Rectangle.
3. Locate the Size section. In the Width edit field, type 60e-6.
4. In the Height edit field, type 20e-6.
5. In the position section select Base as Corner and type 910e-6 for x and 30e-6 for y.
6. Click Build Selected icon.

Difference 1 (dif1)

1. In the Model Builder window, right-click Geometry 1>Boolean Operation>Difference.
2. Go to the Settings window for Difference.
3. Click on the Objects to add edit field.
4. In the Graphics window click e2 and right click to select.
5. Click on the Objects to subtract edit field.
6. In the Graphics window click r4 and right click to select.
7. Click r4 and right click to select.
8. In the Relative repair tolerance edit field type 1.0e-8.

9. Click Build Selected icon.

Click Form Union (fin) and in the Finalize tab and click Build all icon to complete the geometry.

Material

Material 1

1. Right click the Materials tab and click Open Material Browser.
2. In the Built-In tab right click Silica glass and click Add material to model.
3. In the graphics tab click domain 1, right click to select.
4. Go to the Settings window for Material.
5. Locate the Material Contents section. In the Material contents table, enter the values from Table A-1.

Table A-1: Material properties

Property	Silica Glass	Aluminum	Aluminum_lowK	Unit
Young’s modulus	73.1e9	70e9	70e9	Pa
Poisson’s ratio	0.17	0.33	0.33	
Density	2203	2700	2700	Kg/m^3
Coefficient of thermal expansion	0.55e-6	23e-6	23e-6	1/K
Heat capacity	703	900	900	J/Kg-K
Thermal conductivity	1.38	160	160	W/mK

Material 2

1. Right click the Materials tab and click Open Material Browser.
2. In the Built-In tab right click Aluminum and click Add material to model.
3. In the graphics tab click domain 2 and 3, right click to select.
4. Go to the Settings window for Material.
5. Locate the Material Contents section. In the Material contents table, enter the values from Table A-1 for Aluminum.

Material 3

1. Right click the Materials tab and click Open Material Browser.
2. In the Built-In tab right click Aluminum and click Add material to model.
3. In the graphics tab click domain 4, right click to select.
4. Go to the Settings window for Material.
5. Locate the Material Contents section. In the Material contents table, enter the values from Table A-1 for Aluminum_lowK.
6. Right click Aluminum (2) and click rename. In the new name field type Alluminum_lowK.

Definitions

Identity Pair 1

1. Right click on the Definitions tab and select Identity pair.
2. In the Identity pair 1 Settings window type hot_contact in the Pair name edit field.
3. Click on the Source Boundaries section to choose source boundaries. In the graphics window select boundary 15, 17.
4. Click on the Destination Boundaries section. In the Graphics window select boundary 16, 18.

Probe 1

1. Right click Definitions> Probes>Domain point probe.
2. In the settings windows, type 1e-3 for x and 0 for y coordinates.
3. Right click and select Rename to edit the New name field to be Cantilever Tip.
4. Right click on Cantilever Tip and select Point probe expression.
5. In the Point probe expressions 1 settings window type T_tip in the Probe name edit field.
6. In the expression section type T-293.15 in the Expression edit field. Choose Unit to be K, turn on description and type Temperature in the edit field.
7. Right click on Cantilever Tip and select Point probe expression.
8. In the Point probe expressions 2 settings window type Dz_tip in the Probe name edit field.
9. In the expression section type -v in the Expression edit field. Choose Unit to be μm, turn on description and type Displacement in the edit field.

Probe 2

1. Right click Definitions> Probes>Domain point probe.
2. In the settings windows, type 940e-6 for x and 20.3e-6 for y coordinates.
3. Right click and select Rename to edit the New name field to be Source at contact.
4. Right click on Source at contact and select Point probe expression.
5. In the Point probe expressions 1 settings window type T_source_contact in the Probe name edit field.
6. In the expression section type T-293.15 in the Expression edit field. Choose Unit to be K, turn on description and type Temperature @ source contact in the edit field.

Probe 3

1. Right click Definitions> Probes>Domain point probe.
2. In the settings windows, type 940e-6 for x and 18.8e-6 for y coordinates.
3. Right click and select Rename to edit the New name field to be Cantilever at contact.
4. Right click on Cantilever at contact and select Point probe expression.
5. In the Point probe expressions 1 settings window type T_CL_contact in the Probe name edit field.

6. In the expression section type T-293.15 in the Expression edit field. Choose Unit to be K, turn on description and type Temperature @ cantilever contact in the edit field.
7. Right click on Cantilever at contact and select Point probe expression.
8. In the Point probe expressions 2 settings window type Dz_CL_contact in the Probe name edit field.
9. In the expression section type -v in the Expression edit field. Choose Unit to be μm, turn on description and type Displacement @ cantilever contact in the edit field.

Probe 4

1. Right click Definitions> Probes>Domain point probe.
2. In the settings windows, type 0.8e-3 for x and 0 for y coordinates.
3. Right click and select Rename to edit the New name field to be 200um from tip.
4. Right click on 200um from tip and select Point probe expression.
5. In the Point probe expressions 1 settings window type T_200um_tip in the Probe name edit field.
6. In the expression section type T-293.15 in the Expression edit field. Choose Unit to be K, turn on description and type Temperature @ 200um from tip in the edit field.

Probe 5

1. Right click Definitions> Probes>Domain point probe.

2. In the settings windows, type 700e-6 for x and 0 for y coordinates.
3. Right click and select Rename to edit the New name field to be 300um from tip.
4. Right click on 300um from tip and select Point probe expression.
5. In the Point probe expressions 1 settings window type T_300um_tip in the Probe name edit field.
6. In the expression section type T-293.15 in the Expression edit field. Choose Unit to be K, turn on description and type Temperature @ 300um from tip in the edit field.

Physics

Heat Transfer(ht)

1. In the Model Builder window, click Heat Transfer (ht).
2. In the settings window locate the Domains section and select All domains from the Selection drop down menu.
3. Click on Heat Transfer in Solids 1 tab. Ensure domains 1,2,3 and 4 is selected in the list. Choose from material for all material properties from the drop-down menu.
4. Click Initial Values 1 tab. In the Initial Values section type 293.15 in the Temperature edit field and 0 in Surface Radiosity edit field.
5. Right click on Heat Transfer tab and choose Initial values from the domain level option list.
6. In the Initial Values 2 settings window select Manual from the drop down menu. In the Graphics window click domain 3 and right click to select. In the Initial values section type

293.15+T in the temperature edit field, where T can be any temperature value the model will be used to simulate for.

7. Right click on Heat Transfer tab and choose Temperature from the boundary level option list.
8. In the Graphics Window select boundaries 6,8 and 14. In the Initial Values section type 293.15+T in the Temperature edit field, where, T is the temperature difference the simulation is being solved for.
9. Right click on Heat Transfer tab and choose Temperature from the boundary level option list.
10. In the Graphics Window select boundaries 1 and 3. In the Initial Values section type 293.15 in the Temperature edit field.
11. Right click on Heat Transfer tab and choose Pairs>Heat Continuity.
12. In the Heat continuity settings window locate Pair selection section select Identity Pair 1. Ensure that 15,16,17,18 is selected in Boundaries section.

Solid Mechanics (solid)

1. In the Model Builder window, select Solid Mechanics (solid).
2. Go to the Settings window and type 1 [m] in the Thickness edit field.
3. Locate the 2D Approximation section. From the 2D approximation list, select Plane strain from the drop down menu.
4. In the Model Builder window, select Linear Elastic Material Model.

5. Select Domain 1,2,3,4.
6. Go to the Settings window for Linear Elastic Material Model.
7. Locate the Geometric Nonlinearity section. Select the Include geometric nonlinearity check box.
8. Right click on the Linear Elastic Material Model 1 ans select Thermal Expansion.
9. In the Thermal Expansion 1 settings window select domain 1 and 2.
10. In the Model Inputs choose Temperature (ht/solid1) from the drop down menu.
11. In the Thermal expansion section type 293.15 [K] in the Strain reference temperature edit field.
12. In the Model Builder window, right-click Solid Mechanics (solid) and select Fixed Constraint.
13. Select Boundaries 1, 3, 6, 8, 14.

Mesh

1. In the Mesh 1> Size tab chose Element Size as Finer from the drop down menu.
2. In the Model Builder window, right-click Mesh 1 and select Free Triangular.

3. In the Free Triangular tab select domain and 1,4.
4. In the scale geometry section typ1 1.3 in the x-direction scale edit field. Click Build selected.
5. Right click Mesh 1 and choose Mapped. Select domain 2, 3. Click build selected.

6. Right click Mesh 1 and choose Boundary Layers.
7. In the settings window choose domain 2.
8. In the Advanced Settings widnow select the check box for Boundary layer split at sharp corners. Type 210 as the minimum split angle and 110 as the maximum angle per split.
9. Right click Mesh 1 and choose Boundary Layer Properties.
10. In the settings window choose Boundaries 15, 17.
11. In the Boundary Layer Porperties section type 4 as Number of boundary layers and 1.2 as Boundary layer stretching factor. Keep Thickness of first layer as Automatic.
12. Click Build selected.

Study 1

1. In >Step1: Time dependent settings window type range(0,1e-3,200e-3).
2. Select thr check box for Plot. Choose Probe 1D plot group 1 for drop down menu and Output times in the Update at drop down menu.
3. In the Solver configuration tab, right click and select Show default server.
4. In Solver 1 click mod1_solid_pw and uncheck Solve for this field.
5. In the Time-dependent Solver 1 settings window locate the General section. In the Relative tolerance edit field, type 1e-3
6. In the Absolute Tolerance section type Tolerance 0.001.
7. In the Time stepping section chose Method as Generalized Alpha, Steps taken by solver Manual.

8. Type 1e-4 in the Time step edit field. Amplification for high frequency 0.1 and chose predictor as Linear.
9. In the Results while Solving section check Plot and chose 2D Plot group 2 from the Plot group drop down menu. Chose Time steps from the solver for the Update at drop down menu.
10. In the Time-Dependent Solver 1> Direct 1 tab chose PARDISO as the Solver drop down menu.

Appendix B

Matlab Programs

1. Analytical model for temporal thermomechanical response of the bimaterial cantilever.

```
clc;

length=500e-6;

width=100e-6;

tal=10e-6;tsio2=10e-6;%thickness

m=tsio2/tal; % ratio of thickness

L=linspace(0,length,11);

cpal=900;cpsio2=703; %Specific Heat capacity

gal=160;gsio2=1.38;% thermal conductivity

pal=2700;psio2=2200; % density (Kg/m^3)

aal=23e-6;asio2=0.55e-6;% THermal expansion coefficient

Eal=70e9;Esio2=73.1e9; %Young's Modulus

n=Esio2/Eal; % ratio of young's modulus

time=linspace(0,28e-3,29);

for j=1:11;

    massal(j)=L(j)*width*tal*pal; %mass
```

```
masssio2(j)=L(j)*width*tsio2*psio2; %mass

Gcal(j)=gal*width*tal/L(j);      Gcsio2(j)=gsio2*width*tsio2/L(j);
%thermal conductance;

end

Cal=massal*cpal;

Csio2=masssio2*cpsio2; %heat capacitance

C=(Cal+Csio2)/2; % total equivalent capacitance

%Gcal=gal*width*tal/length;

Gcsio2=gsio2*width*tsio2/length;%thermal conductance

G=Gcal+Gcsio2; % total equivalent thermal conductance.

Thot=313; Tcold=293;

h=tal+tsio2; %height

tl2h=3*length^2/(2*h);

opm2=(1+m)^2;

opmn=1+m*n;

msp1mn=m^2+1/(m*n);

da=aal-asio2;

delT=zeros(2,29);       Tana=zeros(2,29);       Tsim=zeros(2,29);
dzana=zeros(2,29);
```

```
dz(1,1)=0;

for t=1:29

    for k=1:11

        tau(k)=C(k)/G(k);

        dummy2=(t-1)*1e-3/tau(k);

        dummy=exp(-dummy2);

        delT(k,t)=(Thot-Tcold)*dummy;

        Tana(k,t)=Thot-delT(k,t);

        Tsim(k,t)=Thot-delT(k,t);

        dzana(k,t)=tl2h*opm2*(aal-asio2)*(Tana(k,t)-
Tcold)/(3*opm2+opmn*msp1mn);

        dztip(k,t)=0.5e-3*dzana(k,t)/L(k);

        if (t*1e-3)<tau(k);

           dz(k,t)=dzana(k,t);

        elseif t==1

            dz(k,t)=dz(k,t);

        else t>1 && (t*1e-3)>tau(k);

            dz(k,t)=dz(k,t-1);

        end
```

```
    end

end

plot(time,Tana,time,Tsim,'rd')

figure;

plot(time,dz(1:29),time,dz_sim,'rd')
```

2. Analytical model for thermomechanical response of the multilayer cantilever.

```
clc;

clear all;

%responsivity calculation of multilayer cantilever beam

%material =[SU8 Al SiO2]; % from bottom to top.

E=[3.2e9 70e9 73.1e9];% Young's modulus [Pa]

rho=[1.5e6 2.7e6 2.22e6];%density [g/m^3]

alfa=[8.71e-5 23e-6 0.55e-6];%thermal expansion coefficient [m/K]

Gc=[0.2 160 1.38];% Thermal conductivity [W/m-k]

Cp=[2 0.9 0.703];%Specific heat capacity [J/g-K]

%Thickness matrix

t=[7.5e-6  50e-9  1e-6;  15e-6  100e-9  2e-6;  22.5e-6  150e-9  3e-6;
30e-6 200e-9 4e-6; 37.5e-6 250e-9 5e-6; 45e-6 300e-9 6e-6];
```

```
tal=[50e-9 100e-9 150e-9 200e-9 250e-9 300e-9];%Thickness of aluminum [m]
tsio2=[1e-6 2e-6 3e-6 4e-6 5e-6 6e-6];%Thickness of SiO2 [m]
tsu8=[7.5e-6 15e-6 22.5e-6 30e-6 37.5e-6 45e-6];%Thickness of SU8[m]
L=[0.5e-3 1e-3 2e-3 3e-3 4e-3 5e-3 6e-3 7e-3];%[m]
w=L/4;%[m]
% calculating radius of curvature.
%find Ai
 sumaEtw=0;sumEtw=0;sumCEtw=0;
 C(1)=t(6,1);
  for i=2:3
        C(i)=C(i-1)+t(6,i);
        CEtw=C(i)*E(i)*t(6,i)*w(1);
        sumCEtw=sumCEtw+CEtw;
  end
for i=1:3
        aEtw=alfa(i)*E(i)*t(6,i)*w(1);
        Etw=E(i)*t(6,i)*w(1);
```

```
        sumaEtw=sumaEtw+aEtw;
        sumEtw=sumEtw+Etw;
end
    dT=20; %[k] Temperature difference
for i=1:3
    A(i)=(-alfa(i)+sumaEtw/sumEtw)*dT*E(i)*t(6,i)*w(1);
    B(i)=(C(i)-sumCEtw/sumEtw)*E(i)*t(6,i)*w(1);
end
 sumEI=0;
for i=1:3
    I(i)=(t(6,i)^3)/12;%calculating Moment I for each layer
    EI=E(i)*I(i);% and multiplying with Young's modulus
    sumEI=sumEI+EI; %summing
end
sumAC=0;sumBC=0;
for i=2:3
    AC=A(i)*C(i);
    sumAC=sumAC+AC;
    BC=B(i)*C(i);
```

```
    sumBC=sumBC+BC;

end

r=(2*sumAC)/(0+sumBC);% radius of curvature

dy=((L(1)^2)/2)*r % tip deflection
```

Appendix C

SPICE NETLIST

1. SPICE Model of Electrothermal MEMS

```
C1 N001 0 1.244µ
R1 N002 N001 1608.8
R2 N003 N002 2855.6
C2 N002 0 1.94µ
V1 N001 0 PULSE(0 20 1m 1n 1n 50m 100m 2)
C3 N003 0 336.46f
.tran 0 200m 0m .1m
.backanno
.end
```

2. SPICE model of Pyroelectric Current generating Thermoelectric MEMS

```
C1 N002 0 1.244µ
R1 N004 N002 1608.8
R2 N006 N004 2855.6
C2 N004 0 1.94µ
V1 N005 0 PULSE(0 20 1m 1n 1n 50m 100m 2)
C3 N006 0 336.46f
B1 0 N007 I=i(C3)
R3 N007 0 1k
XU1 N003 0 NC_01 0 N001 LT1018
XU2 N004 N002 NC_02 0 N003 LT1001
S1 N002 N005 N001 0 SW
.tran 0 200m 0m .1m
.lib LTC.lib
.lib LTC1.lib
.backanno
.end
```

References

[1]"Key world energy statistics 2010," International Energy agency, 2010.

[2] "Annual Energy Review," U.S. Energy Information Administration, 2009.

[3] "Key World Energy Statistics," International Energy Agency, 2011.

[4] "Annual Enery Outlook," http://www.eia.gov/forecasts/aeo, 2011.

[5] N. R. Lo, , E. C. Berg, S. R. Quakkelaar, J. N. Simon, M. Tachiki, Lee Hee-Jung, K. S. J. Pister, "Parameterized layout synthesis, extraction, and SPICE simulation for MEMS," in *Circuits and Systems, 1996. ISCAS '96., 'Connecting the World'., 1996 IEEE International Symposium on*, 1996, pp. 481-484 vol.4.

[6] J. A. Paradiso and T. Starner, "Energy scavenging for mobile and wireless electronics," *Pervasive Computing, IEEE,* vol. 4, pp. 18-27, 2005.

[7] M. J. Moran and H. N. Shapiro, *Fundamentals of engineering Thermodynamics*, 6th edition ed.: John Wiley and Sonc. Inc., New york, NY, , 2004.

[8] "Conversion of Low-Grade Waste Heat to Electricity," CanmetENERGY, Ottawa CETC Number 2008-56 / 2006-02-28, 2008.

[9] A. V. D. Ziel, "Solar power generation with the pyroelectric effect," *Journal of Applied Physics,* vol. 45, p. 4128, 1974.

[10] (June 24, 2011). *Cogeneration*. Available: http://en.wikipedia.org/wiki/Cogeneration

[11] S. B. Riffat and X. Ma, "Thermoelectrics: a review of the present and potential applications," *Applied Thermal Engineering,* vol. 23, pp. 913-935, 2003.

[12] R. B. Olsen, D. A. Bruno, J. M. Briscoe, J. Dullea,, "Cascaded Pyroelectric Energy Converter," *Ferroelectrics,* vol. 59, pp. 205-219, 1984.

[13] R. B. Olsen, J. M. Briscoe, D. A. Bruno, W. F. Butler, "A Pyroelectric Energy Converter Which Employs Regeneration," *Ferroelectrics,* vol. 38, pp. 975-978, 1981.

[14] R. B. Olsen and D. D. Brown, "High-Efficiency Direct Conversion Of Heat To Electrical Energy-Related Pyroelectric Measurements," *Ferroelectrics,* vol. 40, pp. 17-27, 1982.

[15] R. B. Olsen, D. A. Bruno, J. M. Briscoe, E. W. Jacobs, "Pyroelectric conversion cycle of vinylidene fluoride-trifluoroethylene copolymer," *Journal of Applied Physics,* vol. 57, pp. 5036-5042, 1985.

[16] M. Ikura, "Conversion of low-grade heat to electricity using pyroelectric copolymer," *Ferroelectrics,* vol. 267, pp. 403-408, 2002.

[17] H. Nguyen, A. Navid, L. Pilon, "Pyroelectric energy converter using co-polymer P(VDF-TrFE) and Olsen cycle for waste heat energy harvesting," *Applied Thermal Engineering,* vol. 30, pp. 2127-2137, 2010.

[18] G. Sebald, E. Lefeuvre, D. Guyomar, "Energy harvesting based on Ericsson pyroelectric cycles in a relaxor ferroelectric ceramic," *Smart Material Structures,* vol. 17, p. 5012, February 1, 2008.

[19] D. Guyomar, G. Sebald, S. Pruvost, M. Lallart, "Ambient energy harvesting using ferroelectric materials," 2008, p. 692808.

[20] D. Guyomar, S. Pruvost, G. Sebald, "Energy harvesting based on FE-FE transition in ferroelectric single crystals," *Ieee Transactions on Ultrasonics Ferroelectrics and Frequency Control,* vol. 55, pp. 279-285, Feb 2008.

[21] S. B. Lang, "Pyroelectricity: From Ancient Curiosity to Modern Imaging Tool," *Physics Today,* vol. 58, pp. 31-36, 2005.

[22] J. N. Zemel, "Future directions for thermal information sensors," *Sensors and Actuators,* vol. 56, pp. 57-62, 1996.

[23] W. H. Clingman and R. G. Moore, "Application of ferroelectricity to energy conversion process," *Journal of Applied Physics,* vol. 32, pp. 675-681, 1961.

[24] E. Fatuzzo, H. Kiess and R. Nitsche,"Theoretical efficiency of pyroelectric power converters," *Journal of Applied Physics,* vol. 37, pp. 510-516, 1966.

[25] R. Sanders. (18th July 2011). *Physicists build world's smallest motor using nanotubes and etched silicon*. Available: http://berkeley.edu/news/media/releases/2003/07/23_motor.shtml

[26] S. B. Lang and D. K. Dasgupta, *Handbook of Advanced Electronic and Photonic Materials and Devices* vol. 4. San Diego, Ca: Academic Press, 2001.

[27] F. J. Balta Calleja, A. Gonzalez Arche, T. A. Ezquerra, C. Santa Cruz, F. Batllan, B. Frick, E. Lopez Cabarcos, "Structure and properties of ferroelectric copolymers of poly(vinylidine fluoride)," *Advances in Polymer Science,* vol. 108, pp. 1-48, 1993.

[28] M. A. Itskovsky, "Pyroelectric hysteresis loop at ferroelectric phase transition," *Journal of Applied Physics,* vol. 85, pp. 4256-4258, April 1, 1999 1999.

[29] J. Grindlay, *An introduction to phenomenological theory of ferroelectricity*. London

Pergamon Press Ltd., 1970.

[30] (June 27, 2011). *Difference between pyroelectricity and ferroelectricity*. Available: http://www.doitpoms.ac.uk/tlplib/pyroelectricity/polarisation.php

[31] H. M. Bao, J.F. Song, J.Zhang, Q.D. Shen, C.Z. Vang, Q.M Zhang,., "Phase transition and ferroelectric relaxor behavior in P(VDF-TrFE-CFE)," *Macromolecules,* vol. 40, pp. 2371-2379, 2007.

[32] T. Yamada, T. Ueda, T. Kitamaya, ,"Ferroelectric to paraeectric phase transition of vinylidene fluoride-trifluroethylene copolymer," *Journal of Applied Physics,* vol. 52, pp. 948-952, 1981.

[33] Theophrastus and J. Hill, *Theophrastus's history of stones*. London: Printed for the author, 1774.

[34] R. W. Whatmore, "Pyroelectric devices and materials," *Reports on Progress in Physics,* vol. 49, p. 1335, 1986.

[35] R. B. Olsen and D. Evans, "Pyroelectric energy conversion: Hysteresis loss and temperature sensitivity of a ferroelectric material," *Journal of Applied Physics,* vol. 54, pp. 5941-5944, 1983.

[36] D. Guyomar, G. Sebald, E. Lefeuvre, A. Khodayari, "Toward Heat Energy Harvesting using Pyroelectric Material," *Journal of Intelligent Material Systems and Structures,* vol. 20, pp. 265-271, Feb 2009.

[37] D. Guyomar, G. Sebald, S. Pruvost, M. Lallart, A. Khodayari, C. Richard, "Energy Harvesting from Ambient Vibrations and Heat," *Journal of Intelligent Material Systems and Structures,* vol. 20, pp. 609-624, Mar 2009.

[38] G. Sebald*, et al.*, "On thermoelectric and pyroelectric energy harvesting," *Smart Material Structures,* vol. 18, p. 5006, December 1, 2009 2009.

[39] G. Sebald, D. Guyomar, A. Agbossou, "Pyroelectric energy conversion: Optimization principles," *Ultrasonics, Ferroelectrics and Frequency Control, IEEE Transactions on,* vol. 55, pp. 538-551, 2008.

[40] N. Ashcon and P. Laurent, "Pyroelectric energy harvesting using Olsen cycles in purified and porous poly(vinylidene fluoride-trifluoroethylene) [P(VDF-TrFE)] thin films," *Smart Materials and Structures,* vol. 20, p. 025012, 2011.

[41] A. Navid, C. S. Lynch, L. Pilon, "Purified and porous poly(vinylidene fluoride-trifluoroethylene) thin films for pyroelectric infrared sensing and energy harvesting," *Smart Material Structures,* vol. 19, p. 5006, May 1, 2010.

[42] A. Navid, D. Vanderpool, A. Bah, L. Pilon, "Towards optimization of a pyroelectric energy converter for harvesting waste heat," *International Journal of Heat and Mass Transfer,* vol. 53, pp. 4060-4070, 2010.

[43] R. B. Olsen, D. A. Bruno, J.M. Briscoe, E. W. Jacobs, "Pyroelectric Conversion Cycles," *Journal of Applied Physics,* vol. 58, pp. 4709-4716, 1985.

[44] R. B. Olsen, D. A. Bruno, J. M. Briscoe, E. W. Jacobs, "High Electric-Field Resistivity And Pyroelectric Properties Of Vinylidene Fluoride-Trifluoroethylene Copolymer," *Journal of Applied Physics,* vol. 58, pp. 2854-2860, 1985.

[45] R. B. Olsen and D. Evans, "PYROELECTRIC ENERGY-CONVERSION - HYSTERESIS LOSS AND TEMPERATURE SENSITIVITY OF A FERROELECTRIC MATERIAL," *Journal of Applied Physics,* vol. 54, pp. 5941-5944, 1983.

[46] J. Fang, H. Frederich, L. Pilon, "Harvesting Nanoscale Thermal Radiation Using Pyroelectric Materials," *Journal of Heat Transfer,* vol. 132, p. 092701, 2010.

[47] A. Navid and L. Pilon, "Pyroelectric energy harvesting using Olsen cycles in purified and porous poly(vinylidene fluoride-trifluoroethylene) [P(VDF-TrFE)] thin films," *Smart Material Structures,* vol. 20, p. 5012, February 1, 2011 2011.

[48] D. Vanderpool, J. H. Yoon, L. Pilon, "Simulations of a prototypical device using pyroelectric materials for harvesting waste heat," *International Journal of Heat and Mass Transfer,* vol. 51, pp. 5052-5062, Oct 2008.

[49] D. Vanderpool, "Numerical and experimental study of a pyroelectric energy converter for harvesting waster heat," Masters, Mechanical Enginnering, University of California, Los Angeles, 2008.

[50] S. Bravina, N. Morozovsky, B. Guiffard, L. Lebrun, D. Guyomar, "Peculiarities of pyroelectric resonance-antiresonance phenomena in PZT ceramics," *Journal of the American Ceramic Society,* vol. 91, pp. 2223-2227, Jul 2008.

[51] D. Guyomar and G. Sebald, "Pyroelectric/electrocaloric energy scanvenging and cooling capabilities in ferroelectric materials," *International Journal of Applied Electromagnetics and Mechanics,* vol. 31, pp. 41-46, 2009.

[52] A. Hajjaji, S. Pruvost, G. Sebald, L. Lebrun, D. Guyomar, K. Benkhouja, "Mechanism of depolarization with temperature for < 001 > (1-x)Pb(Zn1/3Nb2/3)O-3-xPbTiO(3) single crystals," *Acta Materialia,* vol. 57, pp. 2243-2249, Apr 2009.

[53] A. Khodayari, S. Pruvost, G. Sebald, D. Guyomar, S. Mohammadi, "Nonlinear Pyroelectric Energy Harvesting from Relaxor Single Crystals," *Ieee Transactions on Ultrasonics Ferroelectrics and Frequency Control,* vol. 56, pp. 693-699, Apr 2009.

[54] G. Sebald*, et al.*, "Electrocaloric properties of high dielectric constant ferroelectric ceramics," *Journal of the European Ceramic Society,* vol. 27, pp. 4021-4024, 2007.

[55] G. Sebald, S. Pruvost, L. Seveyrat, L. Lebrun, D. Guyomar, B. Guiffard, "Electrocaloric and pyroelectric properties of 0.75Pb(Mg1/3Nb2/3)O-3-0.25PbTiO(3) single crystals," *Journal of Applied Physics,* vol. 100, Dec 2006.

[56] L. Kouchachvili and M. Ikura, "Improving the efficiency of pyroelectric conversion," *International Journal of Energy Research,* vol. 32, pp. 328-335, 2008.

[57] L. Kouchachvili and M. Ikura, "Pyroelectric conversion - Effects of P(VDF-TrFE) preconditioning on power conversion," *Journal of Electrostatics,* vol. 65, pp. 182-188, 2007.

[58] B. Lopez-Walle, M. Gauthier, N. Chaillet, "Dynamic modelling for thermal micro-actuators using thermal networks," *International Journal of Thermal Sciences,* vol. 49, pp. 2108-2116, Nov 2010.

[59] J. Reinke, G. K. Fedder, T. Mukherjee, "CMOS-MEMS Variable Capacitors Using Electrothermal Actuation," *Journal of Microelectromechanical Systems,* vol. 19, pp. 1105-1115, Oct 2010.

[60] C. I. Lee, C. H. Ko, T. C. Huang, F. C. Hsu, "Multiactuation complementary metal-oxide semiconductor radio frequency MEMS switch," *Journal of Micro-Nanolithography Mems and Moems,* vol. 9, Jul-Sep 2010.

[61] X. J. Mu, W. Sun, H. H. Feng, A. B. Yu, K. W. S. Chen, C. Y. Fu, M. Olivo, "MEMS micromirror integrated endoscopic probe for optical coherence tomography bioimaging," *Sensors and Actuators a-Physical,* vol. 168, pp. 202-212, Jul 2011.

[62] J. K. Chu, R. Zhang, Z. P. Chen, "A novel SU-8 electrothermal microgripper based on the type synthesis of the kinematic chain method and the stiffness matrix method," *Journal of Micromechanics and Microengineering,* vol. 21, May 2011.

[63] M. Hassan, "Pt/3C-SiC electrothermal cantilever for MEMS-based mixers," *Microsystem Technologies-Micro-and Nanosystems-Information Storage and Processing Systems,* vol. 17, pp. 425-428, Mar 2011.

[64] B. Ando, S. Baglio, N. Savalli, C. Trigona, "Cascaded "Triple-Bent-Beam" MEMS Sensor for Contactless Temperature Measurements in Nonaccessible Environments," *Ieee Transactions on Instrumentation and Measurement,* vol. 60, pp. 1348-1357, Apr 2011.

[65] P. I. Oden, P. G. Datskos, T. Thundat, R. J. Warmack, "Uncooled thermal imaging using a piezoresistive microcantilever," *Applied Physics Letters,* vol. 69, pp. 3277-3279, Nov 1996.

[66] L. R. Senesac, J. L. Corbeil, S. Rajic, N. V. Lavrik, P. G. Datskos, "IR imaging using uncooled microcantilever detectors," *Ultramicroscopy,* vol. 97, pp. 451-458, Oct-Nov 2003.

[67] S. R. Hunter , R. A. Amantea, L.A. Goodman, D.B. Kharas, S. Gershtein, J. R. Matey, S. N. Perna, Y. Yu, N. Maley, L. K. White,"High-sensitivity uncooled microcantilever infrared imaging arrays," 2003, pp. 469-480.

[68] P. G. Datskos, N. V. Lavrik, S. Rajic, "Performance of uncooled microcantilever thermal detectors," *Review of Scientific Instruments,* vol. 75, pp. 1134-1148, Apr 2004.

[69] D. Grbovic, N. V. Lavrik, P. G. Datskos, D. Forrai, E. Nelson, J. Devitt, B. McIntyre, "Uncooled infrared imaging using bimaterial microcantilever arrays," *Applied Physics Letters,* vol. 89, Aug 2006.

[70] L. Wu and H. K. Xie, "A Millimeter-Tunable-Range Microlens for Endoscopic Biomedical Imaging Applications," *Ieee Journal of Quantum Electronics,* vol. 46, pp. 1237-1244, Sep 2010.

[71] T. Kobayashi, H. Okada, T. Masuda, R. Maeda, T. Itoh, "A digital output accelerometer using MEMS-based piezoelectric accelerometers and arrayed CMOS inverters with satellite capacitors," *Smart Materials & Structures,* vol. 20, Jun 2011.

[72] M. Sato, S. Tsuda, I. Kanno, H. Kotera, O. Tabata, "Development of piezoelectric MEMS deformable mirror," *Microsystem Technologies-Micro-and Nanosystems-Information Storage and Processing Systems,* vol. 17, pp. 931-935, Jun 2011.

[73] J. Johari, J. Yunas, A. A. Hamzah, B. Y. Majlis, "Piezoelectric Micropump with Nanoliter Per Minute Flow for Drug Delivery Systems," *Sains Malaysiana,* vol. 40, pp. 275-281, Mar 2011.

[74] S. J. Chen, C. Y. Lee, E. S. Kim, "Integration of piezoelectric tunable capacitors and bonded-wire inductors for contactless RF switch and tunable filter," *Sensors and Actuators a-Physical,* vol. 165, pp. 73-78, Jan 2011.

[75] C. Dehoff, A. Hennings, C. Kugeler, T. Schneller, U. Bottger, "Piezoelectric actuated MEMS for use in microwave switching and filtering applications," *Physica Status Solidi a-Applications and Materials Science,* vol. 208, pp. 343-356, Feb 2011.

[76] B. Op het Veld, D. Hohlfeld, V. Pop, "Harvesting mechanical energy for ambient intelligent devices," *Information Systems Frontiers,* vol. 11, pp. 7-18, 2009.

[77] M. Al Ahmad and H. N. Alshareef, "Modeling the Power Output of Piezoelectric Energy Harvesters," *Journal of Electronic Materials,* vol. 40, pp. 1477-1484, Jul 2011.

[78] G. G. Stoney, "The tension of metallic films deposited by electrolysis," *Proceedings of the Royal Society of London Series a-Containing Papers of a Mathematical and Physical Character,* vol. 82, pp. 172-175, May 1909.

[79] S. Timoshenko, "ANALYSIS OF BI-METAL THERMOSTATS," *J. Opt. Soc. Am.,* vol. 11, pp. 233-233, 1925.

[80] Y. T. Hu, H. Xue, T. Hu, H. P. Hu, "Nonlinear interface between the piezoelectric harvesting structure and the modulating circuit of an energy harvester with a real storage battery," *Ieee Transactions on Ultrasonics Ferroelectrics and Frequency Control,* vol. 55, pp. 148-160, Jan 2008.

[81] Y. M. Liu., G. Tian, Y. Wang, J. H. Lin, Q. M. Zhang, H. F. Hofmann, "Active Piezoelectric Energy Harvesting: General Principle and Experimental Demonstration," *Journal of Intelligent Material Systems and Structures,* vol. 20, pp. 575-585, Mar 2009.

[82] M. Lallart and D. J. Inman, "Low-Cost Integrable Tuning-Free Converter for Piezoelectric Energy Harvesting Optimization," *IEEE Transactions on Power Electronics,* vol. 25, pp. 1811-1819, Jul 2010.

[83] P. C. P. Chao, C. I. Shao, C. X. Lu, C. K. Sung, "A new energy harvest system with a hula-hoop transformer, micro-generator and interface energy-harvesting circuit," *Microsystem*

Technologies-Micro-and Nanosystems-Information Storage and Processing Systems, vol. 17, pp. 1025-1036, Jun 2011.

[84] Y. K. Ramadass and A. P. Chandrakasan, "An Efficient Piezoelectric Energy Harvesting Interface Circuit Using a Bias-Flip Rectifier and Shared Inductor," *Ieee Journal of Solid-State Circuits,* vol. 45, pp. 189-204, Jan 2010.

[85] M. M. Yovanovich., J. R. Culham, P. Teertsra, "Calculating interface resistance," *Electronics Cooling,* vol. 3, pp. 24-29, 1997.

[86] J. Y. Fu., D. P. Chen, T. C. Ye, B. B. Jiao, Y. Ou, "Modeling and optimal design of multilayer thermal cantilever microactuators," *Science in China Series E-Technological Sciences,* vol. 52, pp. 1167-1170, May 2009.

[87] T. Bechtold, E. B. Rudnyi, J. G. Korvink, "Automatic generation of compact electro-thermal models for semiconductor devices," *Ieice Transactions on Electronics,* vol. E86C, pp. 459-465, Mar 2003.

[88] T. Bechtold, E. B. Rudnyi, J. G. Korvink., "Dynamic electro-thermal simulation of microsystems - a review," *Journal of Micromechanics and Microengineering,* vol. 15, pp. R17-R31, Nov 2005.

[89] T. Bechtold, E. B. Rudnyi, J. G. Korvink *, Fast simulation of electro-thermal MEMS: Efficient dynamic compact models*: Springer, 2007.

[90] V. Szekely, "THERMODEL: a tool for compact dynamic thermal model generation," *Microelectronics Journal,* vol. 29, pp. 257-267, Apr-May 1998.

[91] P. Szabó and V. Székely, "Characterization and modeling of electro-thermal MEMS structures," *Microsystem Technologies,* vol. 15, pp. 1293-1301, 2009.

[92] U. A. Bakshi and A. V. Bakshi, *Circuit Anlaysis -II*: Technical Publications, 2009.

[93] P. Ramos., F. J. Meca, J. Mendiola, E. Martin, "A simple thermal and electrical model of an infrared pyroelectric detector using spice," *Ferroelectrics,* vol. 271, pp. 1969-1974, 2002.

[94] C. G. Wei, T. L. Ren, J. Zhu, L. T. Liu, "A ferroelectric capacitor mathematical model for spice simulation," *Integrated Ferroelectrics,* vol. 64, pp. 101-111, 2004.

VITA

Salwa Mostafa completed her schooling from Holycross Girls High School and Holy Cross College in 2001. She graduated with a Bachelor of Science in Electrical and Electronics Engineering from Bangladesh University of Engineering and Technology in June, 2007. She pursued a direct Doctor of Philosophy degree in Electrical Engineering in the department of Electrical Engineering and Computer Science at University of Tennessee, Knoxville since January 2008 under the supervision of Dr. Syed Kamrul Islam.

Her research interests include low power analog circuits, analog to digital converters, device modeling and characterization, sensor and signal processing circuits, MEMS and energy harvesting systems. She has penned six journal papers and fifteen conference proceedings. During her tenure at University of Tennessee, Knoxville, she has been cited chancellor's honor for "Exceptional Professional Promise" and received Athletics department award as high-quality doctoral student.

She is married to Ashraf B Islam. She enjoys reading, crafting, physical activities and social networking.